High-Speed Imaging in the Refinement of a Fluid Dynamics-Based Sensory Light for Mental Well-being Enhancement

A thesis submitted for the degree of Masters of Science in
Engineering with Innovation & Entrepreneurship
by
Edoardo Gambacorta, BEng

Department of Mechanical Engineering
University College London

I, Edoardo Gambacorta, confirm that the work presented in this thesis is my own. Where information has been derived from other sources, I confirm that this has been specified in the thesis.

September 2023

Student number: 22231205
Total number of words: 11,984

I give permission to UCL to make this report public after the end of my studies, so UCL students and staff can access it.

☐ YES ☒ NO

Abstract

The present research delves into the development and refinement of a sensory light fixture “Breathe”, leveraging principles of fluid mechanics to offer a multisensory experience aimed at alleviating mental health issues. By synchronising visual input, movement, and auditory senses, “Breathe” aims to create a multisensory connection, fostering a cognitive feedback loop that relaxes the user into a state of presence. The initial prototype, inspired by the traditional bubble tube sensory light, presented some drawbacks. High-speed imaging played a vital role in the refinement of the prototype. Through assessment of key parameters such as droplet velocity, aspect ratio, generation time, and size, the prototype was iteratively improved. A set of performance criteria were devised based on the insights from the initial high-speed imaging experiments and user feedback. The improved prototype exhibited a considerable reduction in droplet velocity and longer generation times, especially in the critical 0–45-degree angle range, resulting in a more immersive and engaging sensory experience. “Breathe’s” business plan highlighted the product’s potential scalability, envisioning various product ranges, from personal deskside to public installations. The projected profits of £197'955 by 2024, combined with a lean operational approach, highlighted the product's commercial viability. While the improved prototype showcased improvements under set design criteria, further research is necessary to optimize droplet dynamics and explore various fluid compositions, tube configurations, and chamber geometries. The potential of “Breathe” sensory fixture for therapeutic and relaxation applications is vast, and its exploration promises a unique amalgamation of fluid dynamics, design, and well-being.

Acknowledgements

I want to express my sincere gratitude to Mark Miodownik, the project's supervisor, who provided invaluable insights for the refinement of the sensory light. My gratitude extends to Stavroula Babalabani for providing the resources for the high-speed imaging experiment which were essential for the project’s success. I am also deeply appreciative of Anastasios Koulogiannis for his assistance and knowledge in carrying out the high-speed imaging experiments. Their collective guidance and commitment have been pivotal to the fruition of this research.

Table of Contents

Nomenclature

- **Aspect Ratio (of a droplet)**: The proportion of its width to its height. Offers insights into the stability and morphology of droplets formed within the sensory light fixture.
- **Capillary Number (Ca)**: A dimensionless parameter comparing the influence of surface tension and viscous forces in the movement of fluid interfaces.
- **Droplet**: A small amount of liquid that has been detached from the main bulk, is often spherical. Droplet formation is the main visual component driving the multisensory experience within the light fixture.
- **Droplet Coalescence**: When two droplets merge together to form a single, larger droplet.
- **Droplet Generation Time**: The period of time between the genesis of subsequent droplets.
- **Droplet Size**: Measured as the diameter of individual droplets
- **Hydrodynamic Focusing**: A technique for controlling droplet formation, often confining one fluid stream within another
- **Liquid-Liquid Instabilities**: When two immiscible liquids come into contact, resulting in intricate flow patterns, as presented in the sensory light
- **Rayleigh-Taylor Instability**: An instability that occurs at the interface between two fluids of different densities, under the influence of a gravitational or acceleration field. This principle is employed in the sensory light to enhance the visual experience.
- **Reynold's Number (Re)**: A dimensionless parameter describing a fluid's flow regime indicating whether the flow is laminar or turbulent
- **Sensory Light**: A lighting device that fosters tranquility through multisensory (auditory, tactile, visual) stimulation
- **Surface Tension**: The property of a liquid's surface that allows it to resist external forces. It plays a fundamental role in droplet formation and stability.
- **Viscosity**: A measure of a fluid's resistance to shear or flow. Different viscosities can lead to varied droplet behaviors and visual effects in the sensory light.

List of Tables

List of Figures

1 Introduction

1.1 Mental Health and Phone Addiction

In an era where digital screens dominate our waking hours, one must pose the question: "How does excessive screen time affect our mental well-being?" The average individual spends nearly 7 hours a day on screen, from smartphones to computers, accounting for over 40% of their waking hours [1][2][3]. Such individuals are unwittingly exposing themselves to a plethora of adverse health effects, including dietary issues, sleep disturbances, vision problems, and mental health concerns[4]. A study conducted by Twenge, J. M., et al. found that excessive screen time contributed to depressive symptoms, stress, anxiety and decreased attention span in young adolescents in the United States [5]. This has been frequently associated with extensive social media use, resulting in brain alterations that disrupt emotional regulation and cognitive function, as well as physical, psychological, and neurological problems [6]. It is a catalyst for ADHD-related behavior, closely coinciding with substance dependence effects, for its ability to activate dopamine receptors and reward pathways[6]. This phenomenon, known as the "Red Mind" effect, is a psychological state characterized by overstimulation, stress, and hyperactivity, negatively impacting mental well-being, cognitive function, and overall health [7]. Smartphones are becoming more accessible with social media presence more established in the day-to-day, causing screen-time related health effects to worsen. It is imperative, therefore, to explore avenues such as sensory fixtures and multisensory therapy, offering a promising solution to the detrimental effects of digital saturation.

Figure 1 A sensory light fixture in use

1.2 Sensory Tools & Technologies for Mental Health and Phone Addiction

Sensory light fixtures (see Fig. 1[8]) have been shown to provide significant therapeutic benefits in the realm of multisensory therapy[9]. This project encompasses the design and optimization of an existing prototype of a sensory light fixture created by the principal researcher of this report (See Previous Work). The technical examination of this existing prototype forms a core part of this study, aiming to identify and rectify its flaws through a rigorous high-speed imaging experiment. The proposed design incorporates droplet formation to offer a soothing and engaging focal point, grounding users in a sense of tranquility while providing cognitive stimulation[10][11]. The novelty of this project lies in the application of these sensory fixtures to a broader context, as a means to divert attention of screens and provide therapeutic benefits that address the core problem of phone addiction.

1.3 Technical Examination of the Existing Prototype

“Breathe”, the presented sensory fixture prototype, stands as a testament to the potential of fluid mechanics in therapeutic applications. This project is a rigorous technical examination of the existing prototype, requiring further refinement and optimization. It will investigate the calming effects produced by oil-water flows and Rayleigh-Taylor Instabilities. The literature review incorporates an examination of fluid dynamics principles, which form the foundation of the sensory light. A high-speed imaging experiment will be conducted on the sensory light at different angles of inclination to measure the existing prototype’s performance, providing insights on parameters such as “Droplet Velocity, Aspect Ratio, Generation Time & Size”. The shortcomings of the current prototype will be critically analyzed to determine what needs to be fixed, helping to develop and optimize the sensory light during the prototyping stage. High-speed imaging will be re-conducted on the refined prototype, utilizing pre-established design parameters to assess its performance. This iterative process will pave the way for subsequent stages, ensuring the final product is therapeutically effective.

1.4 Project Overview

The design aim of this project is to examine and quantify previously constructed sensory light design through a high-speed imaging experiment. The sensory light stimulates visual, auditory, and tactile senses using Rayleigh-Taylor Instabilities in oil-water flows. Users can physically manipulate the fixture to generate varying fluid dynamics effects. Experiments using high-speed imaging serve as a design reference for both the initial and improved prototypes. These observations help to create a business and production plan for mass market deployment, together with market research.

1.5 Aim

- Utilize fluid dynamics principles to refine existing sensory light fixture in order to deliver therapeutic advantages through multisensory therapy, with a focus on phone addiction and mental health issues.

1.6 Objectives

- Carry out a high-speed imaging experiment to analyze the behavior of Rayleigh-Taylor instabilities in oil-water flows, providing insights for the refinement of the new sensory light fixture prototype.
- Prototype, test and refine the sensory light fixture, ensuring its design effectively incorporates insights gained from the high-speed imaging experiment, by establishing a set of design criteria
- Re-conduct high speed imaging on refined prototype, assessing performance against design criteria
- Develop a comprehensive business plan that outlines the strategies for producing the sensory light fixture

The following literature will examine Rayleigh-Taylor instabilities in oil-water flows and related droplet generation mechanisms, laying the foundations for the sensory fixture's therapeutic potential.

2 Literature Review

2.1 Overview

The following literature review delves into principles of fluid dynamics, emphasizing their relevance in the sensory light prototype. It explores the behaviors of oil-water flows, highlighting phenomena like Rayleigh-Taylor Instabilities and their therapeutic implications[12], [13]. It aims to highlight primary mechanisms of droplet generation such as hydrodynamic focusing and droplet coalescence. The review underscores the psychological benefits of observing fluid motion, referencing established concepts like the "Blue Mind" effect[14], [15]. The significance of high-speed imaging in capturing these fluid behaviors is also discussed, emphasizing its role in the design and refinement of sensory fixtures.

2.2 Fundamentals of Fluid Dynamics in Sensory Light Therapy

Fluid dynamics, a subfield of fluid mechanics, uncovers fluid flow behavior across diverse scenarios, from ocean tides and weather patterns to blood circulation and design of complex engineering systems[16]. Pertinent to this investigation, it deciphers the underlying mechanism behind the proposed sensory light effect. This refers to the visual and tactile stimulation produced by the movement of fluids, particularly Rayleigh-Taylor Instabilities within oil-water flows within the sensory light fixture. Consideration of factors like surface tension, viscosity difference, manipulated by surfactants, is crucial. These principles will be pivotal in optimizing the performance and design characteristics of the sensory fixture.

2.2.1 Liquid-to-liquid flows & instabilities

Understanding liquid-to-liquid flows and instabilities is crucial in oil-water systems. Such flows can arise from the interaction of immiscible liquids, like oil and water, leading to various flow regime and instabilities, from interphase mixing to stratified flows. The viscosity of oil and water can affect these flow pattens, dictating how the two fluids interact at the interface. Factors such as surface tension forces, wall-wetting properties, and tube material also affect oil-water systems, Brauner finds [17]. Liu et al. identified a correlation between flow split ratio and oil/water separation, which consistent across diverse Reynold’s

numbers. Reynold's numbers, a dimensionless quantity, represents the ratio of inertial forces to viscous forces and describe the flow regime of fluid systems.

Liquid-liquid systems can result in a wide variety of flow patterns, as discussed by Brauner, with visual representations observed in Fig 2 [17]. These can be categorized into four essential prototypes: stratified layers (Fig 2a/b), large slugs (Fig 2q/r), dispersed fine drops (Fig 2i/j) and annular flow (Fig 2m/n) [17].

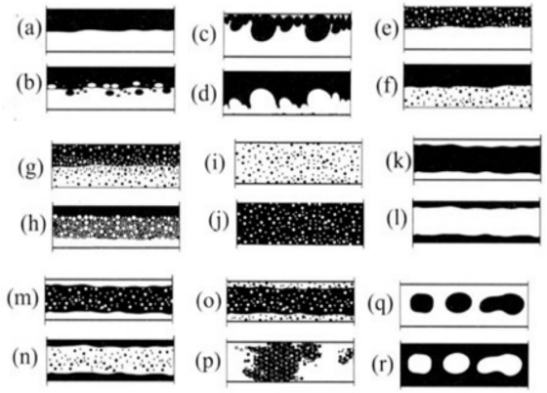

Figure 2- various possible flow patterns observed in horizontal liquid to liquid systems

The complexity of these patterns poses challenges in predicting their behavior, but also offers a plethora of possibility for its applications within the desired sensory light effect.

2.2.2 Rayleigh-Taylor Instability

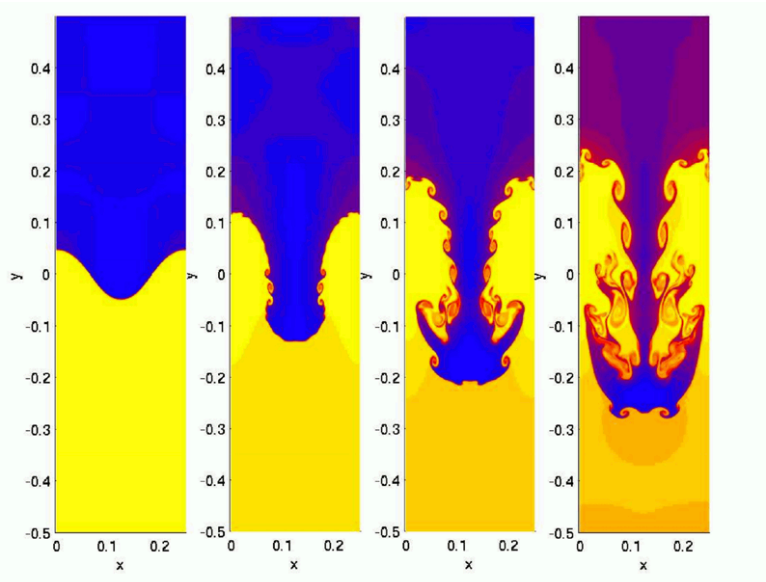

Figure 3– Rayleigh-Taylor Instability development over time

Rayleigh-Taylor Instability occurs when a denser fluid is placed over a lighter fluid, leading to the growth of perturbations at their interface, which is significant in the context of sensory light therapy due to its captivating visual patterns (see Fig. 3). Flow patterns are highly dependent on fluid properties (i.e., viscosity), flow rates and the system's geometry, Garoosi et. al finds [18]. The early-stage prototype, which is targeted for optimization, consists of a circular chamber divided into two identical parts, linked by acrylic tubes. When the denser fluid (waster) is placed on top, it forms a downwards droplet effect, while the oil droplet rises upwards to keep the system in equilibrium. This creates a visually captivating, synchronized spectacle of droplet formation, potentially useful for the sensory fixture. Ueda et al. found droplet formation is influenced by an upward hydrodynamic force due to the wake and a downward force due to gravity[19]. Factors like system velocity, gravity and surface tension may also impact the magnitude of Rayleigh-Taylor Instability [19].

2.2.3 Application to the sensory light fixture

Understanding the behaviors of oil and water under various conditions, is key in optimizing the design and functionality of the sensory light fixture, ensuring optimal visual effects. Sensory light fixtures, predominantly used for therapeutic aid in children with learning impairments, are designed to alleviate stress and anxiety by stimulating multiple senses simultaneously [20][21]. The study conducted by Ashby et. al validates the advantages of sensory light therapy as a calming exercise, offering a feeling of security and unique simulation at the discretion of the user[22]. This all-engaging, multisensory experience, aims to reduce stress and anxiety levels, as confirmed by Chan et. al [23].

2.2.4 Mechanisms of Droplet Generation and Interaction in Liquid-Liquid Flows

Droplet Generation: The sensory light fixture utilizes Rayleigh-Taylor instability in oil-water flows to generate droplets. The denser fluid (water drops) is forced downwards while the oil drops are propelled upwards, creating a spectacle of droplet formation. Lovick et al. state this process is comparable to the breakdown of disturbance waves, (as confirmed by Hewitt and Hall-Taylor), with both phases destabilizing each other, resulting in the generation of oil and water droplets [24][25].

Droplet Coalescence: Droplets often interact, merging to form larger droplets, creating a visually fascinating spectacle [26]. Material used for the tube influences drop size distributions, with steel pipes producing smaller droplets when compared to acrylic pipes, under identical flow conditions, as disputed by Angeli et al. [27]. Droplet coalescence, an important separation mechanism in oil-water flows is a non-linear function of time, as deducted by Hafskjold et al. [28]. Wang et al. devised a model to represent coalescence in oil droplets, where different stages were observed including droplet convergence, using high speed imaging techniques (see Fig 4)[29] [30][31]. High-speed imaging will be used in this investigation to examine fluid motion, including drop coalescence, within the sensory light.

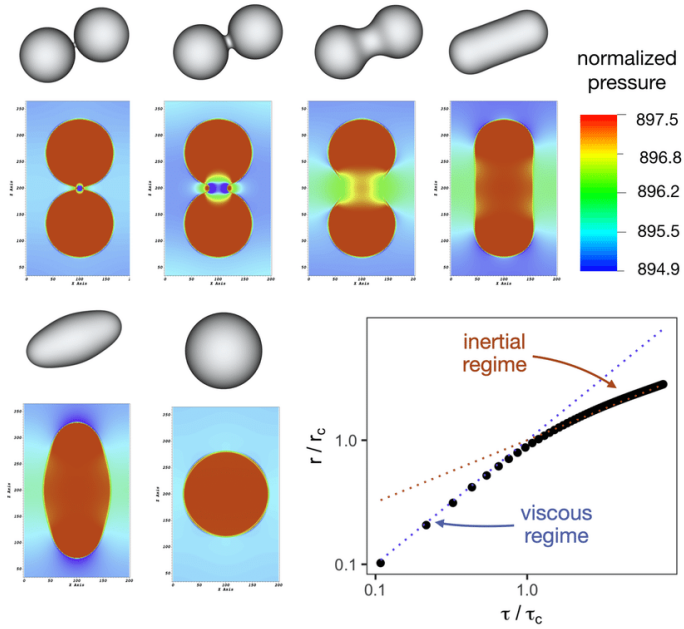

Figure 4– Evolution of droplet coalescence

Hydrodynamic focusing: As evidenced by Chang et al., this element is crucial in guiding flows within a system and has established applications and droplet creation tools[32]. The water and oil are directed through two tubes, causing the water to drop and the oil to rise to maintain equilibrium. The fluids are hydrodynamically focused through cylindrical tubes, resulting in spherical droplet formation, as deducted by Funfschilling et al (see Fig 5) [33][34]. Foroughi et al deduces a relationship between slug, annular and droplet flow patterns and could provde insights into oil-water behavior within the sensory light [35]. The width of the focused stream may be influenced by adjusting the relative volumetric flow rates of central and side streams, Babakhani et. al concluded [36] [32]. Quantifying hydrodynamic focus of the flow and associated parameters allows for consistent and controlled fluid flow in the light fixture, enhancing the sensory experience.

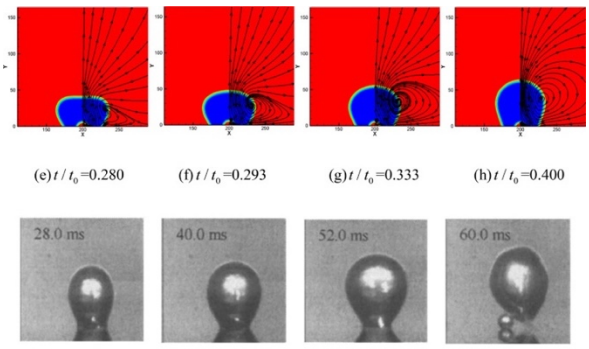

Figure 5– Hydrodynamic Focusing occurring at the tube

2.2.5 Influence of Surface Tension & Viscosity on Oil-Water Dynamics

The roles of surface tension and viscosity, especially the variance in viscosity, are essential in modifying oil-water flows and related instabilities [37][38][39]. In Rayleigh Taylor instabilities, surface tension's success in stabilizing disturbances is dependent on the growth rate, representing the pace of fluid system perturbation, as deducted by El-Ansary et al. [40] [41]. Variations in surface tension impact mixing and dispersion behavior in oil-water flow, thus droplet formation, as disputed by Chen et al. [42]. Surface tension can be manipulated or reduced by adding surfactants in oil-water systems. This agrees with findings by Xu et al, with sodium dodecyl-di(oxyethylene) ether sulfate (AES) deemed to be the most effective agent in reducing surface tension [43]. Surfactant concentration may also impact the degree of ordering of the interfacial oil molecules, as deducted by Hosseinpour et al. [44].

Viscosity, a measure of the fluid's resistance to shear flow, plays a significant role in the behavior of Rayleigh-Taylor Instabilities [45]. Mikelian et al. demonstrates that viscosity directly influences perturbations at the interface [46]. This is congruent with the findings of Loh et. al., observing a higher viscosity ratio result in a limited flow pattern, when comparing low and high viscous oil-water flows in pipelines [47]. Use of drag-reducing polymers, such as polyacrylamides and polysaccharides can modify flow dynamics by reducing drag, as argued by Al-Yaari et al. [47] [48]. Incorporating substances such as glycerol to oil can alter the viscosity contrast, impacting the interfacial tension and phase inversion dynamics in oil water flows [49][35]. Analyzing the effects of additives like surfactants on surface tension and viscosity is crucial for the sensory light's development.

While fluid dynamics can provide the foundational principles of the sensory light's behavior, it's essential to delve into the therapeutic implications of such fluid motions.

2.3 Mental Health Benefits and Neurostimulations of Fluid Motion

2.3.1 Sensory rooms and their impact on mental health

Sensory rooms, designed to offer safe and interactive sensory stimulation, are particularly beneficial for individuals with mental illness (such as Autism, Dementia and Asperger's), addiction, sensory processing disorders or trauma history, Chalmers et al. finds [50][51]. These rooms offer a variety of stimuli including sounds, colors, lights, tactile features, and aromas, resulting in auditory, proprioceptive, tactile, vestibular, olfactory, and visual stimuli[50][52] Studies reveal a significant stress reduction in patients after exposure to the sensory room, indicating its mental health benefits, in agreement with the findings of Knight et al. [51][53]. Multisensory therapy (or Snoezelen) can induce relaxation, improve focus, reduce aggressive behavior while promoting overall positive behaviors[23] [54].

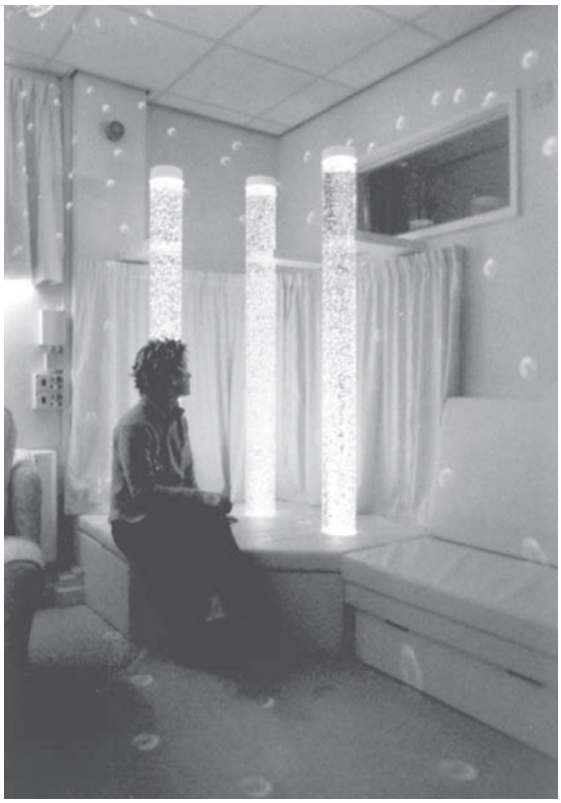

Figure 6 - Bubble Tube sensory light fixture under observation to achieve multisensory stimulation.

2.3.2 Psychological Benefits of Observing Fluid Motion

Sensory light fixtures, often featuring droplet formation, are a staple in Snoezelen therapy. They offer a soothing, engaging focus points for patients, grounding the user to a sense of tranquility while providing cognitive stimulation (See Fig. 6) [51][50]. Pusuluri et al. developed the bubble tube, a cylindrical water-filled pipe equipped with an air blower and LED lights, aiming to provide both visual and auditory stimuli in sensory therapy [10]. A study conducted by Ashby et. al, show significant improvement in patient attention span and positive emotions after 8-10 multisensory therapy sessions with the bubble tube [55][56]. Exposure to the bubble tube led to decreased heart rates and behavioral disturbances, as observed Hotz et al. in children recovering from brain injury[57]. While the bubble tube offers visual patterns, it lacks physical interactivity for the user. The following case study affirms the project's motivation for producing a fluid based sensory light that links physical interaction with visual stimuli to establish a stronger multisensory connection.

2.3.3 Grounding & Therapeutic Influence of Fluid Motion

Wallace J. Nichols "Blue Mind" effect describes the tranquility and well-associated with observing water, contrasting the anxiety-inducing "Red Mind" effect of digital overstimulation, as discussed by Tajane et al. [15][58]. Nichols argues observing chaotic fluid motion can stimulate mood-enhancing neurotransmitters, akin to meditation[15] [59]. This agrees with the findings of White et al., concluding environments with larger bodies of water tend to have a significant impact on affection and grounding [59]. Observing fluid motion increasea dopamine while decreasing cortisol (stress hormone), as disputed by Conrad et al. [14]. A 2016 survey in Wellington New Zealand, reported higher exposure to blue spaces resulted in lower psychological distress [14][60]. Looking at water can also reduce risk of death by 12-17%, as argued by Crouse et al. when examining Canadians residing by the coast. The European Union introduced Blue Health in 2020, a four-year cross-disciplinary project, exploring the multitude of positive psychological effects of observing aquatic environments [61]. These studies underscore the potential of manipulating fluid motion through Rayleigh-Taylor instabilities in a sensory light can mimic the calming and grounding effects of observing water.

2.3.4 Potential of Fluid Dynamics in Neurostimulation and Promoting Positive Mental Health

Fluid motion's therapeutic potential for neurostimulation and multisensory therapy is a burgeoning field. The bubble tube case study confirms the efficacy of utilizing chaotic fluid motion in Snoezelen therapy, as shown by Novakovic et al.[62]. Multi-sensory therapy is designed to stimulate senses simultaneously, providing a holistic sensory experience, strengthening the overall physiological and psychological effects [13]. The proposed sensory light aims to provide a holistic sensory experience by combining visual stimuli of fluid motion combined with the user's physical interaction, creating a calming cognitive feedback loop as argued by Staal et al. [63]. The "Blue Mind" effect, which associates observation of fluids with reduced stress further justifies the context of this study [59][14]. Exploring Rayleigh-Taylor instabilities in sensory lights ensures a fascinating, ever-changing pattern of fluid motion and a novel approach to multisensory therapy.

Having established the therapeutic potential of fluid motion, it's crucial to understand the methodologies employed to study these fluid behaviors.

2.4 Investigating Oil-Water Flows through High-Speed Imaging Experiment

2.4.1 Introduction to High-Speed Imaging & Its Applications In Sensory Light Design

High-speed imaging captures intricate fluid behaviors, such as droplet creation and Rayleigh-Taylor Instabilities, at unparalleled rates [64][65][66]. It offers insights into droplet dynamics, such as velocity, generation time, aspect ratio and size, essential for the sensory light's design. Key parameters, including frame rate, spatial resolution, and lighting conditions, dictate the reliability and accuracy in data sampling [67][68][69].

2.4.2 High Speed Imaging in Oil-Water flows and Rayleigh-Taylor Instability

Within the context of oil-water flows, high-speed imaging accurately reveals flow pattern morphologies, including the dynamics of Rayleigh-Taylor Instabilities [70]. It is instrumental in understanding the behavior of droplets in oil-water flows, including their formation, coalescence, and the influence of factors like surface tension and fluid composition [71] [72][73].

2.4.3 Challenges & Limitations of High-Speed Imaging

Despite its capabilities, high-speed imaging presents challenges, such as limited depth of field and refractive differences in oil-water flows [74] [75]. However, recent advancements, like deep-learning algorithms, offer solutions to these challenges, enhancing image resolution and capturing accuracy [76] [77].

2.4.4 Role of High-Speed Imaging in the Design and Refinement of the Sensory Fixture

The project leverages high-speed imaging to inform the sensory light's design, focusing on droplet dynamics at varied angular inclinations. Measuring and quantifying the interactivity of the sensory light, emphasizes the therapeutic potential of varied droplet formations, with the sensory light's visual-tactile feedback loop being a key stress-reliever [78] [79][9]. This will allow for prototype refinement, assessing performance against design criteria deducted in light of the high-speed imaging experiments.

With this foundational knowledge, one can now review the previous work on the prototype, understanding its strengths and areas of improvement.

3 Previous Work

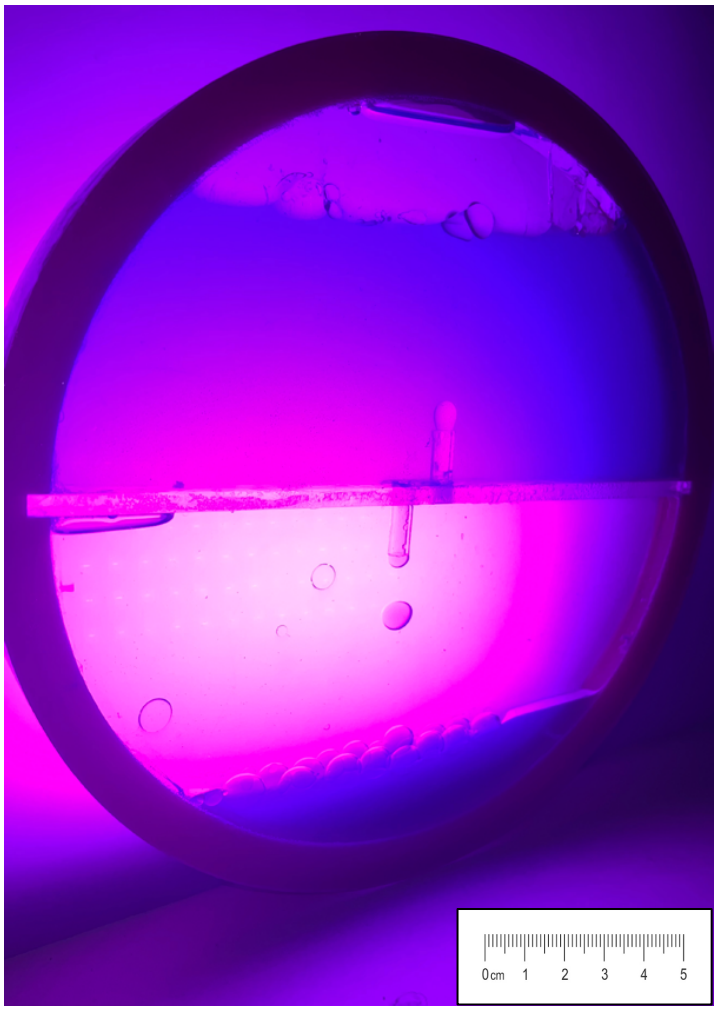

Figure 7– Previously made prototype of "Breathe" sensory light aimed to be used for high-speed imaging study

This section delves into the features and critiques of the previously developed prototype of the sensory light, emphasizing its potential in multisensory therapy.

3.1 Introduction to Previous Work

The "Breathe" sensory light, an innovative blend of fluid mechanics principles and sensory therapy, consists of a circular chamber divided into two sections interconnected by tubes (see Fig. 7). The structure aims to create an ergonomic feel, with the circular structure symbolizing continuity and functionality. When with fluids of different densities (distilled water on top, mineral oil on the bottom), and flipped, the chamber showcases the Rayleigh-Taylor Instability. This phenomenon involves the interplay of two fluids of different

densities, results in a mesmerizing, rhythmic droplet formation resulting due to hydrodynamic focusing at the tubes, offering a soothing visual experience[41], [80]. The prototype is also aided by a backlighting component, aiming to highlight the effect and strengthen the multisensory connection. The proposed sensory light demonstrates how fluid mechanics can extend beyond traditional applications, such as tackling mental health through multisensory therapy[10].

3.2 Current Prototype's Therapeutic Potential

The sensory fixture product introduces Rayleigh-Taylor Instability to multisensory therapy, a novel concept. The droplet formation engages visual, tactile, and auditory senses for an all-engaging therapeutic tool[22].Snoezelen therapy benefits mental health, especially in children with learning disabilities[10], [57]. The sensory fixture enhances this effect with its dynamic visual element - the rhythmic movement of droplets. This calming spectacle encourages focus on the present, diverting attention from stressors.

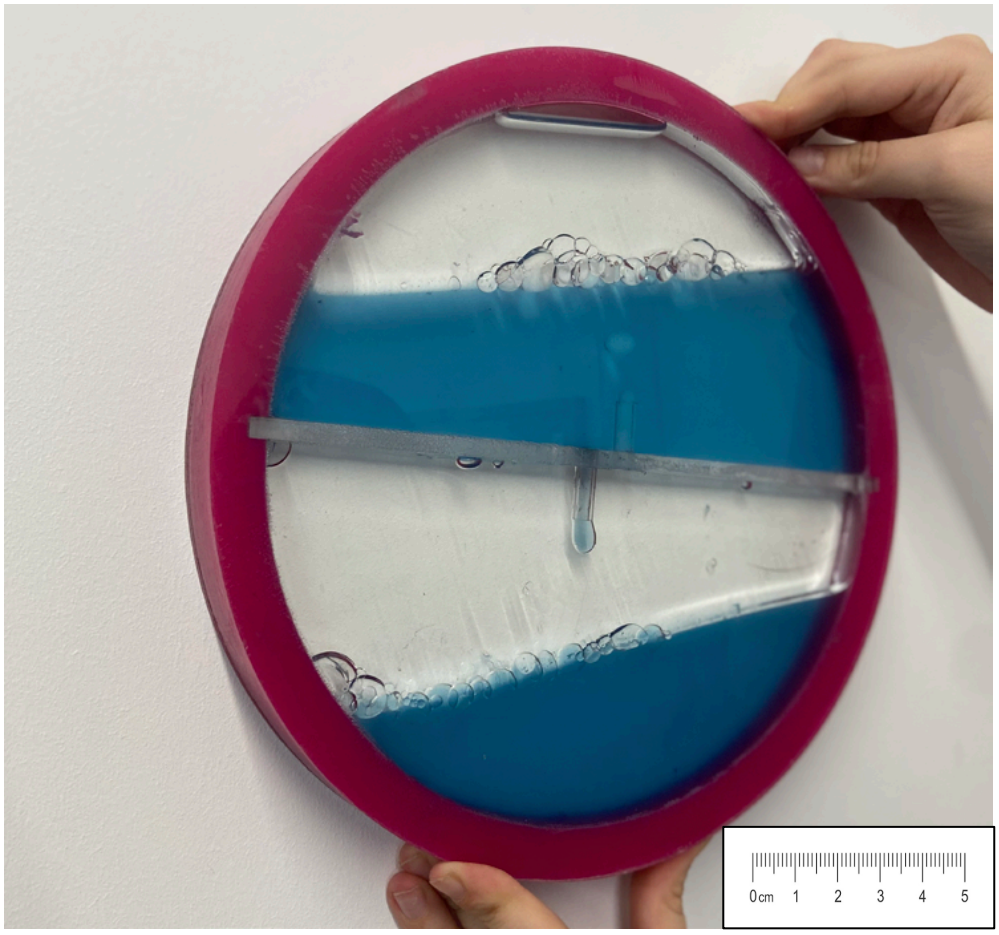

Figure 8– User interacting with sensory light

The ergonomic circular shape was designed to invite physical interaction, as shown by Fig. 8. Users manipulate the fixture to initiate the effect and control droplet flow, enhancing therapeutic benefits[12]. Physical manipulation is central to its therapeutic potential, creating a cognitive feedback loop that foster's presence in the user[10], [55]. Unlike the bubble tube (see Fig 6.) which is stationary, the proposed design offers a more engaging experience through multisensory interaction[10]. It's alignment with high-speed imaging, with its flat surface and circular shape, facilitates precise angle measurement, critical in assessing the current prototype's drawbacks[65], [81].

3.3 Critique of the Sensory Light Prototype and High-Speed Imaging Approach

While the current sensory light prototype holds promise, it exhibits limitations, especially at varied angles of inclination. Achieving optimal visual display dynamics and maintaining user engagement at stepper angles requires a deeper understanding of droplet generation times and velocity, along with extensive testing and user feedback [82].

A high-speed imaging experiment was designed to measure the angles that restrict the Rayleigh-Taylor Instability and user interaction and quantify the effects of changing angles on visual outputs, including droplet velocity, size, generation time and aspect ratio[40]. The insights from this method will be pivotal in identifying flaws and guide future prototyping.

Given the insights and drawbacks highlighted in previous work, the challenge lies in devising a methodology that not only addresses these limitations but also amplifies the sensory light's therapeutic potential.

4 Methodology

4.1 Experiment Set Up

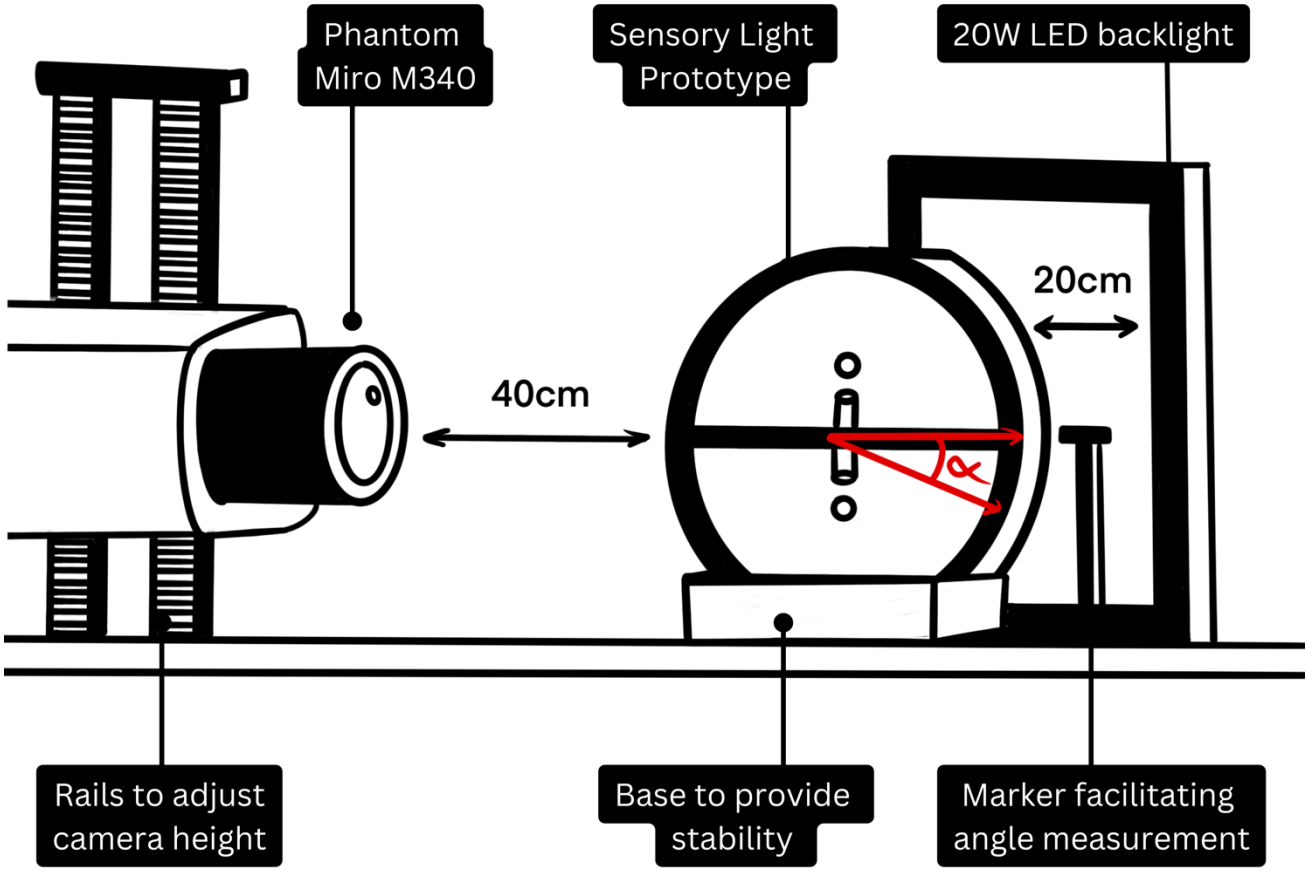

Figure 9– Experimental Set Up

The high-speed imaging experiment was designed to ensure accurate capture of the fluid dynamics aspects of the sensory light, with a central focus on the droplet formation on the top and bottom of the circular chamber resulting from the Rayleigh-Taylor Instability[81], [83]. The experiment utilized the Phantom Miro M340 high-speed camera, positioned 40cm away from the sensory light, focusing on the target zone, as shown by Fig 9 [84]. The prototype is positioned on a base, ensuring stability throughout the collection period. The angle of inclination, denoted as α, was varied in increments of 15 degrees, ranging from 0 (horizontal) to 135 degrees. The high-speed capture was aided by a 20W LED backlight placed 20cm behind the sensory fixture, and a marker placed next to the sensory light to facilitate angle measurements[84]. Thus, allowing for observation of droplet formation at different angles, quantifying the multi-sensory connection achieved from physical manipulation and resulting

varied visual output[10], [62]. The set-up distance was marked and maintained throughout the entire data collection procedure to ensure accuracy in results, and to provide a suitable reference point for converting pixel distance to millimeters in post-processing[67], [75]. The camera was paired with image capture software Dantec Dynamic Studio.

Different frequencies were established for each angle of inclination (Table 1). This setup facilitated the recording of droplet generation at varying velocities, frame rates and intervals[65], [67]. At the case of 0 degrees, droplet formation is extremely rapid, requiring a higher frequency due to the shorter time frame. Whereas at 135 degrees, where droplet generation is delayed, was captured with a low frequency, to capture necessary details throughout the longer time period[67].

Table 1 - Frequency (Hz) used for each angle.

Angle (°)	Frequency (Hz)
0	90
15	90
30	90
45	90
60	90
75	90
90	45
105	45
120	15
135	5

4.2 Data Collection

Quantifying droplet formation within the sensory light allowed for measurement of key parameters. These include droplet generation time, droplet velocity, droplet size and aspect ratio and its variation upon inclination angles. This was crucial in understanding how the visual output of the fluid dynamics within the sensory light varies as the light is physically manipulated. Such is the main mechanism driving the multi-sensory connection, as the user physically interacts with the light, resulting in a clear change of the fluid motion within[12], [13]. This creates cognitive feedback loop that is desired in multisensory or Snoezelen therapy, driving positive mental health effects such as decreased stress and anxiety levels while grounding and providing focus to the user [53]. Measurements were collected for both

the top and bottom chamber of the sensory light in order to investigate which are most effective in offering multisensory stimulation throughout the various angles. Quantifying the fluid dynamics behind the multisensory effect of the sensory light will provide fundamental basis for confirming and optimizing it's benefits in the next prototype iteration.

4.3 Post-Processing of Images

Post-processing is a critical step within the project methodology, where raw data collected from the high-speed imaging experiment is transformed into a format that can be analyzed and interpreted[81]. This procedure was carried out on the ImageJ software, a powerful open-source tool that provides a range of functionalities for image processing and analysis[85].

4.3.1 Image Sequence Integration:

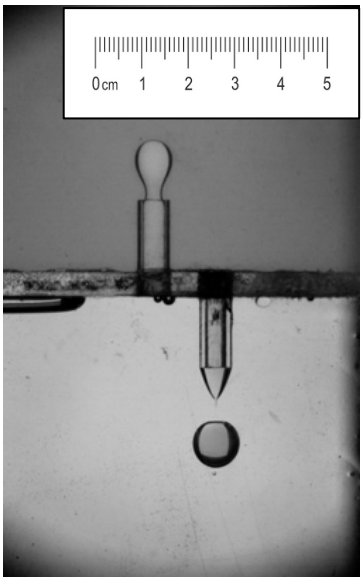

Figure 10– Line marking the trajectory of the droplet throughout the sampling period.

This step entails loading the image series into ImageJ. This software is capable of handling large volumes of data, making it an ideal tool for managing the extensive image sequences generated by the high-speed camera used. Fig 10. shows a sample of the raw image sequence imported into ImageJ before conducting any sort of post-processing[85]. In the given cases where the angle was varied (15-135), the image sequence was rotated by that given angle to ensure data collection was horizontal for the entire post processing step. Once the images are integrated, the next step involves manipulating the image to be optimal for data sampling.

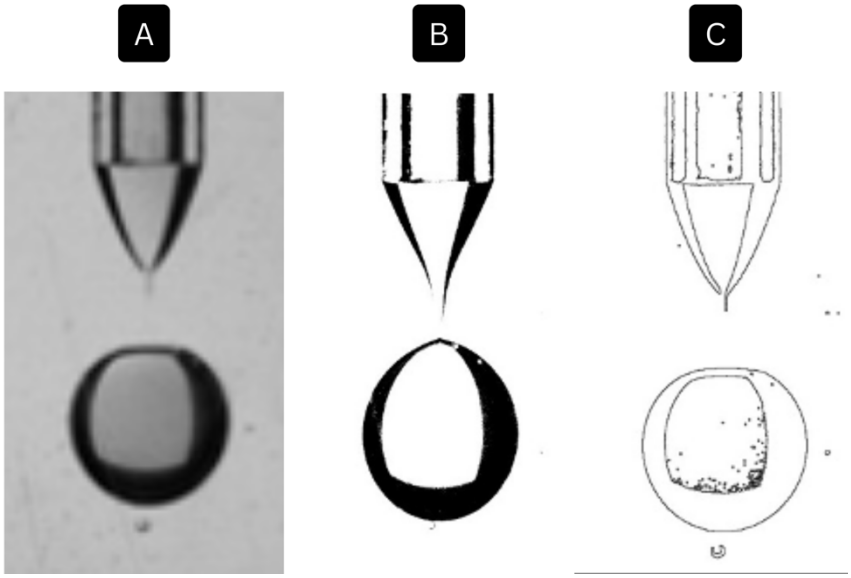

Figure 11– Image Processing Workflow: (a) Raw Image Sequence, (b) Brightness and Contrast Manipulation, and (c) Binarization Function Application

4.3.2 Cropping, Brightness and Contrast Manipulation:

Once the image sequence is imported, the desired section is cropped (see Fig 11A) and the brightness and contrast of the images are manipulated (see Fig 11B). This step is crucial for enhancing the visibility of the droplets in the oil-water flows and reducing the noise from the sampling[67]. The goal here is to obtain a clear 2D image of the droplet, which will increase the accuracy of the subsequent measurements and analyses, as argued by Damsohn et al [70].

4.3.3 Binarization and Outline Function Application:

Images are binarized into 2D black and white format after being adjusted for brightness and contrast to improve droplet visibility. The outline function is then applied to the binarized images (see Fig 11C). This function outlines the shape of the droplet, focusing on the outer structure, which is the area of interest for this study[67], [70]. The processes of binarization and outlining are vital for distinguishing the droplets and readying the images for subsequent in-depth measurements[85].

4.4 Measuring Velocity:

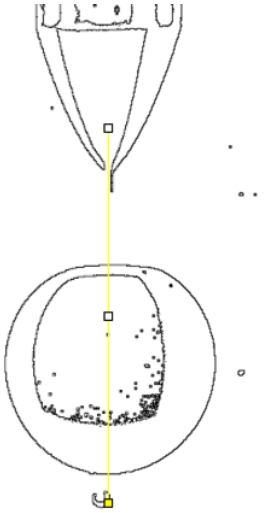

Figure 12– Line marking the trajectory of the droplet throughout the sampling period.

4.4.1 Velocity Measurement Process:

Measuring droplet velocity involved tracking their trajectory throughout the sampling period and extracting relevant data. A line was drawn vertically through the droplet (as shown in Fig. 12) in the binarised image sequence, marking the path of the droplet's movement. This method allowed for the tracking of the droplet's position over time, providing the necessary data for velocity calculation[67], [68].

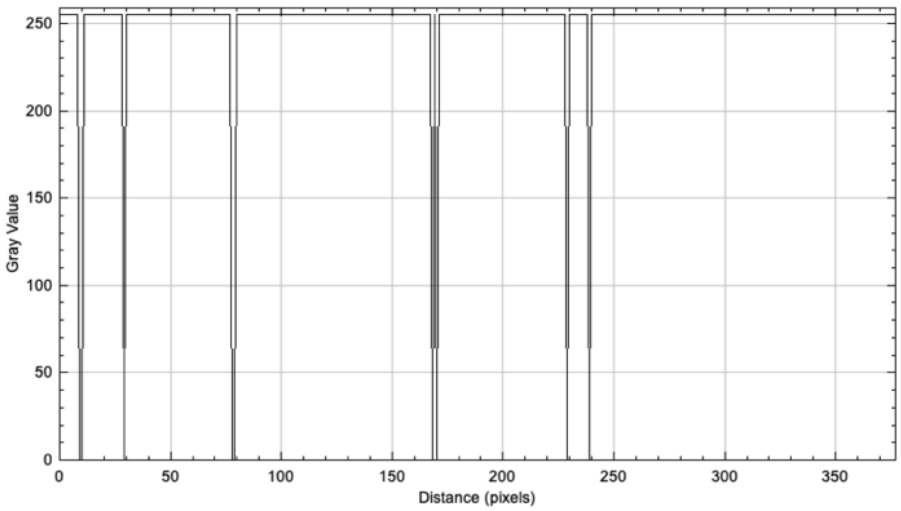

Figure 13 – Plot profile for a given frame

4.4.2 Data Extraction and Manipulation:

The StackProfileData macro plugin (see Appendix A) was employed to generate CSV files that contained the profile plot data over time for the given line (see Fig 12)[85]. The color values for each pixel are shown (255 for white, 0 for black). In order to identify the droplet's outer boundary for falling droplets, CSV data analysis was utilized to retrieve the last black value from each frame. The plot profile was used to understand which relevant values to extract for each case, as seen by Fig 13 above[67].

4.4.3 Data Smoothing and Cropping:

The extracted data was slightly noisy and required smoothing for accurate velocity calculations. Spline fitting was performed on the position data using a polynomial of degree 3, which was chosen empirically. The data was then cropped to focus on one droplet generation, providing a more focused dataset for velocity calculation[81], [86].

4.4.4 Velocity Calculation:

The velocity of the droplets was calculated from the smoothed and cropped position data. Velocity was computed as the rate of change of position over time, formulated as (pos_frame_2-pos_frame_1)/dt, with dt being 1/frequency (Eq. 1). This calculation was performed using Python code, which is provided in Appendix B for reference. This procedure was executed for the bottom section of the sensory light, for 0, 30 and 60 degrees. Velocity measurements were disregarded for the superior chamber as three-way flows are present here, skewing results, as evidenced by Thoroddsen et al. [81].

4.5 Measuring Droplet Generation Time:

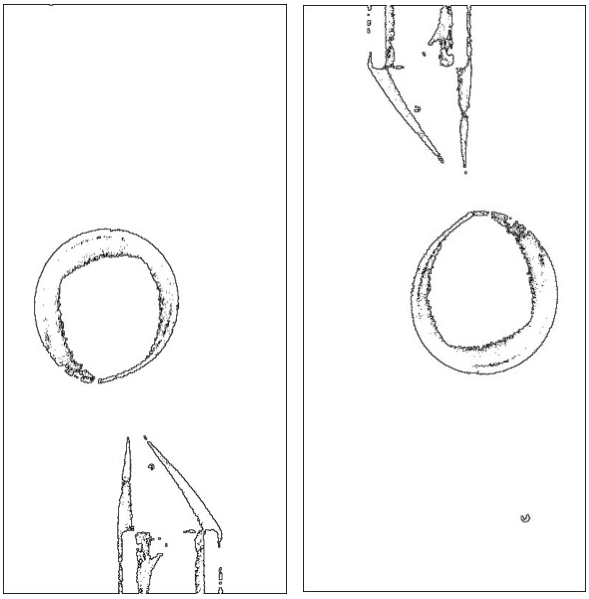

Figure 14 Droplet release points for 15 degrees, top (left) and bottom (right) chambers of the sensory light

4.5.1 Determination of Droplet Release Points:

Utilizing the high-resolution image sequence capture, the exact point of droplet detachment from the tube were identified. Establishing a standardized point where the droplet is released throughout the top and bottom, and the complete range of angles ensured that the data captured was both accurate and representative of the fluidic behavior within the sensory light [67], [86]. Fig 14 illustrates the droplet generation time for a 15-degree inclination, identifying the release between frames 11 and 82.

4.5.2 Calculation of Generation Time:

By comparing the frame rates of consecutive droplet releases, the generation time was computed as the difference between the two frames, divided by the inverse of the recording frequency.

$$Bubble\ Generation\ Time = \frac{Frame\ \#\ Bubble\ Release\ Point\ 2 - Frame\ \#\ Bubble\ Release\ Point\ 1}{\frac{1}{Frequency}} \quad \text{(Eq. 2)}$$

This approach provided a quantitative measure of the time taken for each droplet to form and detach, allowing for a standardized measurement to be taken across all sampling points[86].

This measurement process was systematically executed for both the top and bottom sections of the sensory light, varying angle of inclination from 0 to 135 degrees at 15-degree increments.

4.6 Measuring Droplet Aspect Ratio Over Time:

In order to measure the droplet's aspect ratio over time, the images were binarized as shown in Fig 11B. This binarization process isolated the droplets from the background, enabling a precise analysis of their shape and size [87]. The images were converted to a monochrome display and interpreted using Matlab's imread function as a 2D matrix [85].

This method helped determine the droplet's aspect ratio over time by identifying x and y direction peaks at different inclination angles.[88]. The aspect ratio, identified as the height to width ratio of the droplet, was assessed by examining droplet from generation to release. bAspect ratio will vary based on how the droplet behaves at different angles, quantifying the effect of manually adjusting the angle on the sensory light's visual feedback.

4.7 Measuring Droplet Size for Each Inclination Angle

A pivotal aspect of the study was the quantification of droplet size as a function of the sensory light's orientation. To ensure consistency and accuracy in measurements, specific points within the image sequence were earmarked for analysis, particularly focusing on the moment of droplet release[65], [81]. This criterion was chosen as it provided a clear and unobstructed view of the droplet, facilitating precise diameter measurements.

Measuring the diameter of each droplet, involved calculating the conversion between pixels and millimeters. This was executed by measuring the width of the release tube in pixels and knowing its width in millimeters allowed for an accurate conversion to be carried out. In this case, 1mm was equated to 24 pixels[85]. This approach ensured precision in gauging the droplet diameters across different observation points throughout the 0-135 degree range.

Having outlined the methodology and steps undertaken for data collection and image processing, presented below are initial findings derived from the high-speed imaging experiment.

5 Results from First Prototype Iteration

5.1 Overview

The high-speed imaging findings emphasized on four principal parameters: droplet velocity analysis, droplet generation time assessment, aspect ratio examination & droplet size distribution study[82], [87], [89], [90]. These metrics were selected to bridge theoretical predictions with tangible performance criteria, while quantifying the interactivity of the sensory light itself.

5.2 Droplet Velocity Analysis

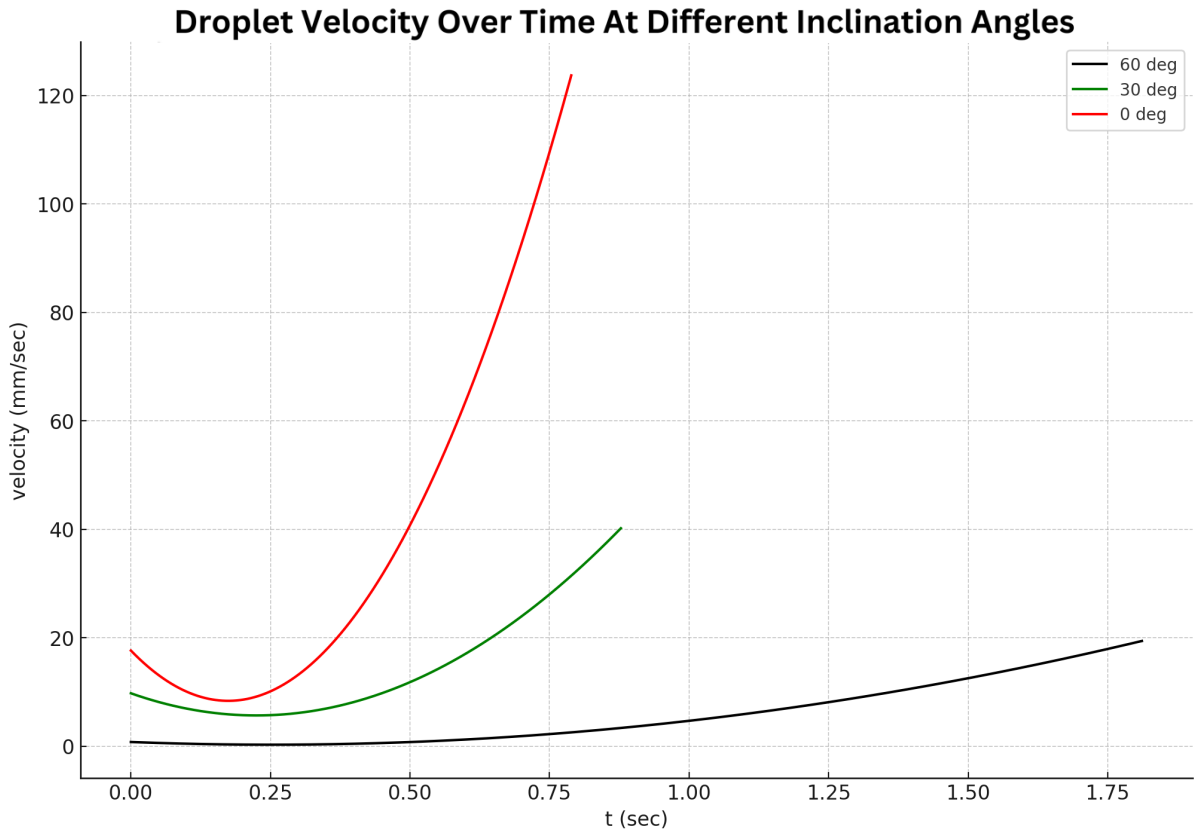

Figure 15 Velocity of droplets over time in top chamber at different inclination angles

Fig. 15 shows the velocity trajectory of the droplets varies significantly according to the angle of inclination a phenomenon also observed in droplet dynamics on inclined surfaces[91]. The initial decrease in velocity across all angles is primarily due to hydrodynamic focusing caused by the tube during the nascent phase of droplet formation [92] [93]. As droplets fully detach, their dynamics are significantly influenced by buoyancy and viscous drag from surrounding oil. This causes the velocity to approach an asymptotic value of terminal velocity for a particular inclination angle [94]. The inclination angle's influence, predominantly introducing tangential kinetic energy. This causes a temporal lag, evident from 0 to 60 degrees, suggesting at steeper angles, the droplet necessitates extended duration for complete detachment from the conduit, and commence its free ascent[95], [96].

At a flat 0 degrees, gravitational forces expedite velocity stabilization [95]. Conversely, at 30 degrees, there's a pronounced delay in stabilization [91], [97]. By 60 degrees, the detachment process is far more prolonged, leading to a further delay in reaching its terminal velocity.

5.3 Droplet Generation Time Assessment

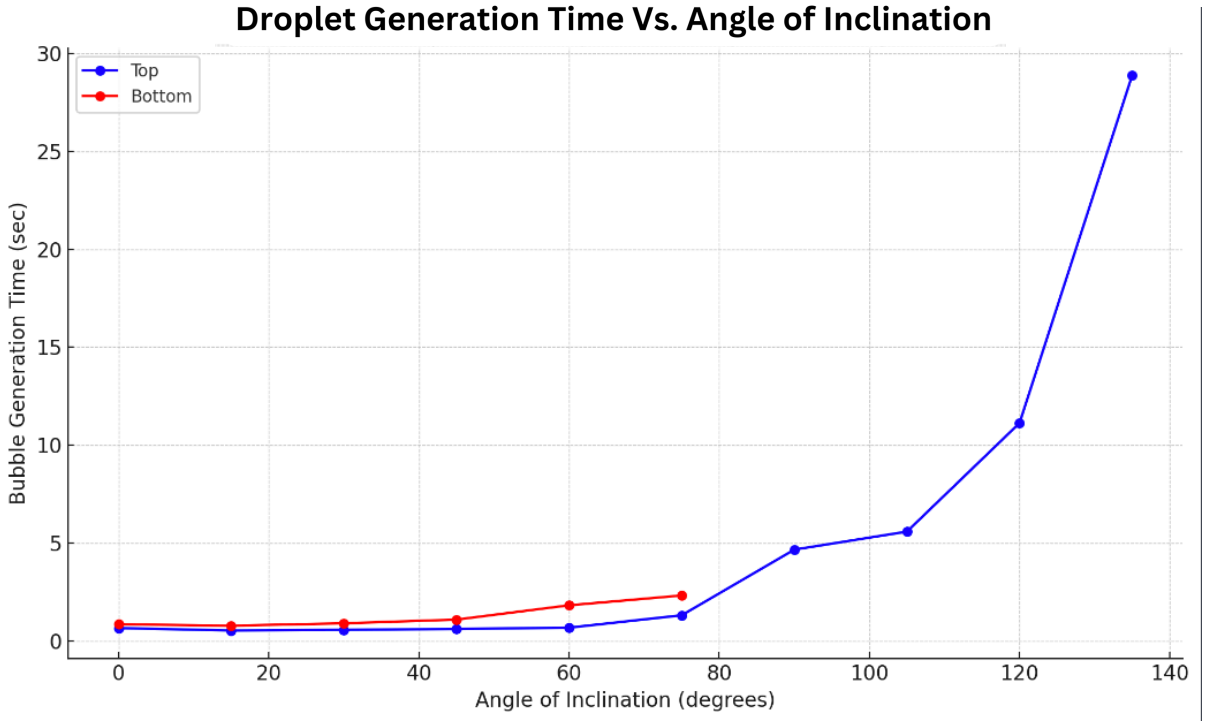

Figure 16 Droplet generation time for top and bottom chamber of sensory light at varying angles of inclination

Fig. 16 exhibits droplet generation time across superior and inferior chambers of the sensory light at varying angles of inclination. The superior chamber displays a marked increase in generation time, especially from 75-135 degrees, escalating from 4.6 to 28.8 seconds. Contrarily, droplet generation time remains fairly consistent within the inferior chamber, exhibiting minimal variance from 0.6 to 2.3 seconds. Within this section, a cessation in droplet formation is evident within the 90–135-degree, attributed to changes in surface tension and pressure variances[89][98]. At lower inclination angles, generation time remains congruent, but as the angle increases, a divergence is observable.

5.4 Aspect Ratio Examination

Examining aspect ratio over time at various angles of inclination allowed for observation of the transformative effects of angle inclination on droplet morphology. The aspect ratio, defined by width/height provided key insights into droplet's shapes dynamics in relation to the measured angle[98]. A value less than 1 indicates a droplet that is elongated vertically more the horizontally, and a high variation in aspect ratio indicates higher interactivity[99].

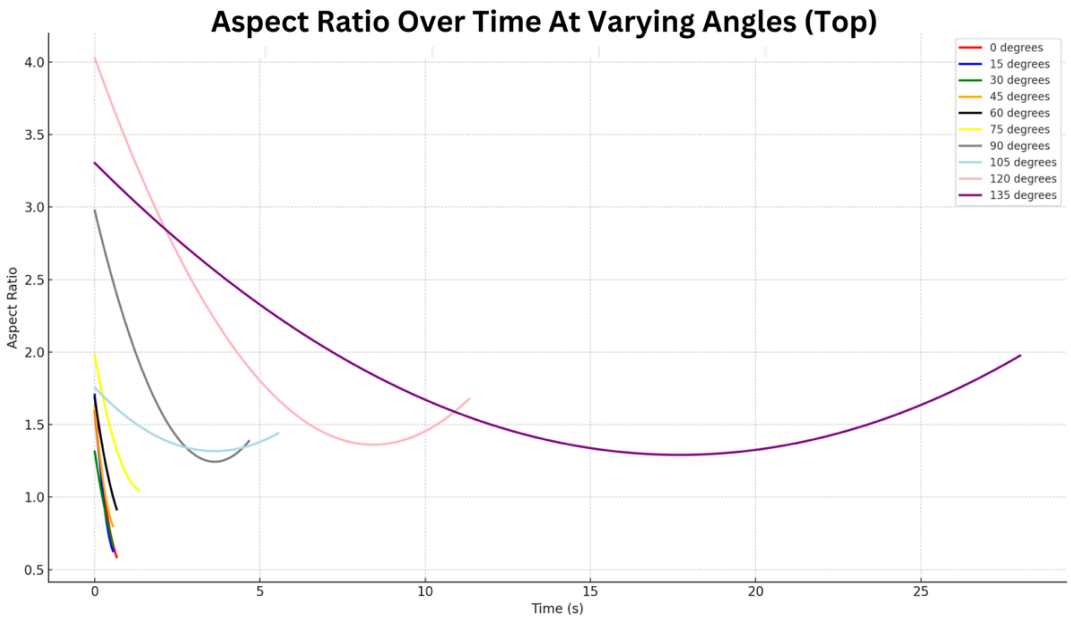

Figure 17. Aspect ratio at varying angles of inclination over time, top of the sensory light

Fig. 17 delineates the temporal evolution of aspect ratio across various inclination angle for the top of the sensory light, resulting in a distinct curve change. As the angle increases, a variation in the rate of change of aspect ratio over time is observed. At higher angle ranges the aspect ratio surges, implying a more pronounced horizontal stretch upon exiting the tubes.

The rate of decrease also varies with angle, with a steeper decrease observed for 90 and 105 degrees, corroborated by experimental findings showing droplets transition from spherical to ellipsoidal regimes[87][100]. Certain angles, including 75 and 135, show a slight increase in aspect ratio towards final cycles of generation, indicating the droplet is stretching horizontally at key points due to the inclination.

See Appendix C-E for Supplementary Graphs for Aspect Ratio Over Time

5.5 Droplet Size Distribution Study

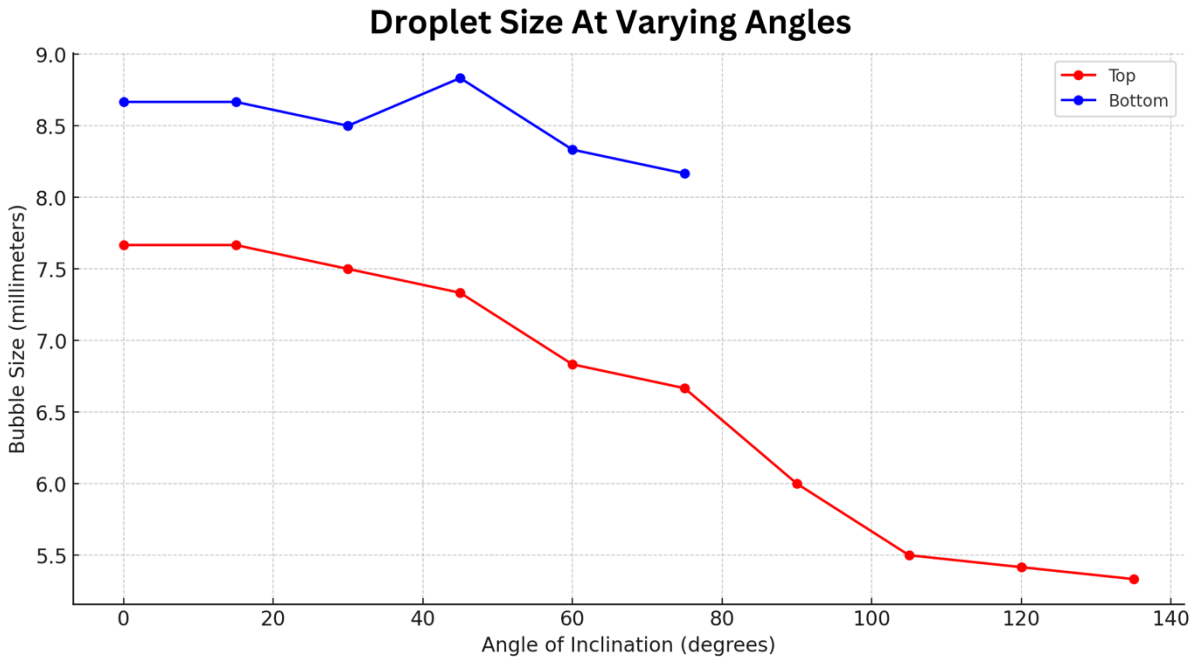

Figure 18 Droplet size distribution study at various angles of inclination

Fig. 18 illustrates droplet size distribution across measured angles of inclination. From 0 to 30 degrees, both top and bottom sections exhibit droplet formation of consistent sizes and minor fluctuations. As angle of inclination increases, the top section displays a decreasing trend in droplet size. The bottom tends to produce larger droplets across all angles, hinting at different dominant forces of droplet formation [101]. The 75-degree range emerges as a notable angle, where beyond this, the size of the droplets of top section drops more precipitously, suggesting the influence of counterbalancing effects of surface tension forces and inlet momentum direction changes[101], [102].

These results show a distinct relationship between droplet morphology and inclination angles. The detailed analysis presented below will contextualize findings and identify refinements for future prototype iterations.

6 Discussion from First Prototype Iteration

6.1 Droplet Velocity Analysis

The study focused on the inferior section of the sensory light for velocity analysis. The presence of air in the top section and resulting three-way flows could introduce discrepancies in the results.

6.1.1 Findings

Irrespective of the inclination angle, droplet velocity displays an initial reduction in velocity as the droplet commences its exit through the tube, stabilizing and reaching terminal velocity post detachment. This behavior aligns with Weber et al.'s insights on inclination's impact on velocity [103]. At steeper angles, surface tension and viscous forces at the tube counteract gravitational forces, causing droplets to remain attached for longer [102][103], [104]. This extended detachment, influenced by buoyant forces dependent on density difference between oil and water, leads to calmer visual dynamics and overall reduced interactivity within the 75–135-degree range.

6.1.2 Insights

Resistance faced by the droplet during exit indicates surface tensions caused by the tube and potential improvements. Curved, helical, or fluted tubes, might facilitate droplet detachment at higher angles of inclination [105][104]. Measuring droplet velocity in terms of incline angle has introduced a dynamics control parameter for the sensory light. Different angles can offer varied visual outputs, ranging from rapid droplet movements as observed at 0 degrees to slower, elongated attachments at steeper angles. This confirms the multisensory stimulation achieved by manipulating the sensory light. The surrounding fluid's viscosity plays a pivotal role in shaping these dynamics[101], [105].

6.1.3 Identified Prototype Adjustments

Introducing a dynamic base in prototype refinement will allow users to manipulate the inclination in real time and enhance user interactivity. Adjusting the oil-water composition, through addition of surfactants or glycerol, can manipulate droplet velocity and therefore enhance the sensory experience [82] [106].

6.2 Droplet Generation Time Assessment

6.2.1 Findings

The droplet generation time graph delineates the relationship between the sensory light's top and bottom chambers across 0-135 degrees. Beyond 90 degrees, the inferior section ceases droplet formation. The 0–75-degree range reveals a steeper rate of increase for the bottom section, indicating droplet formation challenges beyond this inclination[107]. The 75-degrees mark emerges as a critical angle, with impediments in droplet formation, possibly due to an increased dominance of one fluid phase over the other and chamber constraints[108].

6.2.2 Insights

Post 75-degree range reveals intricate force dynamics, attributed to increased viscous drag and altered surface dynamics [109][104]. Uniform changes in droplet generation times across inclination angles are crucial for the sensory fixture's performance. Prolonged generation times at higher angles diminish user engagement, so focus will be shifted to promote interactivity across the lower angle ranges (0-60). The top chamber presents inconsistencies with its three-way flows, causing unpredictable droplet behavior, an identified flaw in the prototype.

6.2.3 Identified Prototype Refinements

The refined prototype targets to reduce viscosity contrast, slows droplet generation while permitting interaction within the 0-60 degrees range, where the sensory light operation should be focused to preserve interactivity. Modifying surface tension characteristics can optimize sensory light duration and interactivity[82], [101]. Exploring microstructures in the chamber, serving as nucleation points, might foster more predictable droplet formation [110].

6.3 Aspect Ratio Examination

6.3.1 Findings

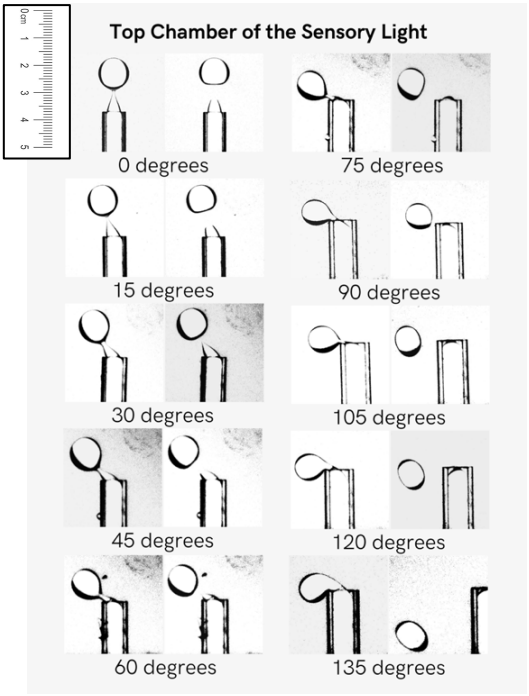

Figure 19 Examination of droplet elongation and release at various angles of inclination, top chamber of the sensory light

The top chamber's analysis reveals a pronounced angle dependency on the aspect ratio of droplets. Notably droplet elongation tends to distort horizontally after 15 degrees. Beyond the 45-degree mark, inconsistencies arise in aspect ratio evolution, suggesting the influence of surface tension from the detachment tube directly impacts droplet morphology, as shown by Fig 19[111]. This could be attributed to a shift in dominant forces governing the Rayleigh-Taylor Instability and variations in contact angles [46], [80] Frictional forces also play a role, restricting droplet flow at higher angles of inclination [112]. The rate of shape changes correlates directly to time, with droplet formation time rising as angle increases[112].

Regardless of inclination, all droplets tend to become more circular as they exit the tube, with an average aspect ratio after release to be around 0.985.

See Appendix F for droplet elongation and release at the bottom of the sensory light.

6.3.2 Insights

This study focused on the top chamber due to its capacity to inspect a broader range of angles. Despite the presence of three-way flows, it provided more consistent results in terms of aspect ratio. The three-way flows, involving air, oil, and water, introduce complexities, yet the top chamber's results remained more consistent, underscoring its reliability for this study.

6.3.3 Identified Prototype Refinements

Consistent droplet formation could be achieved by altering the fluid composition, such as introducing a viscous agent to the oil, or substituting the type of oil all together [113], [114][108]. Aiming for a sustained dynamic effect, refinements include achieving higher variations in aspect ratio across inclination angles and incorporating an easy-to-navigate user interface. The high-speed imaging experiment underscores the variability in visual output due to physical manipulation. Manipulating the air gap, responsible for the top section's three-way flow, can modulate droplet dynamics by either intensifying their chaotic nature (more air) or rendering them more predictable (less air) [115][116]. Understanding the means for either slowing down or speeding up droplet generation, whilst validating this shift in results will be key in refining next prototype iteration.

6.4 Droplet Size Distribution Study

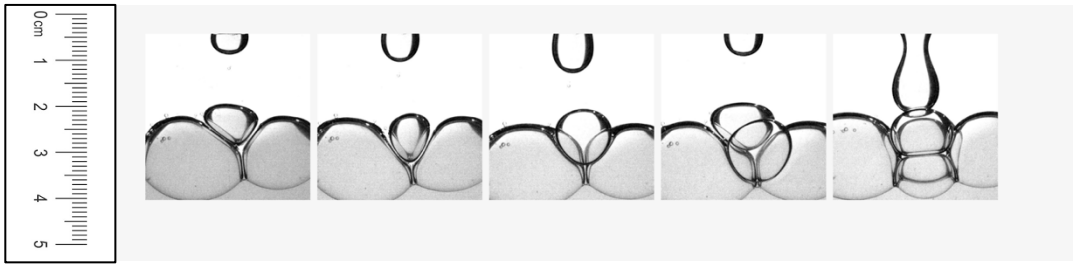

Figure 20 Evolution of droplet swerving occurring at the bottom section of the sensory light.

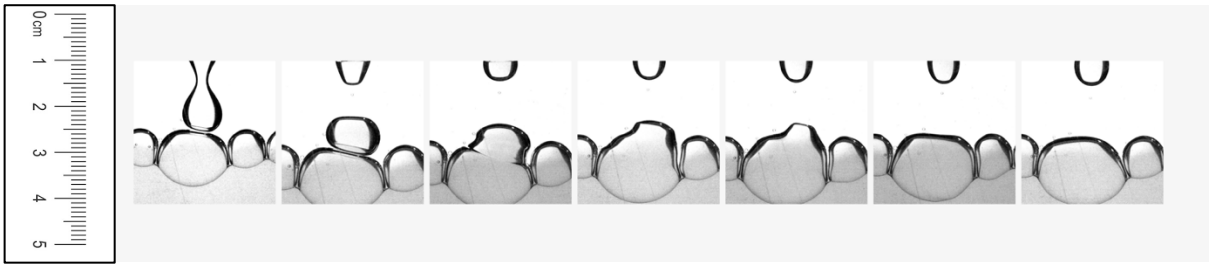

Figure 21 - Evolution of droplet coalescence occurring at the bottom section of the sensory light.

6.4.1 Findings & Insights

The droplet size was determined by analyzing diameter post-droplet release across the various inclinations. The droplet size varies by merely 2mm throughout the top and bottom chamber, indicating higher predictability within these arrangements[117]. As observed by Fig 20, droplets tend to swerve each other and eventually burst after navigating in the liquid pool. In contrast, when colliding at the appropriate angle, gravitational and surface tension conditions, droplets tend to coalesce as depicted in Fig 21 [118], [119]. Beyond 75-degree mark, there is a noticeable reduction in diameter, likely due to diminished gravitational influence and pressure variance, impacting fluid volume in droplets. [115]. The reduction in size underscores the sensory fixture's dynamic adaptability based on its orientation, confirming the multisensory connection as previously established.

6.4.2 Identified Prototype Refinements

Orientation influences droplet size. Lower angles generate consistent droplet sizes, coupled with faster generation times. As inclination increases, droplet diameter decreases as droplet formation slows, emphasizing the angle's role in influencing droplet morphology[116], [117]. Beyond 75 degrees, the top sections experience a reduced volume, varying 2.5mm throughout the entire sampling range. Droplet size is governed by factors like viscosity, surface tension and density variations. The addition of additives to modulate viscosity could potentially promote larger droplet formation at higher angles[114]. Adjusting fluid composition might enhance certain attributes at the expense of others, so combining these adjustments with user feedback is essential to achieve the desired sensory experience [82], [106].

6.5 Qualitative Error Analysis

Despite careful setup, potential errors may arise, introducing minor uncertainties to the presented data. The camera's frame rate and resolution might influence droplet velocity and aspect ratio data accuracy [81], [83]. Variations in lighting conditions can affect image quality and subsequent data extraction[83], [84]. The marker aiding angle measurements, if misaligned, can skew angle data, impacting interpretations of droplet dynamics. Additionally, converting pixel distance to millimeters may introduce scaling errors if setup distances vary.

High-speed imaging demonstrated that visual dynamics change with the angle of inclination, and adjusting fluid composition can alter droplet velocity. Determining the optimal velocity requires user feedback, leading to the next phase focused on user perspectives.

7 User Interviews & Feedback

The refinement of the existing sensory light prototype is rooted in a comprehensive understanding of the target audience's needs and preferences. A series of interviews, both in person and online, were conducted with various demographic group. These sessions prioritized hands on interaction with the sensory light, allowing participants to physically engage and establish a multisensory connection. Interviews also tackled user’s daily challenges with stress, anxiety, and mobile addiction, thereby enhancing comprehension and potential impact of “Breathe” sensory fixture better[3].

7.1 Feedback on the First Prototype and Suggestions for Improvement

The interviewees were presented with a demo of the first prototype of the Sensory Fixture. 55-year-old Swiss woman Monica enjoyed the droplet effect but emphasized sustainability and classic design. Mihai, a 21-year-old university student, valued the calming effect of the lamp and suggested improvements within the base to ensure easier transition between angles of inclination.

7.2 User Preferences for Droplet Velocity & Identified Trade-Offs

The high-speed imaging experiment demonstrated that the controllability and user interaction is quantified by measuring inclination angle versus parameters like droplet velocity and generation time[65], [67]. This proves the multisensory potential of the sensory light. However, there's a trade-off: more interactive and dynamic droplet movements might speed up the duration of the sensory light, potentially reducing its calming effect. Interestingly, 70% of the interviewees preferred the slower movement, while 30% favored a faster pace. This occurs because, slower droplets decrease the user's neurological pace, leading to a more pronounced sense of grounding and awareness[120]. The sensory light shows potential in droplet generation in both directions, necessitating further research on optimal dynamics and user exposure to varied experiences. Cognitive stimulation will be measured using heart rate, skin conductance, eye-tracking, and EEG (electroencephalogram) analysis[121].

7.3 Presentation of Insights

1. **Stress and Anxiety Management**: Allison (psychologist) and Victor (student) acknowledged the impacts of stress and anxiety on a regular basis using diverse techniques like time management, music, and outdoor walks for relief.

2. **Excessive Screen Time & Mental Health**: Many respondents emphasised how inconvenient phones and social media can be, with many like Daniel admitting phoning addiction. The link between extensive screen time and negative emotional impacts was also universally recognized. [6], [58].

3. **Aesthetics and Functionality of Lamps**: Many, like Rebeca, prioritized the aesthetic appeal of lamps, while also valuing features like adjustable brightness and ergonomic design.

7.4 Presentation of Insights from a Psychologist

An interview with Allison, a 48-year-old psychologist with 15 years of experience, provided a professional perspective on the application of Rayleigh-Taylor instability within a sensory

light. Allison's insights into stress management and the calming effects of aesthetic lamps were aligned with the project's objectives. Her endorsement of the potential of multisensory therapy, particularly the variation in patterns and effects achievable within the realm of fluid mechanics, added a layer of scientific validation to the project[55], [62].

7.5 Synthesis of Findings and Conclusion

The interviews collectively revealed the complexity of human interaction with sensory stimuli and the nuanced preferences that must be considered in the development of a sensory fixture product [62], [79].

Technical input from friends and family struck a compromise between the relaxing impact of slower motion and the requirement for rapid droplet engagement for interactivity at higher angles of inclination.

Presented below are the main findings from the interviews:

- **Ergonomics and Interactivity**: The majority favoured a slower, soothing droplet pace, highlighting the the need for enhanced interactivity and ergonomic design.
- **Fluid Dynamics and User Experience**: High-speed imaging experiments quantified the potential in manipulating fluid composition. Glycerol was considered to decelerate droplet velocity, as this slower motion was preferred by the majority[49].
- **Aesthetics and Functionality**: Aesthetics are crucial for a calming ambiance, but must harmonize with functional features, as feedback on the prototype emphasized.
- **Future Research Directions**: Determining optimal droplet velocity remains a research priority. Upcoming studies will measure cognitive and relaxing stimulation through heart rate, EEG readings, and other metrics[121].

Insights provided from the high-speed imaging experiments along with user feedback, provided a clear understanding for the next prototype iteration. These findings, coupled with the empirical data, paved the way for the deduction of quantifiable design criteria, used to assess the refined prototype in the second round high speed imaging experiment.

8 Final Design & Selected Performance Criteria

Figure 22 - CAD rendering & visualization of Breathe Sensory Light in living space

8.1 Key Insights from High-Speed Imaging Experiment

The high-speed imaging experiments provided empirical evidence on pivotal metrics, namely: droplet velocity, aspect ratio, generation time and size.

Droplet Velocity: Experimental findings indicated a counterproductive effect of faster droplet velocities on the intended calming visual sensation[92]. A challenge was observed wherein reduced droplet velocity led to diminished interactivity at increased inclination angles. Thus, the design imperative became evident: achieving an optimal balance between reduced droplet velocity and preserved interactivity in the critical angle range.

Droplet Aspect Ratio: Low variation in droplet aspect ratio across varying inclination angles were evident in the initial prototype. A higher variation in aspect ratio is essential for a dynamic & chaotic sensory experience, aiding its interactive multisensory potential[12], [62].

Droplet Generation Time: The temporal gap between successive droplet genesis was identified as a key metric. It was posited that a rhythmic and consistent droplet generation pattern would be imperative for a soothing sensory experience[50][122]. Design modifications in the refined prototype aimed to prolong this inter-droplet temporal gap at various angles of inclination.

Droplet Size: Congruent with velocity and aspect ratio, the diameter of the droplets emerged as a significant factor influencing the overall visual experience[90]. The refined prototype aimed to achieve a higher variation in droplet size.

8.2 Selected Quantitative Performance Criteria for Prototype Refinement

Given the empirical data and insights from the initial high-speed imaging experiments, the following quantitative success criteria were delineated for the refined prototype (see Fig 22):

1. **Reduced Droplet Velocity**: A targeted reduction in average droplet velocity by at least 15%[103], [123].
2. **Increased Droplet Generation Time**: An increase in the temporal gap between successive droplets by at least 30% [122].
3. **Higher Variation in Aspect Ratio**: Target a droplet aspect ratio range of 5.0-0.5[87].
4. **Maintained Interactivity**: Ensure interactivity is preserved up to 60 degrees for the bottom section and 120 degrees for the top.
5. **Droplet Size Variability**: A minimum droplet size variation of 2 millimeters across 0-120 degrees[88].
6. **Improved Base:** Prototype a dynamic vase that allows seamless transition between inclination angles.
7. **Smooth Droplet Detachment**: Seamless detachment of droplets, indicative of minimal turbulence.
8. **Droplet Velocity Variation**: A pronounced variation in droplet velocity throughout 0-120 degrees[49].
9. **Droplet Longevity**: Requirement for droplets to remain in the chamber for 5 seconds post-detachment.
10. **Enhanced Interactivity**: Increased interactivity via droplet coalescence and swerving.

These criteria directly correlate with the observed inconsistencies and user feedback gathered from the initial design. Emphasis on droplet velocity reduction and increased generation time was inferred directly from user feedback[13]. Similarly, the criterion regarding aspect ratio variability was influenced by the observed deviations from the high speed imaging experiment.

The outlined performance criteria will serve as benchmarks, against which the efficacy of this design in delivering the intended sensory experience will be evaluated in the second round high speed imaging experiment. This will inform subsequent prototyping and testing phase, ensuring that the tangible representation of theoretical concepts is in alignment with our research findings and user feedback.

9 Physical Prototyping & Testing

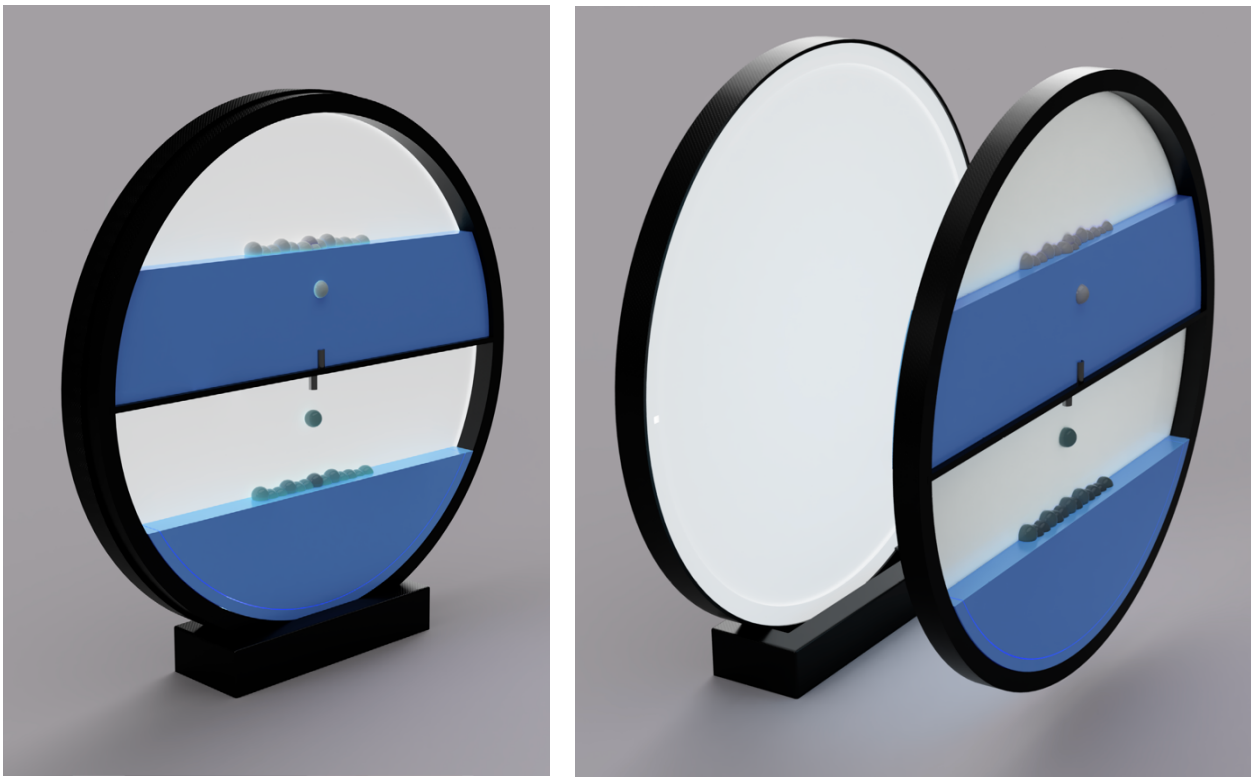

Figure 23 - CAD rendering for Refined Prototype of the "Breathe" sensory light, fully attached (left), separated from lighting component (right)

The prototyping process was a crucial phase in the development of the "Breathe" sensory light, providing a tangible representation of theoretical concepts explored within the high speed imaging experiment while allowing for real-world testing and refinement.

The final prototype rendering equipped with a dynamic base and backlit panel, is shown in Fig. 23 above.

9.1 Fluid Composition & Droplet Velocity

The primary objective was to slow down droplet generation to enhance the calming effect of the device. To achieve this, glycerol was added to the oil composition. The optimal glycerol to oil ratio for was found to be between 2-5% for optimal droplet generation and coalescence, according to Wang et al[49], [114] . Other fluids such as blue dye, distilled water, and industrial-grade mineral oil were also employed in the prototypes.

9.2 Initial Prototyping for Glycerol Composition Testing

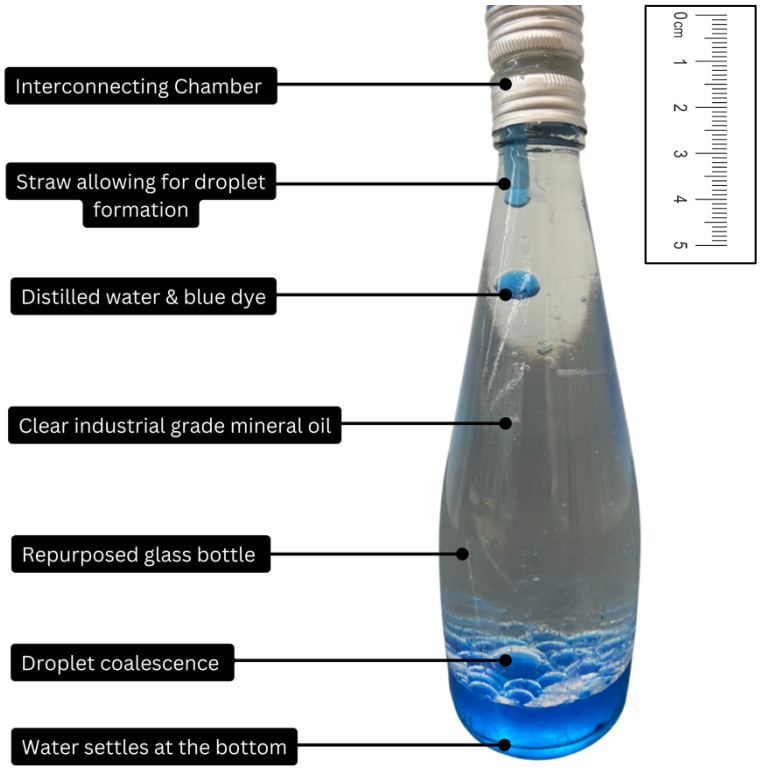

.

Figure 24 - Configuration of initial glycerol testing

Initial testing for fluid composition was constructed using two glass bottles. Their metal caps were hot-glued together, and two 5mm holes were drilled into each cap. Straws of 20mm length were then glued into these holes. One bottle was filled with mineral oil and the other with water. The bottles were quickly screwed together using the modified metal caps, creating a chamber that mimicked the Rayleigh-Taylor Instability observed in the sensory

light (see Fig 24). This initial prototype was crucial for testing various glycerol compositions. Four different glycerol concentrations (2%, 3%, 4%, and 5%) were tested [49], [114]. Qualitative observations were made on droplet coalescence for each configuration (see Fig 24). The 3% glycerol composition was found to be optimal, based on both visual assessments by peers and the effectiveness of the Rayleigh-Taylor Instability[49].

9.3 Refinement and Validation of the New Prototype

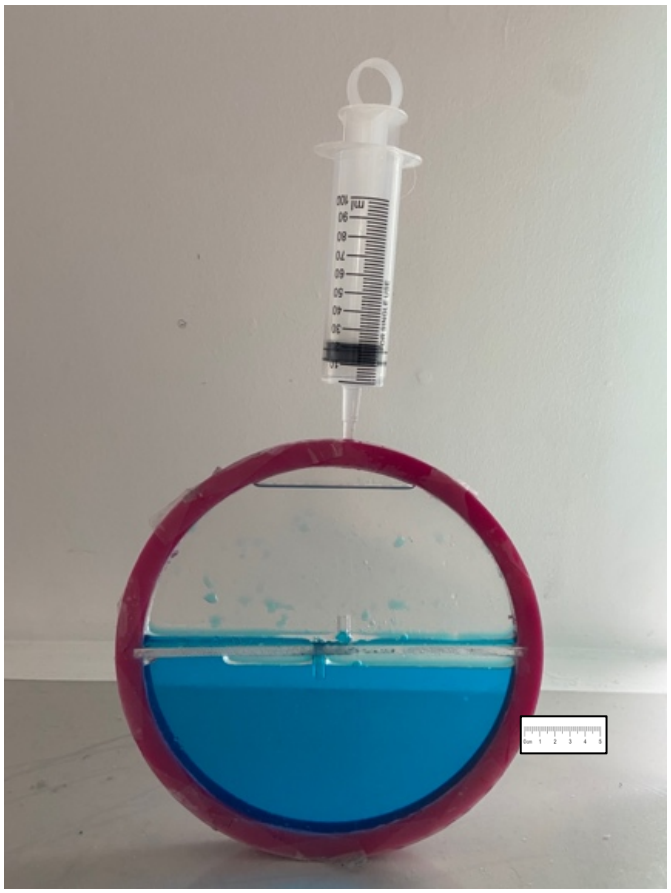

Figure 25 - filling up refined prototype (3% glycerol composition) with syringe

With the optimal glycerol composition identified, attention was turned to the new prototype. A hole was drilled into the chamber to empty the existing fluids. The chamber was then filled with a 100ml syringe, the 3% glycerol-oil composition on one side and distilled water and blue dye on the other. The hole was sealed with a 5mm acrylic dowel, ensuring an airtight fit (see Fig 25). To ensure accurate comparison with the previous prototype in second round high speed imaging, the air gap was measured and maintained the same.

Figure 26- 3mm laser cut borders for the sensory light, spraypainted black.

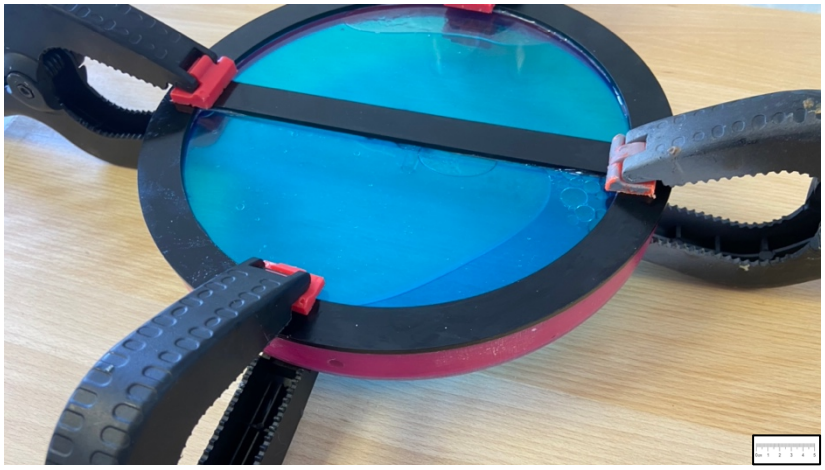

Figure 27 Gluing border using Epoxy adhesive and clamping for adhesion

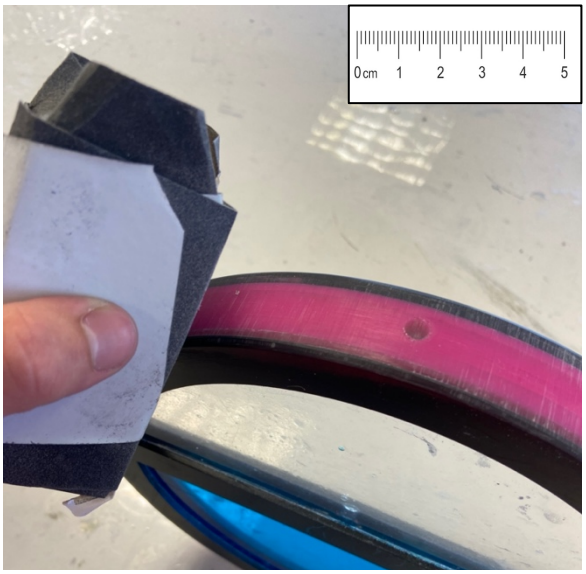

Figure 28 - Wet Sanding & polishing from 180-1000 grit sand-paper.

Additional refinements included the use of two-part epoxy glue to seal the chamber, laser-cut acrylic borders for aesthetic enhancement (see Fig 26-27), and meticulous sanding and polishing to achieve an ergonomic design (see Fig 28). The sensory light was then spray-painted black, providing a seamless finish.

The wooden base of the sensory light was also constructed and refined through a similar process of sanding, wet sanding, and polishing. Hard plastic corners were added to the bottom of the base for stability.

9.4 Displaying the Sensory Light

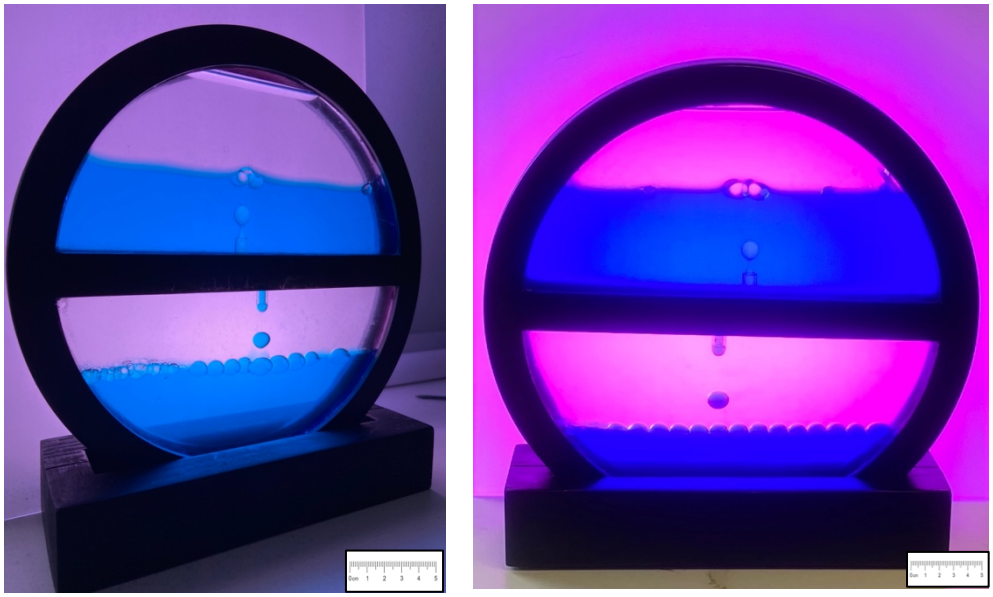

Figure 29 - Display of refined sensory light design (left), testing the effect under various color configuration (right)

The latest prototype has not yet integrated the backlit panel, planned to be a 250mm circular LED lighting component. For display purposes, a frosted acrylic sheet was placed behind a 50W light to complete the sensory light fixture (see Fig 29, left). Various colors configurations were tested for its compatibility with the sensory effect (see Fig 29, right).

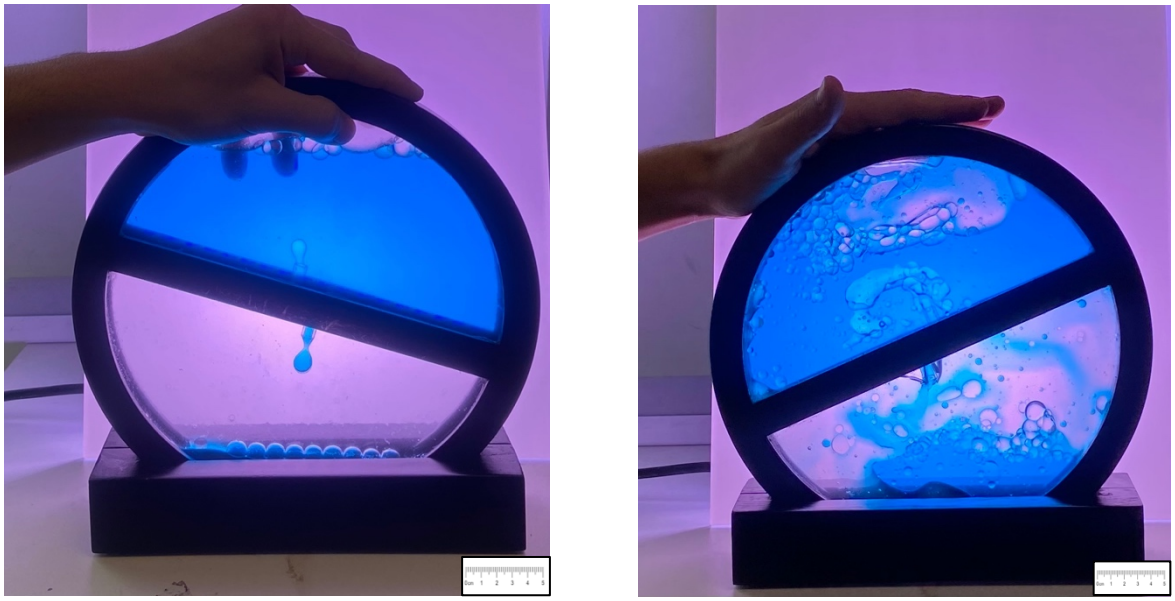

Figure 30 - User physically modifying angle of inclination (left), user generating turbulent liquid-liquid flows from fast rotation(right)

The integration with the refined base ensured users could easily switch between different inclination angles, tailoring the sensory experience to their preferences (see Fig 30, left). This was achieved by polishing and achieving a smooth finish on both the sensory light and the base, allowing smooth angle transition without the need for bearings or support bracket. Interestingly, rotating the sensory light rapidly generated turbulent liquid-liquid flows, a supplementary layer of interactivity to be explored in future prototyping stages (see Fig 30, right).

Initial observations showed generation cycle of the sensory light was extended from 7:40 minutes to approximately 10:00 minutes with the refined prototype, offering a more prolonged and immersive user experience [57]. Having established design criteria and refined the prototype, it is re-evaluated using high-speed imaging in subsequent sections to validate the refined prototype's performance.

10 Results from Refined Prototype

10.1 Overview

In the pursuit of refining the "Breathe" sensory light, high-speed imaging was employed to analyze the performance of the second prototype iteration. The primary aim was to contrast observed results with pre-established performance criteria (see Final Design), determining the prototype's effectiveness. The inclusion of glycerol, which influenced droplet morphology & generation times, was a significant design choice validated via this analysis[49], [114].

10.2 Presence of Three-Way Flows & Data Accuracy

In the assessment of droplet generation time, size, and velocity, only the bottom of the sensory light was analyzed due to the superior section's three-way flows caused by the air gap, compromising result accuracy[82], [92]. However, aspect ratio was examined for the top section, given its importance in assessing variability and availability of more sampling points.

10.3 Droplet Velocity Analysis

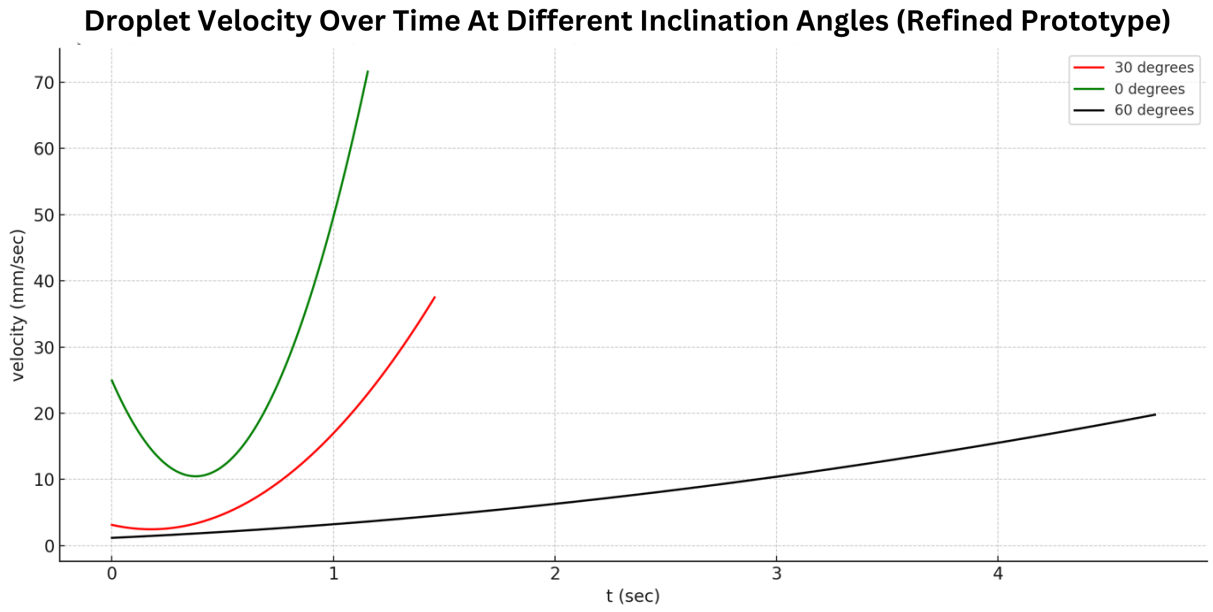

Figure 31 - Velocity of droplets over time in bottom chamber at different inclination angles, refined prototype

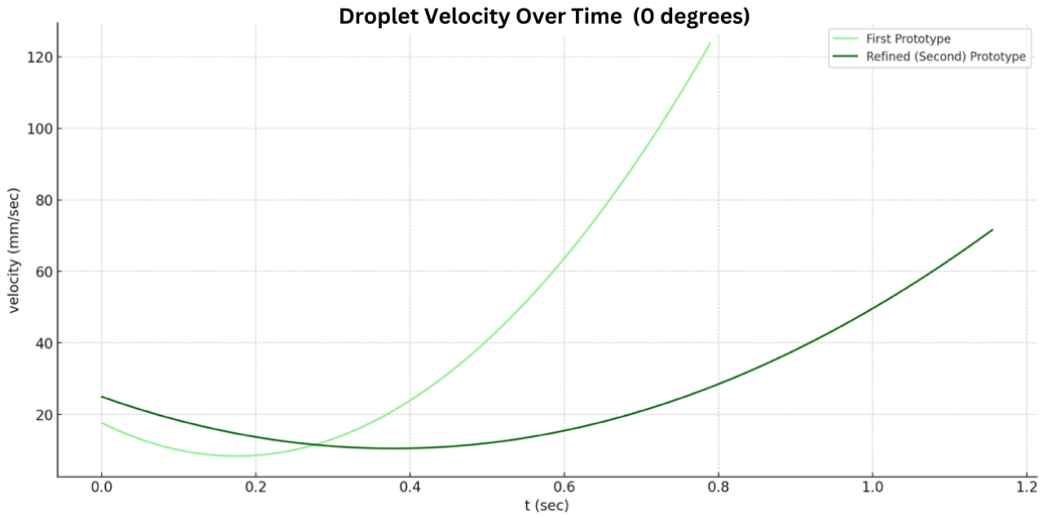

Figure 32 - Velocity of Droplets over time, 0 degrees, First vs Refined Prototype

The refined prototype's droplet trajectory was plotted for inclination angles of 0, 30, and 60 degrees, (see Fig 31). Direct comparisons between the first and refined prototype, revealed significant variations. At 0 degrees, the refined prototype had a reduced initial velocity difference of 77.03%, which slightly reduced to -14.77% by the end of the observation period (see Fig 32). Graphical representations for 30 and 60 degrees are displayed in Appendix G-H. At 0 and 60 degrees, the temporal lag and slower droplet generations resulted in an overall velocity difference of -19.75% and -14.77%, respectively. On aggregating the data, the refined prototype's velocity was marginally lesser by -15.41% on average.

10.4 Droplet Generation Time Assessment

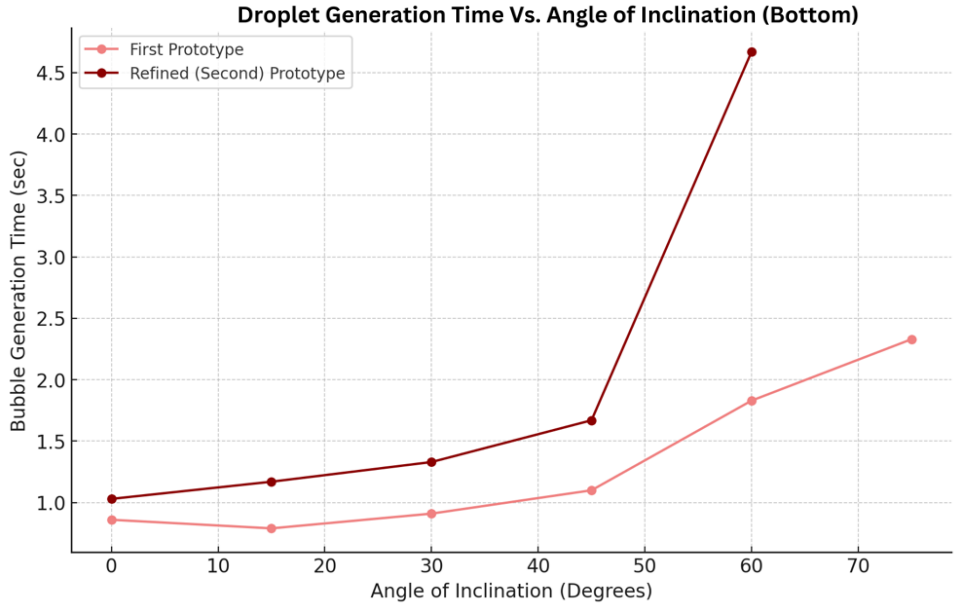

Figure 33 - Droplet generation time vs angle of inclination, bottom chamber, First vs Refined Prototype

The refined prototype, especially in the bottom section, consistently took longer to generate droplets across various angles (see Fig 33). For instance, at inclinations like like 0°, 15°, and 60°, the refined prototype showed increases of about 19.77%, 48.10%, and 155.19%, respectively. Similarly for the top section, the refined prototype exhibited a consistent increase in droplet generation time up to 60 degrees, with a pronounced spike beyond 75 degrees (see Appendix K). Quantitatively throughout all inclination angles, the refined prototype exhibited a 247.56% and 64.21% increase in droplet generation time, respectively.

10.5 Aspect Ratio Examination

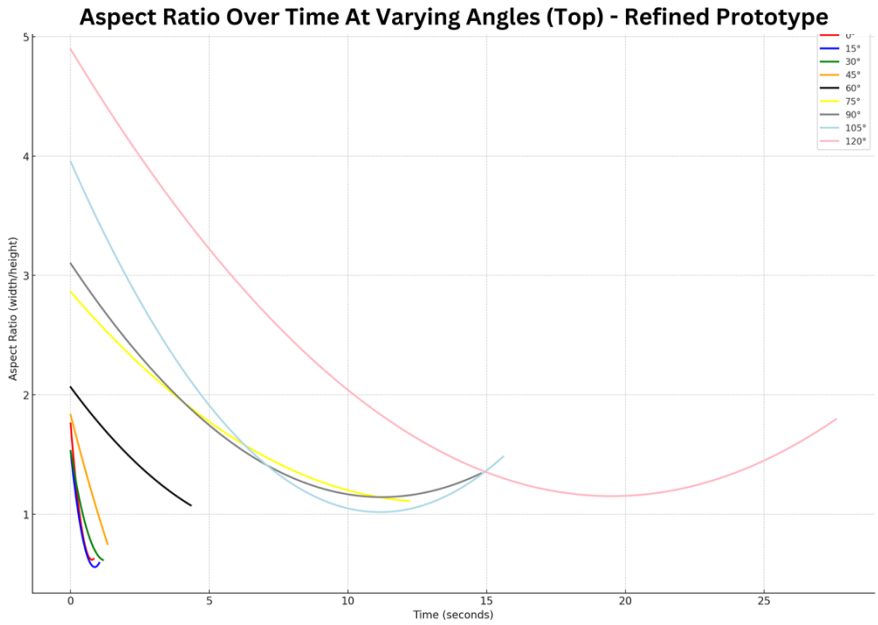

Figure 34 - Aspect ratio over time at varying angles of inclination, top chamber, Refined Prototype

In the top section, the refined prototype exhibited a pronounced decrease in aspect ratio over time, indicating droplets elongating vertically, enhancing the dynamic and chaotic sensory experience (see Fig. 34). Aspect ratio varied between 4.8-0.5 for the refined prototype, a substantial increase compared to the 4.0-0.6 observe in the first prototype. Analyzing the bottom section, the refined prototype displayed a steeper decline in aspect ratio between 0 and 60 degrees, emphasizing the influence of the refined design on droplet morphology (see Appendix I). Direct comparisons at specific angles, such as 30 and 45 degrees, emphasized the refined prototype's superior performance (See Appendix J-b and J-d). At 30 degrees, aspect ratios were about 24.66% higher, while at 45 degrees, the difference was around 35.94%

10.6 Droplet Size Distribution Study

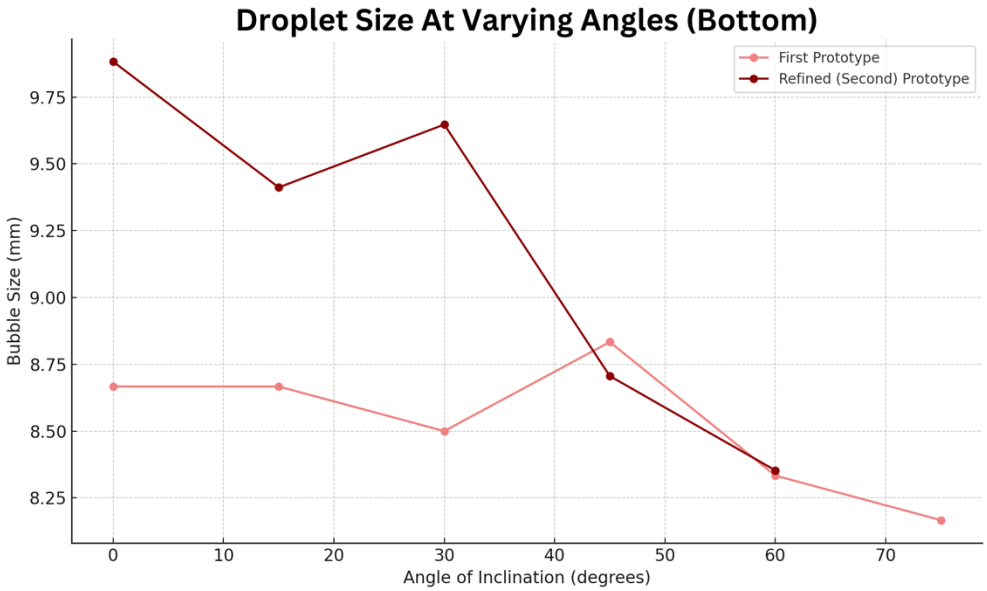

Figure 35 - Droplet size vs angle of inclination, bottom chamber, First vs Refined Prototype

The bottom section showcased a sharper decline in droplet size for the refined prototype between 0 and 60 degrees. At 0 degrees, the refined prototype's droplets were about 14.03% larger. Yet, from 75 degrees onwards, droplet generation ceased in the refined prototype, indicating challenges at higher angles (see Fig 35). On average, the refined prototype displayed an increase of 5.05% and 6.98% in droplet size in the top (see Appendix L) and bottom sections, respectively, compared to the first prototype.

Following detailed analysis of the refined prototype's results, the subsequent discussion aims to contextualize these findings against the set performance criteria.

11 Discussion of Performance of Refined Prototype Against Evaluated Performance Criteria

11.1 Evaluating Droplet Velocity Against Performance Criteria

The introduction of glycerol to the mineral oil in the refined prototype has influenced droplet dynamics. Its higher viscosity, combined with mineral oil, alters the viscosity contrast, leading to a marked decrease in droplet velocities[49], [114]. The heightened surface tension due to glycerol can impact droplet generation time, potentially leading to larger, slower-forming droplets[122]. This viscosity-surface tension interplay indicates a transition towards laminar flow regime in the refined prototype, resulting in smoother droplet detachment[96].

Reduced Droplet Velocity: The refined prototype achieved an average velocity reduction of 15.41%, aligning closely with the targeted 15% reduction. While velocity was measured at angles of 0, 30, and 60 degrees, it's imperative to extend this analysis to other angles, ensuring uniformity across the sensory light's spectrum.

Higher Variation in Droplet Velocity: The refined prototype's dynamic behavior highlights a pronounced variation in velocity across different inclination angles in comparison to the first prototype, suggesting that fluid alterations have introduced more variability in droplet movement[82], [92].

Droplet Longevity and Enhanced Interactivity: Reduced velocity up to 60 degrees suggests prolonged longevity. Qualitative observations indicate droplets tend to form at a measured pace, averaging a life span of 4 seconds, close to the set 5-second benchmark.

11.2 Evaluating Droplet Generation Time Against Performance Criteria

The incorporation of glycerol into the mineral oil has led to a more controlled ascent of droplets due to reduced buoyancy-driven forces[81], [103]. This is further accentuated by glycerol's propensity to increase surface tension, resulting in a more stable fluid interface and overall longer generation times [108], [124].

Increased Droplet Generation Time: The refined prototype showed an notable in droplet generation time across inclinations, averaging 247.56% for the top and 64.21% for the bottom, aligning it with the 30% target. This elongation generation time, especially beyond 60 degrees in the top section, may pose challenges in maintaining the desired interactivity. This arises as a critical tilt angle where gravitational forces can't overcome increased surface tension and viscosity, inhibiting droplet generation[40], [46]. Future prototypes might investigate various fluid additives or chamber shapes.[125].

Maintained Interactivity: The refined prototype balanced droplet velocity and user engagement, maintaining interaction within the key angle range of 0-45 degrees.

Improved Base: The dynamic base of the sensory light allows angle adjustments (see Fig 30, left), influencing droplet velocity and generation times, and paired with the turbulent effect (see Fig 30, right), it enhances user interaction [53].

11.3 Evaluating Droplet Aspect Ratio Against Performance Criteria

Aspect Ratio Variability and Fluid Dynamics Principles:

The targeted aspect ratio range of 5.0-0.5 was not only met but exhibited a rich variability across different angles of inclination, suggesting a more dynamic evolution in droplet morphology[87]. At inclinations of 0° and 15°, the refined prototype demonstrated steep declines in aspect ratios, indicative of significant vertical droplet elongation. The reduced viscosity contrast and capillary number, a dimensionless parameter that signifies the relative effect of viscous forces over surface tension, has a direct bearing on droplet dynamics, influencing their formation, detachment, and overall morphology[82], [101], [103].

Interactivity and Prototype Performance:

Enhanced interactivity, as evidenced by the observed droplet coalescence and swerving, underscores the refined prototype's performance[28]. Such behaviors are emblematic of fluid systems operating in reduced Reynolds numbers, emphasizing the dominance of viscous forces over inertial ones[96]. Despite diminished interactivity over 60 degrees, the prototype performs best in the 0-45 degrees, the most commonly interacted with range.

11.4 Evaluating Droplet Size Against Performance Criteria

Droplet Size Variability and Fluid Dynamics Implications:

The refined prototype's ability to produce larger droplets, especially from 0 to 60 degrees, is a direct consequence of the altered fluid composition. By modulating the viscosity contrast between the two immiscible fluids, the dynamics at the interface are modified, leading to the formation of larger droplets[90], [126]. Smaller droplets necessitate more energy to overcome the increased interfacial forces, explaining the observed larger droplet sizes in the refined prototype[100]. This observation aligns with the performance criterion targeting a minimum droplet size variation of 2 millimeters across 0-120 degrees.

Having assessed the improved protype performance, and validated the multisensory connection of the refined prototype, subsequent section will delve into the market opportunity for "Breathe" in the commercial landscape.

12 Commercialization of A Novel Sensory Light "Breathe"

12.1 Market Analysis

The ambient lighting industry is anticipated to reach £104.87 billion by 2026, while the worldwide LED market, worth £70.94 billion in 2022, will increase at an 11.0% CAGR through 2024. [127][128]. While "Breathe" is a niche within this sector, these figures underscore a robust market opportunity for its entrance.

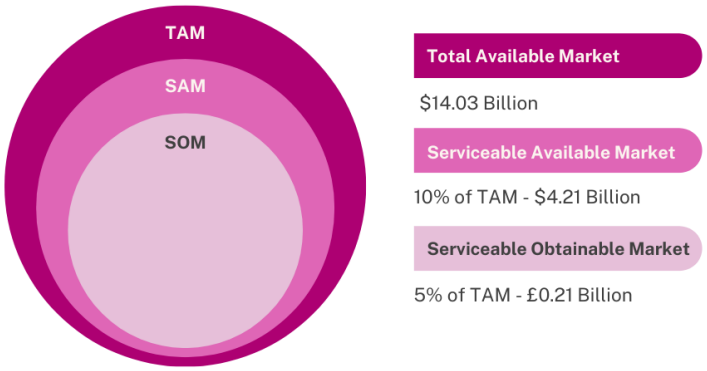

Figure 36 - Geoffrey Moore's bowling alley market strategy

Within this expansive market, "Breathe" focuses on students aged 18-25 as its beachhead segment, aligning with Geoffrey Moore's Bowling Alley Analogy (see Fig. 36)[129]. The UK had approximately 2.66 million students in 2020-21, with an added 562,060 the next year [130]. "Breathe" aims to tap into this demographic, using platforms like Instagram and TikTok for marketing.Using a top-down approach based on the $140 billion LED and ambient lighting sectors, 'Breathe' has a TAM of £14.03 billion. Targeting apt segments, the SAM is £4.21 billion, with an initial SOM of £0.21 billion.

12.2 Competition

Amidst this promising landscape, "Breathe" confronts competition. Notable competitors include Phillips Hue, a customizable smart lighting system; Aurora, a relaxation lamp with mobile-controlled light and sound; Hooga, amalgamating light, sound, and aroma [131]–[133]. Each brings distinct difficulties, such as Philips Hue's strong brand recognition. Yet, "Breathe" distinguishes itself through its spinning feature, circular design, and use of Rayleigh-Taylor Instability, which together create an unparalleled sensory immersion.

12.3 Lean Canvas

Figure 37 - lean canvas for "Breathe" Sensory Light

The Lean Canvas, devised by Ash Maurya, is adept at analyzing start up business ventures like "Breathe", minimizing assumption risks (see Fig 37).

12.3.1 Problem, Solution, and Unique Value Proposition

Rising screen time, averaging 11 hours for adults, is linked to heightened stress and anxiety [1], [7], [58]. "Breathe" leverages water's tranquility, offering a captivating sensory alternative to screens.

12.3.2 Revenue Streams and Cost Structure

"Breathe" adopts a B2C sales strategy, pricing its sensory lights from £44. Distribution includes online marketplaces, specialty stores, and its website. An future mobile app will further enrich user experience. Manufacturing costs vary between £23 and £59, with other costs covering salaries, marketing, and supplier dealings.

12.3.3 Customer Segments

"Breathe" primarily targets students and households. The desk-sized model, tailored for students, also functions as a study timer (see Fig 38). The medium-sized variant caters to adults, providing serene household ambiance (see Fig 39). B2B opportunities arise, with potential installations in restaurants and hotels, leveraging user-generated content and word of mouth promotions (see Fig 40).

Figure 38 – "Breathe" desk side version

Figure 39 – "Breathe" home version

Figure 40 – "Breathe" for public spaces

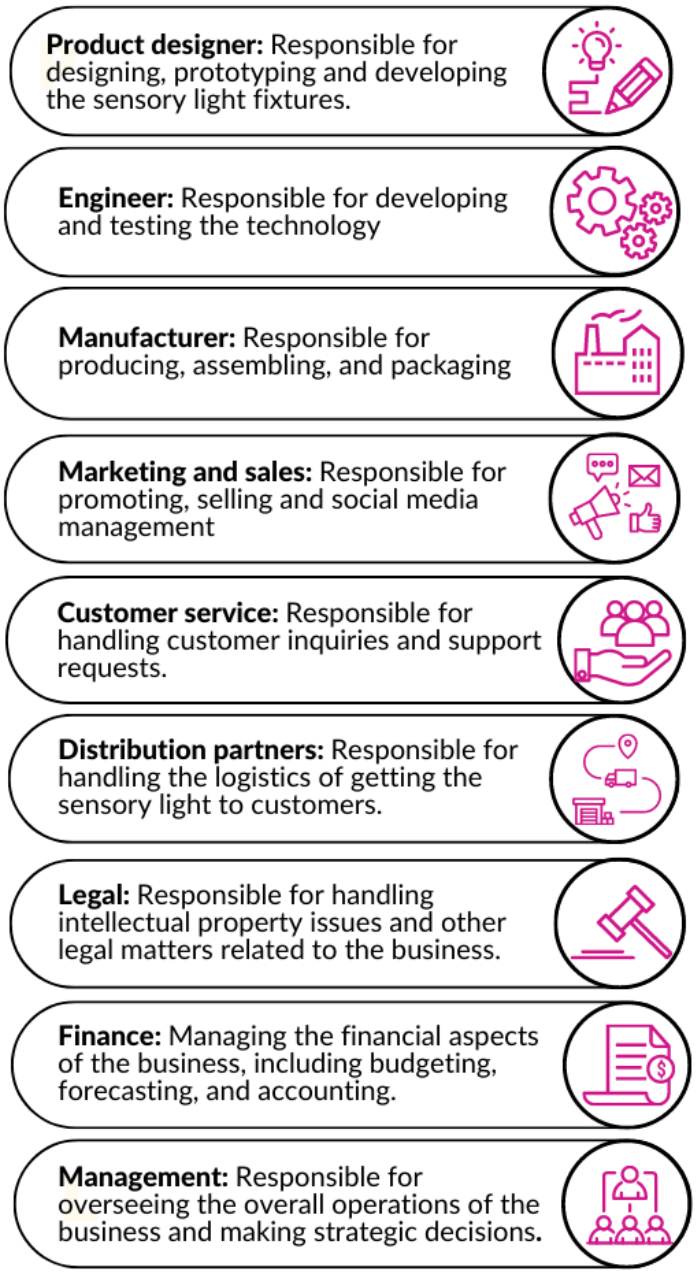

Figure 41 – list of key employees and partners

12.3.4 Key Resources and Partnerships:

Operational efficiency requires strategic partnerships (see Fig. 41). Collaborations with manufacturers, legal consultants, and marketing agencies ensure quality production at cost-effective rates. Potential investments will strengthen “Breathe’s” market entrance.

12.4 Manufacturability and Process Flow Diagram

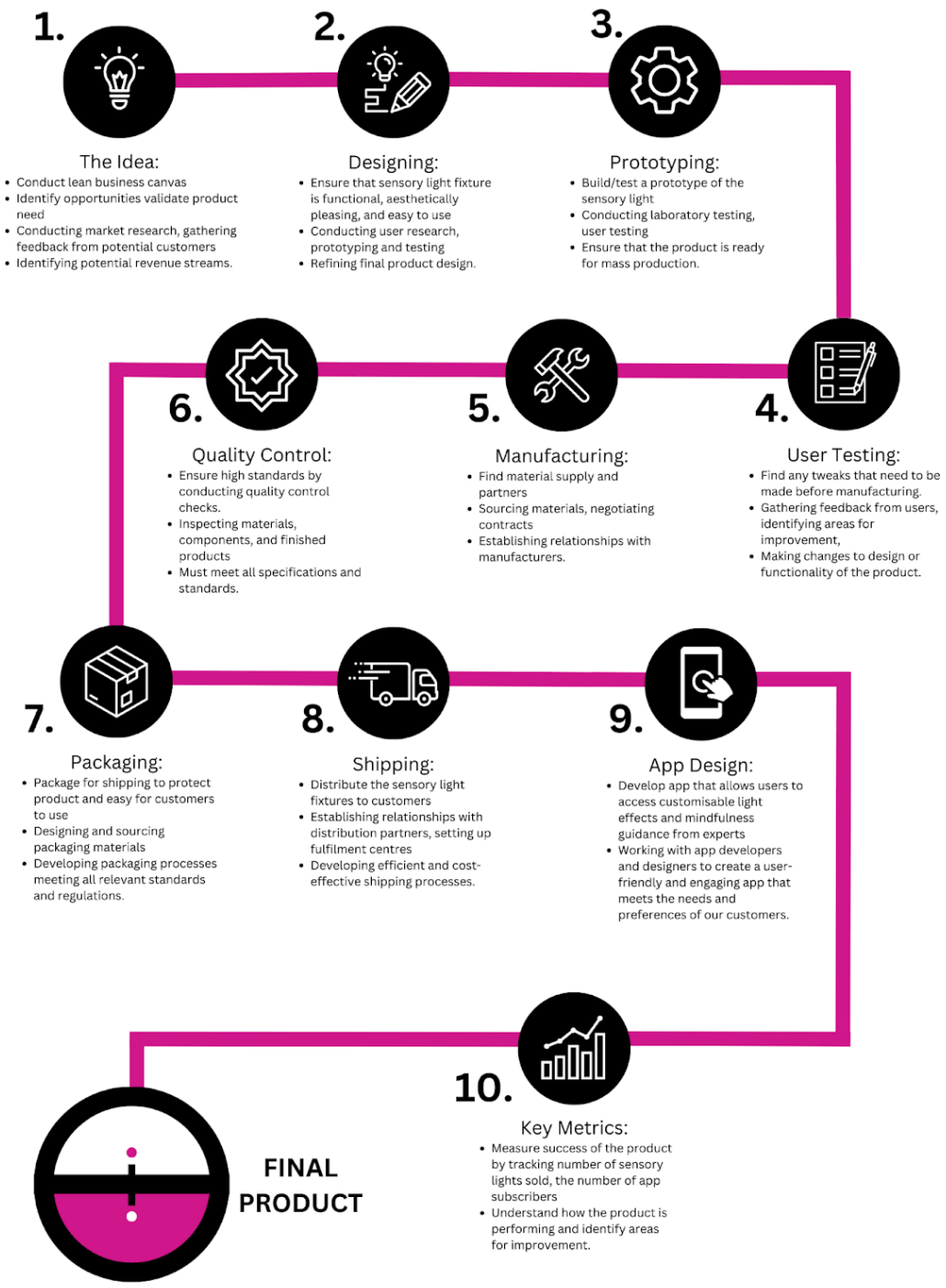

Figure 42 – Breathe process flow diagram

The production of "Breathe" involves a streamlined process flow diagram, ensuring efficient production and cost management. Fig 42 provides a visual representation of the production stages, enabling timely identification of bottlenecks and optimization opportunities. A detailed manufacturing breakdown, which will be periodically reviewed is depicted in Fig 43

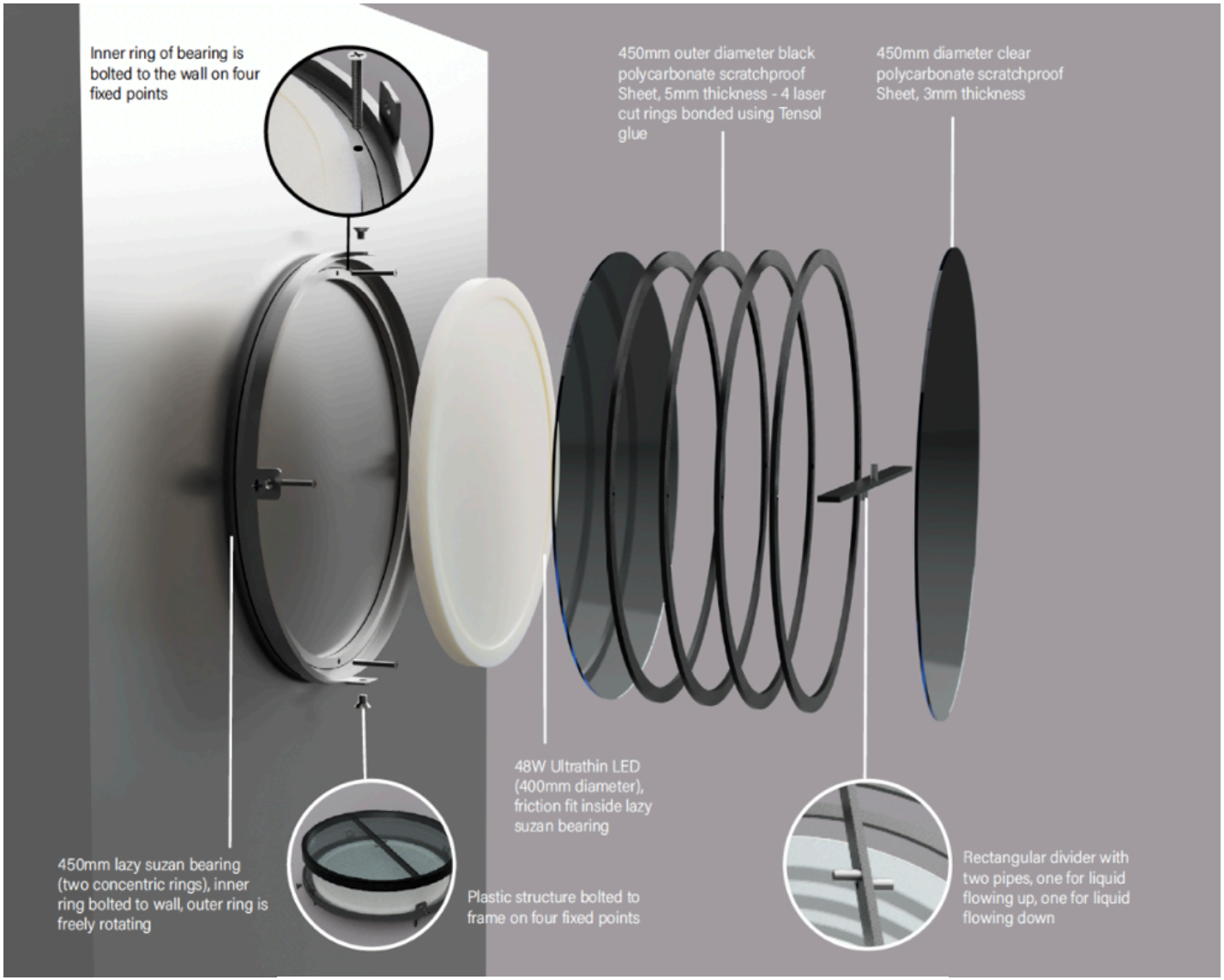

Figure 43 – Manufacturability breakdown for "Breathe" sensory light

12.5 Financial Projections

Potential profitability and long-term viability of "Breathe" was assessed through financial projections, providing a clear fiscal roadmap for the 2024-2026 period.

Table 2 - Component costs, selling price and net per unit margin for "Breathe" desk side and "Breathe" home living

Desk Side Version		Home Living Version	
Components	**Cost**	**Components**	**Cost**
Chamber	£ 9.00	Chamber	£ 5.00
Water & Dye	£ 5.00	Water & Dye	£ 0.50
Mineral Oil	£ 10.00	Mineral Oil	£ 1.00
20W Backlit Panel	£ 15.00	20W Backlit Panel	£ 7.00
Wooden Base	£ 7.00	Wooden Base	£ 3.00
Assembly	£ 5.00	Assembly	£ 2.50
Packaging	£ 3.00	Packaging	£ 1.00
Shipping	£ 5.00	Shipping	£ 3.00
Total Cost	£ 59.00	Total Cost	£ 23.00
Selling Price	£ 109.00	Selling Price	£ 44.00
Net Margin	£ 50.00	Net Margin	£ 21.00

The Desk Side costs £59 per unit with a net margin of £50, translating to a 47.7% margin. In contrast, Home Living version costs £23 per unit, yielding a net margin of £21, a 45% margin (see Table 2). Table 3 shows expected retail price and costs for "Breathe" with projected inflation rates accounted to be 1.8% in 2025 and 2.1% in 2026.

Table 3 Retail price and cost for desk side/home version sensory lights, inflation adjusted at 1.8% in 2025, and 2.1% in 2026

Desk Side			
Year	**2024**	**2025**	**2026**
Retail Price	£ 44.00	£ 44.79	£ 45.73
Cost	£ 23.00	£ 23.41	£ 23.91
Home Version			
Year	**2024**	**2025**	**2026**
Retail Price	£ 109.00	£ 110.96	£ 113.29
Cost	£ 59.00	£ 60.06	£ 61.32

Targeting 5% of the ambient lighting market, sales forecasts (Table 4) are conservative but achievable with strategies like influencer marketing through TikTok and Instagram, positioning e-commerce as the primary revenue source.

Table 4 Sales forecast for "Breathe" desk side and home living, 2024-2026

	Desk Side Version	Home Living Version
Year	**Units Sold**	
2024	7,095	2,682
2025	10,116	3,402
2026	14,425	4,314

Start-up costs for Breathe are around £36,000 (see Table 5), covering essential sectors while operating under a lean approach. Funding plans include crowdfunding like Y-Combinator, and private investments. Additional £ 100,000 is sought in 2024, once production has commenced to ensure smooth operations post-production launch.

Table 5 Start-up costs, initial investment required to commence operation

Product Development	£ 25,000.00
Legal & Accounting	£ 8,000.00
Website Development	£ 3,000.00
Total	£ 36,000.00

As operations expand, variable costs, especially marketing, are set to rise (Table 6). Outsourcing manufacturing inflates these costs initially. Economies of scale are set to be achieved by year 5 of operation. As Breathe transitions to in-house manufacturing and production volume increases, these expenses are aimed to be minimized over time.

Table 6 Variable costs for "Breathe" operation, 2024-2026

Year	2024	2025	2026
Variable Unit Costs	£ 321,423.00	£ 441,139.68	£ 609,436.23
Marketing Costs	£ 11,000.00	£ 15,000.00	£ 22,000.00
Total	£ 332,423.00	£ 456,139.68	£ 631,436.23

Fixed costs, driven by increased workforce and operational needs will rise from £74,230 in 2024 to £163,740 by 2026 (Table 7). Crowdfunding and investment rounds are planned to address potential cost surges, with a £2000 annual contingency fund for added security. Breathe aims to reduce fixed costs by employing a smaller, skilled workforce, allocating 10% of equity for employee premiums.

Table 7 Fixed costs for "Breathe" operation, 2024-2026

Storage & Fulfilment	£	15,000.00	£	18,000.00	£ 21,000.00
Utilities	£	960.00	£	1,040.00	£ 1,580.00
Salaries	£	54,350.00	£	85,680.00	£ 131,480.00
Business Insurance	£	1,400.00	£	2,800.00	£ 6,430.00
Digital Services	£	520.00	£	850.00	£ 1,250.00
General Expenses	£	2,000.00	£	2,000.00	£ 2,000.00
Total	**£**	**74,230.00**	**£**	**110,370.00**	**£ 163,740.00**

Given the following financial assumptions and sales forecasts, presented is a financial summary for revenues and profits obtained (Table 8/9). Profits are expected to be 30% higher for the desk side version despite the lower margins. In coming years, "Breathe" aims to reduce production costs and amplifying marketing efforts for optimal profits.

Table 8 Financial summary for Desk Side Version, 2024-2026

Desk Side Version					
Year	**2024**		**2025**	**2026**	
Units Sold	7095		10116	14425	
Avg. Selling Price	£	44.00	£ 44.79	£	45.73
Yearly Revenue	£	312,224.65	£ 453,150.30	£	659,643.22
Variable Unit Costs	£	163,185.00	£ 236,815.56	£	344,901.75
Yearly Profit	**£**	**149,016.31**	**£ 216,306.17**	**£**	**314,747.76**

Table 9 Financial summary for Home Living Version, 2024-2026

Home Living Version					
2024	**2025**		**2026**		
Units Sold	2682		3402	4314	
Avg. Selling Price	£	109.00	£ 110.96	£	113.29
Yearly Revenue	£	292,383.56	£ 377,480.88	£	488,789.81
Variable Unit Costs	£	158,238.00	£ 204,324.12	£	264,534.48
Yearly Profit	**£**	**134,120.90**	**£ 173,159.49**	**£**	**224,224.61**

By 2024, Breathe projects £ 197'955 in net profit (Table 10 & Fig. 44) which will be allocated to pay back investors for start-up costs and the purchase of new inventory to scale operations in coming years.

Table 10 Projected revenue, expenses and net profit for Breathe, 2024-2026

Year	2024	2025	2026
Total Revenue	£ 604,608.21	£ 830,631.18	£ 1,148,433.03
Total Expenses	£ 406,653.00	£ 566,509.68	£ 795,176.23
Net Profit	**£ 197,955.21**	**£ 264,121.50**	**£ 353,256.81**

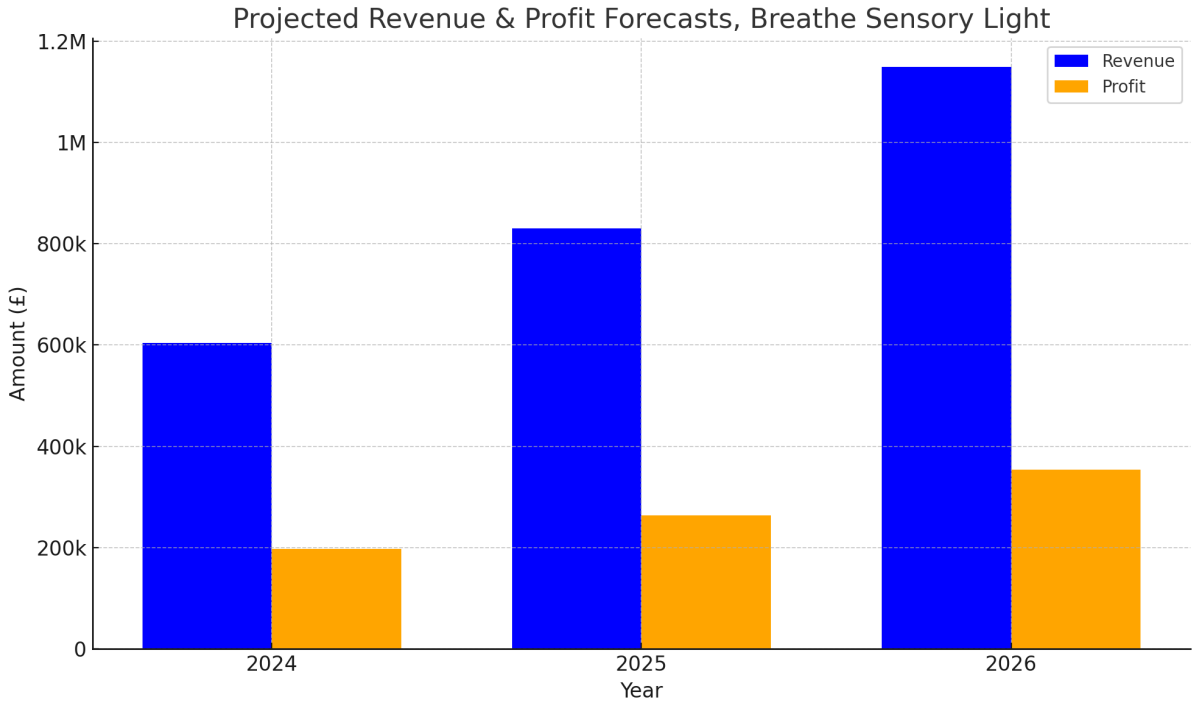

Figure 44 - Projected revenue & profit forecasts for Breathe, 2024-2026

Breakeven analysis is a financial tool that determines the point at which Breathe's revenue will cover its costs, indicating no net loss or gain. Essential for identifying and mitigating associated business risks, this analysis builds confidence in the venture (Table 11). Given the positive projections from similar products, it underscores Breathe's viable business model and its potential for sustained success in the ambient lighting market.

Table 11 Breakeven targets for Breathe, 2024-2026

	Desk Side "Breathe"	Home Living "Breathe"	
Year	Break Even Target (Units Sold)		**Predicted to be achieved? (Y/N)**
2023	4059	1705	Y
2024	5864	2463	Y
2025	8512	3574	Y

12.6 SWOT Analysis

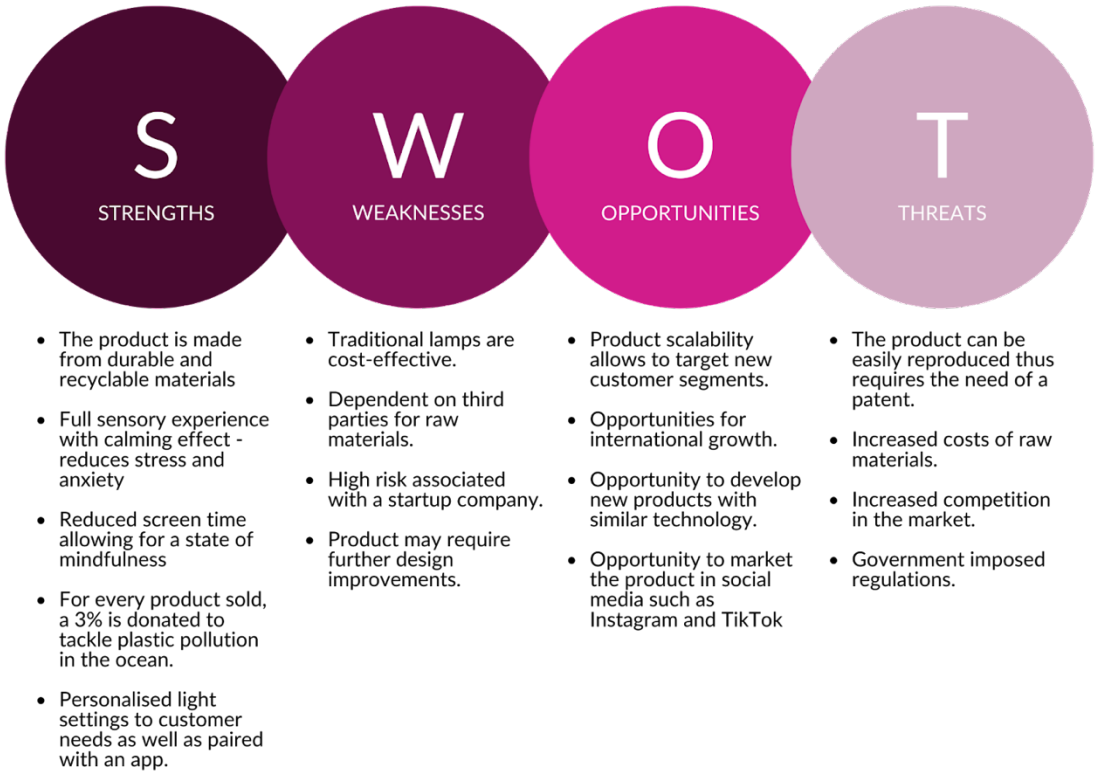

Figure 45 SWOT analysis for Breathe Sensory Light

SWOT analysis (Fig 45) evaluates "Breathe's" Strengths, Weaknesses, Opportunities, and Threats, guiding decision-making and growth strategies.

Having outlined potential strategies for commercialization, it's evident that "Breathe" not only holds a unique position in the market but also showcases undeniable profitability and viability.

13 Conclusion

The modern world has witnessed a significant increase in screen time, with individuals spending nearly 7 hours daily on screens, accounting for 40% of their waking hours[1], [58]. This trend, predominantly among adolescents correlates to a plethora of adverse effects, including sleep disturbances, dietary problems and mental health challenges[4], [7]. Addressing this pressing issue, the project aimed to refine and optimize a sensory light fixture using high speed imaging techniques, targeting mental health and phone addiction by crafting a fluid-based light fixture for multisensory user stimulation.

Fluid-based sensory lights' potential was first recognized through the bubble tube case study, primarily used therapeutically for children with learning disabilities like autism [62][10]. While promising, this visual interaction required more interactivity[10]. The goal was to overcome this by developing a sensory light that connects physical interaction to varied dynamic visual effects, utilizing Rayleigh-Taylor instabilities in oil-water flows[80] [12]. This multisensory approach forms a cognitive feedback loop, acting as a therapeutic anchor, grounding users in the present while fostering relaxation and mental well-being [11].

The initial prototype presented challenges within the fluid dynamics composition. User feedback highlighted the need to decrease droplet velocity for a more calming effect. A high-speed imaging experiment was devised to enhance the dynamics of the visual display by reducing droplet velocity while preserving interactivity at steeper inclinations. Droplet velocity, size, aspect ratio and generation time spanned a 0-135-degree range for both chambers of the sensory light.

Experimental results presented vital insights. The droplet velocity was too high, resulting in unfavorable generation times. Aspect ratios presented minimal variability across the 0–45-degree range, while droplet size diminished at steeper angles. This data was pivotal in setting ten quantifiable performance criteria for the subsequent, quantifying the multisensory connection in tangible fluid dynamics data.

Using these findings, the refined prototype aimed to reduce droplet velocity by 15% and increase droplet generation times by 30%, maintaining interactivity at 120 degrees for the top chamber and 60 degrees for the bottom. Introducing glycerol modified fluid properties, decreasing droplet velocity with a higher variability in aspect ratios.

Another round of high-speed imaging was conducted on the refined prototype. Droplet velocity reduced by 15.41%, and the aspect ratio showcased higher variation, especially in the 0–45-degree range. Droplet generation times increased by 247.56% and 64.21% for the top and bottom respectively, and droplet size varied by 3mm. A dynamic base was integrated, allowing users to swiftly change inclination angles and generate turbulent fluid motion with fast rotation movements, enhancing its multisensory appeal. While the prototype met most performance criteria, it faced challenges in maintaining interactivity beyond 60 degrees. The presence of three-way flows in the top chamber introduced inconsistencies, which future iterations aim to address by reducing this airgap.

The business strategy highlighted “Breathe’s” potential in the rapidly growing ambient projected to grow to **£104.87 billion** by 2026[128]. Targeting students 18-25, "Breathe" adopts a lean operational approach, emphasizing e-commerce and social media marketing. By 2024, projections show revenues of **£604,608.21**, with profits of **£197,955.21**. The scalability presented with an expanded product offering, coupled with the exploration of varying fluid dynamics effects, positions “Breathe” uniquely in the market.

In conclusion, experimental data, user testing and market research have facilitated the refinement of a novel sensory light that leverages fluid dynamics. The refined prototype, backed by rigorous scientific data, stands as a testament to the power of fluid dynamics in creating therapeutic tools. Further research and user testing is imperative to optimize droplet velocity and ensure consistent interactivity across desired angle ranges, ensuring that the sensory light fixture remains not just a product, but a beacon of hope for those grappling with the challenges of the digital age.

14 Limitations & Future Work

The endeavor of developing a sensory light fixture anchored in fluid mechanics has yielded significant results, yet also presents areas for further refinement and exploration. While the project's emphasis was on modulating droplet velocity, other vital fluid dynamics parameters must be explored to amplify the sensory experience.

Future work could delve deeper into fluid composition, particularly the introduction of surfactants to the oil, aiming to increase velocity and interactivity at steeper angles [82], [106]. This would pave the way for creating sensory light variants with diverse droplet dynamics, each tailored to specific user needs. Coupled with user testing, employing advanced neurostimulation measurement tools like EEG and heart rate monitors, one could discern the sensory light version offering the most profound neurostimulatory potential, while maintaining interactivity within the critical 0-45 degree angle range[134].

Beyond fluid properties, the design itself has areas for further refinement. Investigating various chamber geometries and tube configurations could boost interactivity while introducing new fluid dynamics effects beyond Rayleigh-Taylor Instabilities [135], [136]. The scalability of the sensory light offers another exciting avenue. Envisioning variants—from desk-side versions for students to grand installations for public spaces—highlights the adaptability of the product across diverse contexts. Moreover, future designs should consider integrating the light source directly into the sensory fixture, moving away from backlit panels.

In summation, while the current project has laid a robust foundation, the realms of exploration are boundless. “Breathe” with its profound potential, stands poised at the cusp of myriad scientific and design innovations, promising a brighter, more interactive future.

References

[1] "Alarming Average Screen Time Statistics (2023)." https://explodingtopics.com/blog/screen-time-stats (accessed Apr. 18, 2023).

[2] "79 Cell Phone/Smartphone Addiction Statistics." https://www.crossrivertherapy.com/research/cell-phone-addiction-statistics (accessed Jul. 16, 2023).

[3] M. Trott, R. Driscoll, E. Irlado, and S. Pardhan, "Changes and correlates of screen time in adults and children during the COVID-19 pandemic: A systematic review and meta-analysis," *EClinicalMedicine*, vol. 48, Jun. 2022, doi: 10.1016/J.ECLINM.2022.101452/ATTACHMENT/69FDCA19-C825-4966-8C9A-1F09AD83071B/MMC1.DOCX.

[4] G. Lissak, "Adverse physiological and psychological effects of screen time on children and adolescents: Literature review and case study," *Environ Res*, vol. 164, pp. 149–157, Jul. 2018, doi: 10.1016/J.ENVRES.2018.01.015.

[5] J. M. Twenge, T. E. Joiner, M. L. Rogers, and G. N. Martin, "Increases in Depressive Symptoms, Suicide-Related Outcomes, and Suicide Rates Among U.S. Adolescents After 2010 and Links to Increased New Media Screen Time," *https://doi.org/10.1177/2167702617723376*, vol. 6, no. 1, pp. 3–17, Nov. 2017, doi: 10.1177/2167702617723376.

[6] G. Lissak, "Adverse physiological and psychological effects of screen time on children and adolescents: Literature review and case study," *Environ Res*, vol. 164, pp. 149–157, Jul. 2018, doi: 10.1016/J.ENVRES.2018.01.015.

[7] "Screen Time and the Brain | Harvard Medical School." https://hms.harvard.edu/news/screen-time-brain (accessed Apr. 18, 2023).

[8] "Sensory Rooms: Aviation's Latest Trend - Blue Sky PIT News Site." https://blueskypit.com/2019/05/13/sensory-rooms-aviations-latest-trend/ (accessed Aug. 27, 2023).

[9] "Positive impact of the snoezelen concept on children and pupils with health disabilities," *Social Pathology and Prevention*, vol. VII, no. 1, pp. 11–33, 2021.

[10] L. A. Pusuluri, T. Dhiraj, Y. S. Kothuri, A. Malisetty, and S. Kalaivani, "Smart snoezelen bubble tube for mentally challenged and learning disability," *Proceedings of the International Conference on Intelligent Sustainable Systems, ICISS 2017*, pp. 524–526, Jun. 2018, doi: 10.1109/ISS1.2017.8389466.

[11] J. Ball and B. K. Haight, "Creating a multisensory environment for dementia: the goals of a Snoezelen room.," *J Gerontol Nurs*, vol. 31, no. 10, pp. 4–10, 2005, doi: 10.3928/0098-9134-20051001-04.

[12] E. Lavie, M. Shapiro, and M. Julius, "Hydrotherapy combined with Snoezelen multi-sensory therapy," *Int J Adolesc Med Health*, vol. 17, no. 1, pp. 83–87, Jan. 2005, doi: 10.1515/IJAMH.2005.17.1.83/MACHINEREADABLECITATION/RIS.

[13] H. Kaplan, M. Clopton, M. Kaplan, L. Messbauer, and K. McPherson, "Snoezelen multi-sensory environments: Task engagement and generalization," *Res Dev Disabil*, vol. 27, no. 4, pp. 443–455, Jul. 2006, doi: 10.1016/J.RIDD.2005.05.007.

[14] K. Conrad, R. Cleland, and N. Reyes, "The Blue Mind," pp. 59–65, 2021, doi: 10.1007/978-3-030-55012-7_5.

[15] Wallace J Nichols, *Blue Mind: The Surprising Science That Shows How Being Near, In, On, Or Under Water Can Make You Happier, Healthier, More Connected, And Better At What You Do* , 2nd ed., vol. 1. New York: Little Brown & Company, 2014.

[16] I. Esau, "Fluid Mechanics Applications," *Fluid Mechanics: Open Access*, vol. 9, no. 1, pp. 1–1, Jan. 2022, doi: 10.37421/2476-2296.2022.9.213.

[17] N. Brauner, “Liquid-Liquid Two-Phase Flow Systems,” pp. 221–279, 2003, doi: 10.1007/978-3-7091-2538-0_5.
[18] F. Garoosi and T. F. Mahdi, “New benchmark problems for validation and verification of incompressible multi-fluid flows based on the improved Volume-Of-Fluid (VOF) method,” *Colloids Surf A Physicochem Eng Asp*, vol. 648, p. 129313, Sep. 2022, doi: 10.1016/J.COLSURFA.2022.129313.
[19] Y. Ueda, N. Kochi, T. Uemura, T. Ishii, and M. Iguchi, “Numerical Observation of Flow Field around the Water Column behind a Rising Bubble through an Oil/Water Interface,” *ISIJ International*, vol. 51, no. 11, pp. 1940–1942, 2011, doi: 10.2355/ISIJINTERNATIONAL.51.1940.
[20] R. Ghazali, S. Rasidah Md Sakip, I. Samsuddin, U. Teknologi MARA, and B. Baru Seri Iskandar, “A Review of Sensory Design Physical Learning Environment for Autism Centre in Malaysia,” *Quality of Life in the Built & Natural Environment*, vol. 6, pp. 2398–4287, 2018, doi: 10.21834/e-bpj.v3i7.1262.
[21] R. Elizabeth, “Sensory Stimulation Techniques,” *Am J Nurs*, vol. 66, no. 2, p. 281, Feb. 1966, doi: 10.2307/3419874.
[22] M. Ashby, W. R. Lindsay, D. Pitcaithly, S. Broxholme, and N. Geelen, “Snoezelen: its Effects on Concentration and Responsiveness in People with Profound Multiple Handicaps”.
[23] S. W. chi Chan, D. R. Thompson, J. P. C. Chau, W. W. S. Tam, I. W. S. Chiu, and S. H. S. Lo, “The effects of multisensory therapy on behaviour of adult clients with developmental disabilities—A systematic review,” *Int J Nurs Stud*, vol. 47, no. 1, pp. 108–122, Jan. 2010, doi: 10.1016/J.IJNURSTU.2009.08.004.
[24] T. Al-Wahaibi, M. Smith, and P. Angeli, “Transition between stratified and non-stratified horizontal oil–water flows. Part II: Mechanism of drop formation,” *Chem Eng Sci*, vol. 62, no. 11, pp. 2929–2940, Jun. 2007, doi: 10.1016/J.CES.2007.01.036.
[25] J. Lovick and P. Angeli, “Experimental studies on the dual continuous flow pattern in oil–water flows,” *International Journal of Multiphase Flow*, vol. 30, no. 2, pp. 139–157, Feb. 2004, doi: 10.1016/J.IJMULTIPHASEFLOW.2003.11.011.
[26] S. Mashaghi, A. Abbaspourrad, D. A. Weitz, and A. M. van Oijen, “Droplet microfluidics: A tool for biology, chemistry and nanotechnology,” *TrAC Trends in Analytical Chemistry*, vol. 82, pp. 118–125, Sep. 2016, doi: 10.1016/J.TRAC.2016.05.019.
[27] P. Angeli and G. F. Hewitt, “Drop size distributions in horizontal oil-water dispersed flows,” *Chem Eng Sci*, vol. 55, no. 16, pp. 3133–3143, Aug. 2000, doi: 10.1016/S0009-2509(99)00585-0.
[28] B. Hafskjold, T. B. Morrow, H. K. B. Celius, and D. R. Johnson, “Drop-Drop Coalescence In Oil/Water Separation,” *SPE Annual Technical Conference and Exhibition*, Sep. 1994, doi: 10.2118/28536-MS.
[29] “Droplet coalescence leads to fluctuations in the pressure field (color)... | Download Scientific Diagram.” https://www.researchgate.net/figure/Droplet-coalescence-leads-to-fluctuations-in-the-pressure-field-color-due-to-the-rapid_fig2_347398304 (accessed Aug. 31, 2023).
[30] T. Wang, S. I. Andersen, and A. Shapiro, “Coalescence of oil droplets in microchannels under brine flow,” *Colloids Surf A Physicochem Eng Asp*, vol. 598, p. 124864, Aug. 2020, doi: 10.1016/J.COLSURFA.2020.124864.
[31] J. D. Paulsen, J. C. Burton, and S. R. Nagel, “Viscous to inertial crossover in liquid drop coalescence,” *Phys Rev Lett*, vol. 106, no. 11, p. 114501, Mar. 2011, doi: 10.1103/PHYSREVLETT.106.114501/FIGURES/4/MEDIUM.

[32] C. C. Chang and R. J. Yang, “Hydrodynamic focusing effect on two-unmixed-fluid in microchannels,” *International Journal of Nonlinear Sciences and Numerical Simulation*, vol. 9, no. 3, pp. 213–220, Sep. 2008, doi: 10.1515/IJNSNS.2008.9.3.213/MACHINEREADABLECITATION/RIS.
[33] J. Yuan, X. Ye, and Y. Shan, “Modeling of the bubble dynamics and heat flux variations during lateral coalescence of bubbles in nucleate pool boiling,” *International Journal of Multiphase Flow*, vol. 142, p. 103701, Sep. 2021, doi: 10.1016/J.IJMULTIPHASEFLOW.2021.103701.
[34] D. Funfschilling, H. Debas, H. Z. Li, and T. G. Mason, “Flow-field dynamics during droplet formation by dripping in hydrodynamic-focusing microfluidics,” *Phys Rev E Stat Nonlin Soft Matter Phys*, vol. 80, no. 1, p. 015301, Aug. 2009, doi: 10.1103/PHYSREVE.80.015301/FIGURES/4/MEDIUM.
[35] H. Foroughi and M. Kawaji, “Viscous oil–water flows in a microchannel initially saturated with oil: Flow patterns and pressure drop characteristics,” *International Journal of Multiphase Flow*, vol. 37, no. 9, pp. 1147–1155, Nov. 2011, doi: 10.1016/J.IJMULTIPHASEFLOW.2011.06.004.
[36] P. Babakhani Dehkordi, A. Azdarpour, and E. Mohammadian, “The hydrodynamic behavior of high viscous oil-water flow through horizontal pipe undergoing sudden expansion—CFD study and experimental validation,” *Chemical Engineering Research and Design*, vol. 139, pp. 144–161, Nov. 2018, doi: 10.1016/J.CHERD.2018.09.026.
[37] A. Abubakar, Y. Al-Wahaibi, T. Al-Wahaibi, A. Al-Hashmi, A. Al-Ajmi, and M. Eshrati, “Effect of low interfacial tension on flow patterns, pressure gradients and holdups of medium-viscosity oil/water flow in horizontal pipe,” *Exp Therm Fluid Sci*, vol. 68, pp. 58–67, Nov. 2015, doi: 10.1016/J.EXPTHERMFLUSCI.2015.02.017.
[38] “Fluid mechanics of surface tension explained | Britannica.” https://www.britannica.com/video/151076/Explanation-surface-tension (accessed Jun. 14, 2023).
[39] A. C. Bannwart, “Modeling aspects of oil–water core–annular flows,” *J Pet Sci Eng*, vol. 32, no. 2–4, pp. 127–143, Dec. 2001, doi: 10.1016/S0920-4105(01)00155-3.
[40] N. F. El-Ansary, G. A. Hoshoudy, A. S. Abd-Elrady, and A. H. A. Ayyad, “Effects of surface tension and rotation on the Rayleigh–Taylor instability,” *Physical Chemistry Chemical Physics*, vol. 4, no. 8, pp. 1464–1470, Apr. 2002, doi: 10.1039/B106242P.
[41] H. J. Kull, “Theory of the Rayleigh-Taylor instability,” *Phys Rep*, vol. 206, no. 5, pp. 197–325, Aug. 1991, doi: 10.1016/0370-1573(91)90153-D.
[42] H. T. Chen and S. Middleman, “Drop size distribution in agitated liquid-liquid systems,” *AIChE Journal*, vol. 13, no. 5, pp. 989–995, Sep. 1967, doi: 10.1002/AIC.690130529.
[43] J. Xu *et al.*, “Effect of surfactant headgroups on the oil/water interface: An interfacial tension measurement and simulation study,” *J Mol Struct*, vol. 1052, pp. 50–56, Nov. 2013, doi: 10.1016/J.MOLSTRUC.2013.07.049.
[44] S. Hosseinpour, V. Götz, and W. Peukert, “Effect of Surfactants on the Molecular Structure of the Buried Oil/Water Interface,” *Angewandte Chemie International Edition*, vol. 60, no. 47, pp. 25143–25150, Nov. 2021, doi: 10.1002/ANIE.202110091.
[45] “Viscosity | Definition, Facts, Formula, Units, & Examples | Britannica.” https://www.britannica.com/science/viscosity (accessed Jun. 14, 2023).
[46] K. O. Mikaelian, “Rayleigh-Taylor instability in finite-thickness fluids with viscosity and surface tension,” *Phys Rev E*, vol. 54, no. 4, p. 3676, Oct. 1996, doi: 10.1103/PhysRevE.54.3676.

[47] W. L. Loh and V. K. Premanadhan, “Experimental investigation of viscous oil-water flows in pipeline,” *J Pet Sci Eng*, vol. 147, pp. 87–97, Nov. 2016, doi: 10.1016/J.PETROL.2016.05.010.
[48] M. Al-Yaari, A. Soleimani, B. Abu-Sharkh, U. Al-Mubaiyedh, and A. Al-sarkhi, “Effect of drag reducing polymers on oil–water flow in a horizontal pipe,” *International Journal of Multiphase Flow*, vol. 35, no. 6, pp. 516–524, Jun. 2009, doi: 10.1016/J.IJMULTIPHASEFLOW.2009.02.017.
[49] K. H. Ngan, K. Ioannou, L. D. Rhyne, and P. Angeli, “Effect of glycerol addition on phase inversion in horizontal dispersed oil–water pipe flows,” *Exp Therm Fluid Sci*, vol. 35, no. 4, pp. 628–635, May 2011, doi: 10.1016/J.EXPTHERMFLUSCI.2010.12.012.
[50] A. Sánchez, J. C. Millán-Calenti, L. Lorenzo-Ló Pez, and A. Maseda, “Multisensory Stimulation for People With Dementia: A Review of the Literature”, doi: 10.1177/1533317512466693.
[51] A. Chalmers, S. Harrison, K. Mollison, N. Molloy, and K. Gray, “Establishing sensory-based approaches in mental health inpatient care: a multidisciplinary approach,” *http://dx.doi.org/10.1177/1039856211430146*, vol. 20, no. 1, pp. 35–39, Jan. 2012, doi: 10.1177/1039856211430146.
[52] S. Haig and N. Hallett, “Use of sensory rooms in adult psychiatric inpatient settings: A systematic review and narrative synthesis,” *Int J Ment Health Nurs*, vol. 32, no. 1, pp. 54–75, Feb. 2023, doi: 10.1111/INM.13065.
[53] M. Knight, L. Adkison, and J. S. Kovach, “A comparison of multisensory and traditional interventions on inpatient psychiatry and geriatric neuropsychiatry units,” *J Psychosoc Nurs Ment Health Serv*, vol. 48, no. 1, pp. 24–31, 2010, doi: 10.3928/02793695-20091204-03.
[54] S. Houghton *et al.*, “An empirical evaluation of an interactive multi-sensory environment for children with disability,” *http://dx.doi.org/10.1080/13668259800033761*, vol. 23, no. 4, pp. 267–278, 2009, doi: 10.1080/13668259800033761.
[55] M. Ashby, W. R. Lindsay, D. Pitcaithly, S. Broxholme, and N. Geelen, “Snoezelen: its Effects on Concentration and Responsiveness in People with Profound Multiple Handicaps”.
[56] L. E. Haggar and R. B. Hutchinson, “Snoezelen: an approach to the provision of a leisure resource for people with profound and multiple handicaps,” *Journal of the British Institute of Mental Handicap (APEX)*, vol. 19, no. 2, pp. 51–55, 1991, doi: 10.1111/J.1468-3156.1991.TB00620.X.
[57] G. A. Hotz, A. Castelblanco, I. M. Lara, A. D. Weiss, R. Duncan, and J. W. Kuluz, “Snoezelen: A controlled multi-sensory stimulation therapy for children recovering from severe brain injury,” *http://dx.doi.org/10.1080/02699050600832635*, vol. 20, no. 8, pp. 879–888, 2009, doi: 10.1080/02699050600832635.
[58] I. Akulwar-Tajane, K. K. Parmar, P. H. Naik, and A. V Shah, “Rethinking Screen Time during COVID-19: Impact on Psychological Well-Being in Physiotherapy Students,” *International Journal of Clinical and Experimental Medicine Research*, vol. 2020, no. 4, pp. 201–216, doi: 10.26855/ijcemr.2020.10.014.
[59] M. White, A. Smith, K. Humphryes, S. Pahl, D. Snelling, and M. Depledge, “Blue space: The importance of water for preference, affect, and restorativeness ratings of natural and built scenes,” *J Environ Psychol*, vol. 30, no. 4, pp. 482–493, Dec. 2010, doi: 10.1016/j.jenvp.2010.04.004.
[60] D. Nutsford, A. L. Pearson, S. Kingham, and F. Reitsma, “Residential exposure to visible blue space (but not green space) associated with lower psychological distress in

a capital city," *Health Place*, vol. 39, pp. 70–78, May 2016, doi: 10.1016/J.HEALTHPLACE.2016.03.002.
[61] "BlueHealth - European Centre for Environment and Human Health | ECEHH." https://www.ecehh.org/research/bluehealth/ (accessed Jun. 15, 2023).
[62] N. Novakovic, M. P. Milovancevic, S. D. Dejanovic, and B. Aleksic, "Effects of Snoezelen—Multisensory environment on CARS scale in adolescents and adults with autism spectrum disorder," *Res Dev Disabil*, vol. 89, pp. 51–58, Jun. 2019, doi: 10.1016/J.RIDD.2019.03.007.
[63] J. A. Staal *et al.*, "THE EFFECTS OF SNOEZELEN (MULTI-SENSORY BEHAVIOR THERAPY) AND PSYCHIATRIC CARE ON AGITATION, APATHY, AND ACTIVITIES OF DAILY LIVING IN DEMENTIA PATIENTS ON A SHORT TERM GERIATRIC PSYCHIATRIC INPATIENT UNIT*," *Psychiatry Med*, vol. 37, no. 4, pp. 357–370, 2007, doi: 10.2190/PM.37.4.a.
[64] C. Boutsioukis, B. Verhaagen, M. Versluis, E. Kastrinakis, and L. W. M. van der Sluis, "Irrigant flow in the root canal: experimental validation of an unsteady Computational Fluid Dynamics model using high-speed imaging," *Int Endod J*, vol. 43, no. 5, pp. 393–403, May 2010, doi: 10.1111/J.1365-2591.2010.01692.X.
[65] M. Versluis, "High-speed imaging in fluids," *Exp Fluids*, vol. 54, no. 2, pp. 1–35, Feb. 2013, doi: 10.1007/S00348-013-1458-X/FIGURES/14.
[66] M. Amaratunga, H. A. Rabenjafimanantsoa, and R. W. Time, "Comparison of oscillatory flow conditions in Newtonian and non-Newtonian fluids using PIV and high-speed image analysis," *Flow Measurement and Instrumentation*, vol. 70, p. 101628, Dec. 2019, doi: 10.1016/J.FLOWMEASINST.2019.101628.
[67] N. JENSEN, "HIGH-SPEED IMAGE ANALYSIS TECHNIQUES," *Photogrammetric Engineering*, vol. 39n1, Dec. 1973.
[68] G. Meynants, G. Lepage, J. Bogaerts, G. Vanhorebeek, and X. Wang, "Limitations to the frame rate of high speed image sensors".
[69] W. Lauterborn and A. Vogel, "MODERN OPTICAL TECHNIQUES IN FLUID MECHANICS.," *Annu Rev Fluid Mech*, vol. 16, pp. 223–244, 1984, doi: 10.1146/ANNUREV.FL.16.010184.001255.
[70] M. Damsohn and H. M. Prasser, "Droplet deposition measurement with high-speed camera and novel high-speed liquid film sensor with high spatial resolution," *Nuclear Engineering and Design*, vol. 241, no. 7, pp. 2494–2499, Jul. 2011, doi: 10.1016/J.NUCENGDES.2011.04.016.
[71] J. Y. L. Lum, T. Al-Wahaibi, and P. Angeli, "Upward and downward inclination oil–water flows," *International Journal of Multiphase Flow*, vol. 32, no. 4, pp. 413–435, Apr. 2006, doi: 10.1016/J.IJMULTIPHASEFLOW.2006.01.001.
[72] T. Al-Wahaibi, N. Yusuf, Y. Al-Wahaibi, and A. Al-Ajmi, "Experimental study on the transition between stratified and non-stratified horizontal oil–water flow," *International Journal of Multiphase Flow*, vol. 38, no. 1, pp. 126–135, Jan. 2012, doi: 10.1016/J.IJMULTIPHASEFLOW.2011.08.007.
[73] O. Der and V. Bertola, "An experimental investigation of oil-water flow in a serpentine channel," *International Journal of Multiphase Flow*, vol. 129, p. 103327, Aug. 2020, doi: 10.1016/J.IJMULTIPHASEFLOW.2020.103327.
[74] T. Sulchek, R. Hsieh, J. D. Adams, S. C. Minne, C. F. Quate, and D. M. Adderton, "High-speed atomic force microscopy in liquid," *Review of Scientific Instruments*, vol. 71, no. 5, pp. 2097–2099, 2000, doi: 10.1063/1.1150586.
[75] W. Witt, U. Köhler, and J. List, "CURRENT LIMITS OF PARTICLE SIZE AND SHAPE ANALYSIS WITH HIGH SPEED IMAGE ANALYSIS".

[76] Z. Wang *et al.*, “Deep-learning-based super-resolution reconstruction of high-speed imaging in fluids,” *Physics of Fluids*, vol. 34, no. 3, Mar. 2022, doi: 10.1063/5.0078644.
[77] H. Gao, L. Sun, and J. X. Wang, “Super-resolution and denoising of fluid flow using physics-informed convolutional neural networks without high-resolution labels,” *Physics of Fluids*, vol. 33, no. 7, Jul. 2021, doi: 10.1063/5.0054312.
[78] S. Sarkar, B. Karthikeyan, S. S. Ajai, G. D. Kumar, and C. M. Sharath, “Relaxation aid for intellectual disabilities,” *Proceedings of the 2018 International Conference On Communication, Computing and Internet of Things, IC3IoT 2018*, pp. 60–64, Mar. 2019, doi: 10.1109/IC3IOT.2018.8668148.
[79] M. Sirkkola, “Everyday Multisensory Environments, Wellness Technology and Snoezelen ISNA-MSE’s XII World,” 2014, Accessed: Jun. 19, 2023. [Online]. Available: www.hamk.fi/julkaisut
[80] S. B. Dalziel, “Rayleigh-Taylor instability: experiments with image analysis,” *Dynamics of Atmospheres and Oceans*, vol. 20, no. 1–2, pp. 127–153, Nov. 1993, doi: 10.1016/0377-0265(93)90051-8.
[81] S. T. Thoroddsen, T. G. Etoh, and K. Takehara, “High-Speed Imaging of Drops and Bubbles,” *https://doi.org/10.1146/annurev.fluid.40.111406.102215*, vol. 40, pp. 257–285, Jan. 2008, doi: 10.1146/ANNUREV.FLUID.40.111406.102215.
[82] R. M. Griffith, “The effect of surfactants on the terminal velocity of drops and bubbles,” *Chem Eng Sci*, vol. 17, no. 12, pp. 1057–1070, Dec. 1962, doi: 10.1016/0009-2509(62)80084-0.
[83] F. Pierron, R. Cheriguene, P. Forquin, R. Moulart, M. Rossi, and M. Sutton, “Performances and Limitations of Three Ultra High-Speed Imaging Cameras for Full-Field Deformation Measurements,” *Applied Mechanics and Materials*, vol. 70, pp. 81–86, 2011, doi: 10.4028/WWW.SCIENTIFIC.NET/AMM.70.81.
[84] C. W. Hsu, C. W. Chow, I. C. Lu, Y. L. Liu, C. H. Yeh, and Y. Liu, “High Speed Imaging 3 × 3 MIMO Phosphor White-Light LED Based Visible Light Communication System,” *IEEE Photonics J*, vol. 8, no. 6, Dec. 2016, doi: 10.1109/JPHOT.2016.2633395.
[85] M. Abramoff, “ImageJ as an Image Processing Tool and Library,” *Microscopy and Microanalysis*, vol. 13, no. S02, pp. 1672–1673, Aug. 2007, doi: 10.1017/S1431927607079652.
[86] M. Ishikawa, “High-speed Image Processing Devices and Its Applications,” *Technical Digest - International Electron Devices Meeting, IEDM*, vol. 2019-December, Dec. 2019, doi: 10.1109/IEDM19573.2019.8993437.
[87] G. Besagni and N. G. Deen, “Aspect ratio of bubbles in different liquid media: A novel correlation,” *Chem Eng Sci*, vol. 215, p. 115383, Apr. 2020, doi: 10.1016/J.CES.2019.115383.
[88] R. Prakash and S. K. Majumder, “Effect of particle size and concentration on bubble size distribution and aspect ratio in a counter-current microstructured bubble column,” *Journal of Industrial and Engineering Chemistry*, vol. 90, pp. 105–116, Oct. 2020, doi: 10.1016/J.JIEC.2020.07.002.
[89] M. Martín, F. J. Montes, and M. A. Galán, “On the influence of the liquid physical properties on bubble volumes and generation times,” *Chem Eng Sci*, vol. 61, no. 16, pp. 5196–5203, Aug. 2006, doi: 10.1016/J.CES.2006.03.027.
[90] W. Luewisutthichat, A. Tsutsumi, and K. Yoshida, “Bubble characteristics in multi-phase flow systems: Bubble sizes and size distributions,” *Journal of Chemical Engineering of Japan*, vol. 30, no. 3, pp. 461–466, 1997, doi: 10.1252/JCEJ.30.461.

[91] N. Sahoo, G. Khurana, A. R. Harikrishnan, D. Samanta, and P. Dhar, “Post impact droplet hydrodynamics on inclined planes of variant wettabilities,” *European Journal of Mechanics - B/Fluids*, vol. 79, pp. 27–37, Jan. 2020, doi: 10.1016/J.EUROMECHFLU.2019.08.013.
[92] K. Ellingsen and F. Risso, “On the rise of an ellipsoidal bubble in water: oscillatory paths and liquid-induced velocity,” *J. Fluid Mech.*, vol. 440, pp. 235–268, Aug. 2001, doi: 10.1017/s0022112001004761.
[93] J. C. Cano-Lozano, P. Bohorquez, and C. Martínez-Bazán, “Wake instability of a fixed axisymmetric bubble of realistic shape,” *Intl J. Multiphase Flow*, vol. 51, pp. 11–21, May 2013, doi: 10.1016/j.ijmultiphaseflow.2012.11.005.
[94] A. L. Yarin, “DROP IMPACT DYNAMICS: Splashing, Spreading, Receding, Bouncing…,” *https://doi.org/10.1146/annurev.fluid.38.050304.092144*, vol. 38, pp. 159–192, Dec. 2005, doi: 10.1146/ANNUREV.FLUID.38.050304.092144.
[95] C. Clanet, C. Béguin, D. Richard, and D. Quéré, “Maximal deformation of an impacting drop,” *J Fluid Mech*, vol. 517, pp. 199–208, Oct. 2004, doi: 10.1017/S0022112004000904.
[96] H. Jeong and H. Park, “Near-wall rising behaviour of a deformable bubble at high Reynolds number,” *J Fluid Mech*, vol. 771, pp. 564–594, May 2015, doi: 10.1017/JFM.2015.191.
[97] S. Uno and R. C. Kintner, “Effect of wall proximity on the rate of rise of single air bubbles in a quiescent liquid,” *AIChE J.*, vol. 2, no. 3, pp. 420–425, 1956, doi: 10.1002/aic.690020323.
[98] H. Z. Li, Y. Mouline, and N. Midoux, “Modelling the bubble formation dynamics in non-Newtonian fluids,” *Chem Eng Sci*, vol. 57, no. 3, pp. 339–346, Feb. 2002, doi: 10.1016/S0009-2509(01)00394-3.
[99] R. F. Mudde, “Gravity-driven bubbly flows,” *Annu Rev Fluid Mech*, vol. 37, pp. 393–423, 2005, doi: 10.1146/ANNUREV.FLUID.37.061903.175803.
[100] R. Prakash and S. K. Majumder, “Effect of particle size and concentration on bubble size distribution and aspect ratio in a counter-current microstructured bubble column,” *Journal of Industrial and Engineering Chemistry*, vol. 90, pp. 105–116, Oct. 2020, doi: 10.1016/J.JIEC.2020.07.002.
[101] F. Scargiali, A. Busciglio, F. Grisafi, and A. Brucato, “Bubble Formation at Variously Inclined Nozzles,” *Chem Eng Technol*, vol. 37, no. 9, pp. 1507–1514, Sep. 2014, doi: 10.1002/CEAT.201300511.
[102] Z. Xiao and R. B. H. Tan, “A model for bubble-bubble and bubble-wall interaction in bubble formation,” *AIChE Journal*, vol. 52, no. 1, pp. 86–98, Jan. 2006, doi: 10.1002/AIC.10644.
[103] M. E. Weber, A. Alarie, and M. E. Ryan, “Velocities of extended bubbles in inclined tubes,” *Chem Eng Sci*, vol. 41, no. 9, pp. 2235–2240, Jan. 1986, doi: 10.1016/0009-2509(86)85073-4.
[104] K. H. Bendiksen, “An experimental investigation of the motion of long bubbles in inclined tubes,” *International Journal of Multiphase Flow*, vol. 10, no. 4, pp. 467–483, Aug. 1984, doi: 10.1016/0301-9322(84)90057-0.
[105] W. Salman, A. Gavriilidis, and P. Angeli, “On the formation of Taylor bubbles in small tubes,” *Chem Eng Sci*, vol. 61, no. 20, pp. 6653–6666, Oct. 2006, doi: 10.1016/J.CES.2006.05.036.
[106] Y. Zhang and J. A. Finch, “A note on single bubble motion in surfactant solutions,” *J Fluid Mech*, vol. 429, pp. 63–66, Feb. 2001, doi: 10.1017/S0022112000002755.

[107] S. Ramakrishnan, R. Kumar, and N. R. Kuloor, “Studies in bubble formation—I bubble formation under constant flow conditions,” *Chem Eng Sci*, vol. 24, no. 4, pp. 731–747, Apr. 1969, doi: 10.1016/0009-2509(69)80065-5.
[108] H. Z. Li, “Bubbles in non-Newtonian fluids: Formation, interactions and coalescence,” *Chem Eng Sci*, vol. 54, no. 13–14, pp. 2247–2254, Jul. 1999, doi: 10.1016/S0009-2509(98)00294-2.
[109] R. J. Benzing and J. E. Myers, “Low Frequency Bubble Formation at Horizontal Circular Orifices,” *Ind Eng Chem*, vol. 47, no. 10, pp. 2087–2090, Oct. 1955, doi: 10.1021/IE50550A022.
[110] S. H. Kim, G. C. Lee, J. Y. Kang, H. S. Park, and M. H. Kim, “A study of nucleate bubble growth on microstructured surface through high speed and infrared visualization,” *International Journal of Multiphase Flow*, vol. 95, pp. 12–21, Oct. 2017, doi: 10.1016/J.IJMULTIPHASEFLOW.2017.02.007.
[111] C. W. Extrand and Y. Kumagai, “Liquid Drops on an Inclined Plane: The Relation between Contact Angles, Drop Shape, and Retentive Force,” *J Colloid Interface Sci*, vol. 170, no. 2, pp. 515–521, Mar. 1995, doi: 10.1006/JCIS.1995.1130.
[112] A. I. ElSherbini and A. M. Jacobi, “Liquid drops on vertical and inclined surfaces: I. An experimental study of drop geometry,” *J Colloid Interface Sci*, vol. 273, no. 2, pp. 556–565, May 2004, doi: 10.1016/J.JCIS.2003.12.067.
[113] M. A. Norato, C. Tsouris, and L. L. Tavlarides, “Phase inversion studies in liquid-liquid dispersions,” *Canadian Journal of Chemical Engineering*, vol. 76, no. 3, pp. 486–494, 1998, doi: 10.1002/CJCE.5450760319.
[114] W. Wang, J. Gong, K. H. Ngan, and P. Angeli, “Effect of glycerol on the binary coalescence of water drops in stagnant oil phase,” *Chemical Engineering Research and Design*, vol. 87, no. 12, pp. 1640–1648, Dec. 2009, doi: 10.1016/J.CHERD.2009.05.004.
[115] G. D. M. Mackay and S. G. Mason, “The gravity approach and coalescence of fluid drops at liquid interfaces,” *Can J Chem Eng*, vol. 41, no. 5, pp. 203–212, 1963, doi: 10.1002/CJCE.5450410504.
[116] S. Kato, E. Nakayama, and J. Kawasaki, “Types of dispersion in agitated liquid-liquid systems,” *Can J Chem Eng*, vol. 69, no. 1, pp. 222–227, 1991, doi: 10.1002/CJCE.5450690126.
[117] R. Narhe, D. Beysens, and V. S. Nikolayev, “Dynamics of drop coalescence on a surface: The role of initial conditions and surface properties,” *Int J Thermophys*, vol. 26, no. 6, pp. 1743–1757, Nov. 2005, doi: 10.1007/S10765-005-8593-4.
[118] R. Narhe, D. Beysens, and V. S. Nikolayev, “Dynamics of drop coalescence on a surface: The role of initial conditions and surface properties,” *Int J Thermophys*, vol. 26, no. 6, pp. 1743–1757, Nov. 2005, doi: 10.1007/S10765-005-8593-4.
[119] Q. Liao, X. Zhu, S. M. Xing, and H. Wang, “Visualization study on coalescence between pair of water drops on inclined surfaces,” *Exp Therm Fluid Sci*, vol. 32, no. 8, pp. 1647–1654, Sep. 2008, doi: 10.1016/J.EXPTHERMFLUSCI.2008.05.010.
[120] R. Chiba, K. Takakusaki, J. Ota, A. Yozu, and N. Haga, “Human upright posture control models based on multisensory inputs; in fast and slow dynamics,” *Neurosci Res*, vol. 104, pp. 96–104, Mar. 2016, doi: 10.1016/J.NEURES.2015.12.002.
[121] K. A. Nielson *et al.*, “Improved connectivity and cognition due to cognitive stimulation in Alzheimer’s disease,” *Front Aging Neurosci*, vol. 15, p. 1140975, 2023, doi: 10.3389/FNAGI.2023.1140975.
[122] M. Martín, F. J. Montes, and M. A. Galán, “On the influence of the liquid physical properties on bubble volumes and generation times,” *Chem Eng Sci*, vol. 61, no. 16, pp. 5196–5203, Aug. 2006, doi: 10.1016/J.CES.2006.03.027.

[123] J. R. Grace and D. Harrison, “The influence of bubble shape on the rising velocities of large bubbles,” *Chem Eng Sci*, vol. 22, no. 10, pp. 1337–1347, 1967, doi: 10.1016/0009-2509(67)80024-1.
[124] C. C. Maneri and N. Zuber, “An experimental study of plane bubbles rising at inclination,” *International Journal of Multiphase Flow*, vol. 1, no. 5, pp. 623–645, Nov. 1974, doi: 10.1016/0301-9322(74)90022-6.
[125] F. Zavareh, A. D. Hill, and A. L. Podio, “Flow Regimes in Vertical and Inclined Oil/Water Flow in Pipes,” Oct. 1988, doi: 10.2118/18215-MS.
[126] A. Manera, H. M. Prasser, D. Lucas, and T. H. J. J. van der Hagen, “Three-dimensional flow pattern visualization and bubble size distributions in stationary and transient upward flashing flow,” *International Journal of Multiphase Flow*, vol. 32, no. 8, pp. 996–1016, Aug. 2006, doi: 10.1016/J.IJMULTIPHASEFLOW.2006.03.005.
[127] “LED Lighting Market Size, Share & Industry Analysis, 2029.” https://www.fortunebusinessinsights.com/led-lighting-market-106832 (accessed Aug. 28, 2023).
[128] “Ambient Lighting Market Size & Share Analysis - Industry Research Report - Growth Trends.” https://www.mordorintelligence.com/industry-reports/ambient-lighting-market (accessed Aug. 28, 2023).
[129] “How to Identify Follow-on Markets (With a Great Bowling Analogy).” https://leanb2bbook.com/blog/identify-follow-on-markets/ (accessed Aug. 28, 2023).
[130] “Higher education in numbers.” https://www.universitiesuk.ac.uk/latest/insights-and-analysis/higher-education-numbers (accessed Aug. 28, 2023).
[131] “Smart lighting | Philips Hue UK.” https://www.philips-hue.com/en-gb?origin=p68512890054&gclid=Cj0KCQjwi7GnBhDXARIsAFLvH4ktsuYZeXGglv4ZLC1trPCPr4wlLNPrNG8EMQFFvczqOZL8F6pGjZ4aApLNEALw_wcB&gclsrc=aw.ds (accessed Aug. 28, 2023).
[132] “Red Light Therapy Devices For Pain, Skin Health, Energy, and Recovery – Hooga.” https://hoogahealth.com/ (accessed Aug. 28, 2023).
[133] “Aurora Volcano Lamp.” https://isaacstreasures.com/products/aurora-volcano-lamp (accessed Aug. 28, 2023).
[134] E. T. Attar, V. Balasubramanian, E. Subasi, and M. Kaya, “Stress Analysis Based on Simultaneous Heart Rate Variability and EEG Monitoring,” *IEEE J Transl Eng Health Med*, vol. 9, 2021, doi: 10.1109/JTEHM.2021.3106803.
[135] E. Shashi Menon, “Fluid Flow in Pipes,” *Transmission Pipeline Calculations and Simulations Manual*, pp. 149–234, 2015, doi: 10.1016/B978-1-85617-830-3.00005-5.
[136] J. L. Trallero, C. Sarica, and J. P. Brill, “A Study of Oil/Water Flow Patterns in Horizontal Pipes,” *SPE Production & Facilities*, vol. 12, no. 03, pp. 165–172, Aug. 1997, doi: 10.2118/36609-PA.

Appendix

Appendix A – *Macro plug-in which extracts the profile plot generated in ImageJ into a .csv file*

```
// StackProfileData
// This ImageJ macro gets the profile of all slices in a stack
// and writes the data to the Results table, one column per slice.
//
// Version 1.0, 24-Sep-2010 Michael Schmid

macro "Stack profile Data" {
    if (!(selectionType()==0 || selectionType==5 || selectionType==6))
      exit("Line or Rectangle Selection Required");
    setBatchMode(true);

    run("Plot Profile");
    Plot.getValues(x, y);
    run("Clear Results");
    for (i=0; i<x.length; i++)
       setResult("x", i, x[i]);
    close();

    n = nSlices;
    for (slice=1; slice<=n; slice++) {
       showProgress(slice, n);
       setSlice(slice);
       profile = getProfile();
       sliceLabel = toString(slice);
       sliceData = split(getMetadata("Label"),"\n");
       if (sliceData.length>0) {
          line0 = sliceData[0];
          if (lengthOf(sliceLabel) > 0)
             sliceLabel = sliceLabel+ " ("+ line0 + ")";
       }
       for (i=0; i<profile.length; i++)
          setResult(sliceLabel, i, profile[i]);
    }
    setBatchMode(false);
    updateResults;
}
```

Appendix B – *Generating velocity from plot profile, for 0, 30, 60 degrees.*

```
from matplotlib import pyplot as plt
import numpy as np
from scipy.interpolate import splrep, splev
import pandas as pd

max_index = []
df = pd.read_csv ('/Users/edoardogambacorta/Desktop/0-bottom V1/Results0.csv')
for i in range(2,len(df.keys())):
    max_index.append(np.argmin(df[df.keys()[i]]))

pos = np.array(max_index)/24
t = np.arange(len(pos))/90

plt.plot(t,pos)
plt.xlabel('t (sec)')
plt.ylabel('position (mm)')
plt.show()


spl = splrep(t[51:123], pos[51:123],k=3,s=5)
t2 = np.linspace(np.min(t[51:123]), np.max(t[51:123]), 10000)
pos2 = splev(t2, spl)
plt.plot(t2,pos2)
plt.xlabel('t (sec)')
plt.ylabel('position (mm)')
plt.show()

plt.plot(t2, pos2)
plt.xlabel('t (sec)')
plt.ylabel('position (mm)')
plt.show()

plt.plot(t2, np.gradient(pos2,t2))
plt.xlabel('t (sec)')
plt.ylabel('velocity (mm/sec)')
plt.show()

from matplotlib import pyplot as plt
import numpy as np
from scipy.interpolate import splrep, splev
import pandas as pd

max_index = []
df = pd.read_csv ('/Users/edoardogambacorta/Desktop/0-bottom V1/Results30.csv')
for i in range(2,len(df.keys())):
    max_index.append(np.argmin(df[df.keys()[i]]))

pos = np.array(max_index)/24
t = np.arange(len(pos))/90

plt.plot(t,pos)
plt.xlabel('t (sec)')
plt.ylabel('position (mm)')
plt.show()

spl = splrep(t[35:115], pos[35:115],k=3,s=5)
t2_30 = np.linspace(np.min(t[35:115]), np.max(t[35:115]), 10000)
pos2_30 = splev(t2_30, spl)
plt.plot(t2_30,pos2_30)
plt.xlabel('t (sec)')
plt.ylabel('position (mm)')
plt.show()

plt.plot(t2_30, pos2_30)
plt.xlabel('t (sec)')
plt.ylabel('position (mm)')
plt.show()

plt.plot(t2_30, np.gradient(pos2_30,t2_30))
plt.xlabel('t (sec)')
plt.ylabel('velocity (mm/sec)')
plt.show()

from matplotlib import pyplot as plt
import numpy as np
from scipy.interpolate import splrep, splev
import pandas as pd

max_index = []
df = pd.read_csv ('/Users/edoardogambacorta/Desktop/0-bottom V1/Results60.csv')
for i in range(2,len(df.keys())):
    max_index.append(np.argmin(df[df.keys()[i]]))

pos = np.array(max_index)/24
t = np.arange(len(pos))/90

plt.plot(t,pos)
plt.xlabel('t (sec)')
plt.ylabel('position (mm)')
plt.show()


spl = splrep(t[99:263], pos[99:263],k=3,s=5)
t2_60 = np.linspace(np.min(t[99:263]), np.max(t[99:263]), 10000)
pos2_60 = splev(t2_60, spl)
plt.plot(t2_60,pos2_60)
plt.xlabel('t (sec)')
plt.ylabel('position (mm)')
plt.show()

plt.plot(t2_60, pos2_60)
plt.xlabel('t (sec)')
plt.ylabel('position (mm)')
plt.show()

plt.plot(t2_60, np.gradient(pos230,t2_60))
plt.xlabel('t (sec)')
plt.ylabel('velocity (mm/sec)')
plt.show()

plt.plot(t2_60-t2_60[0], np.gradient(pos2_60,t2_60), label='60 deg')
plt.plot(t2_30-t2_30[0], np.gradient(pos2_30,t2_30), label='30 deg')
plt.plot(t2-t2[0], -np.gradient(pos2,t2), label='0 deg')
plt.xlabel('t (sec)')
plt.ylabel('velocity (mm/sec)')
plt.legend()
```

Appendix C – *Aspect ratio over time at 0-75 degrees of inclination, top of the sensory light*

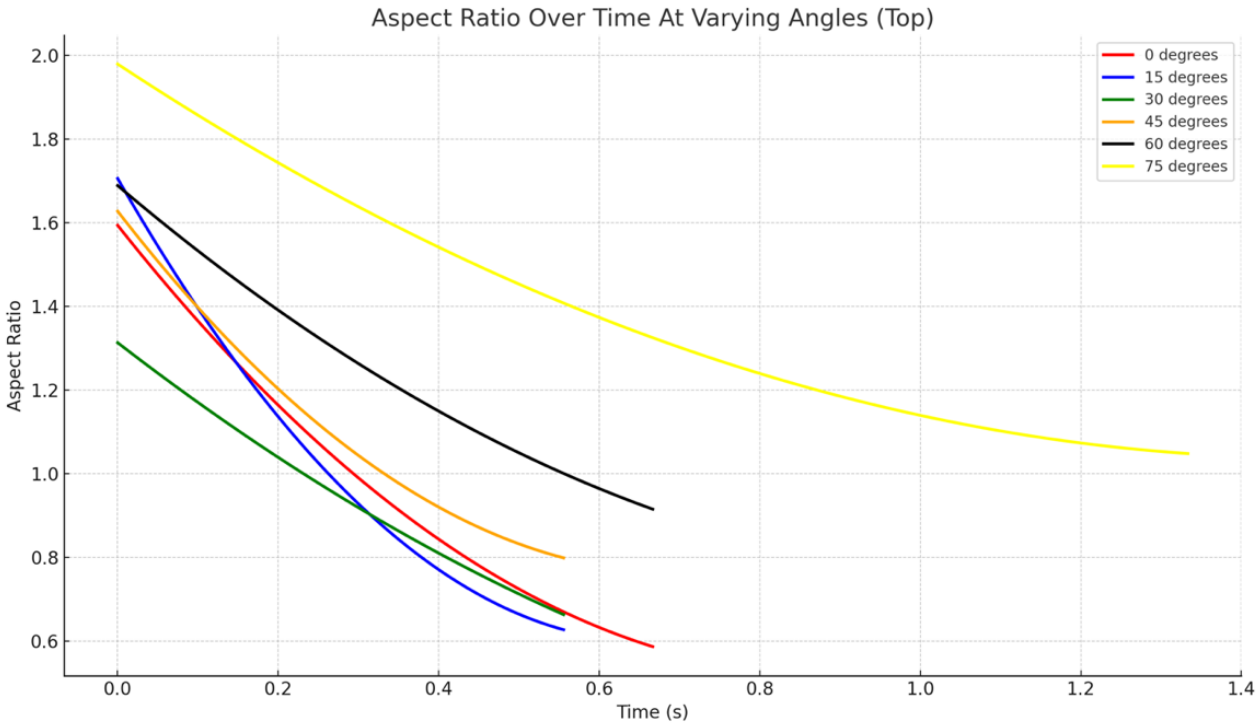

Appendix D - *Aspect ratio over time at 0-75 degrees of inclination, bottom of the sensory light*

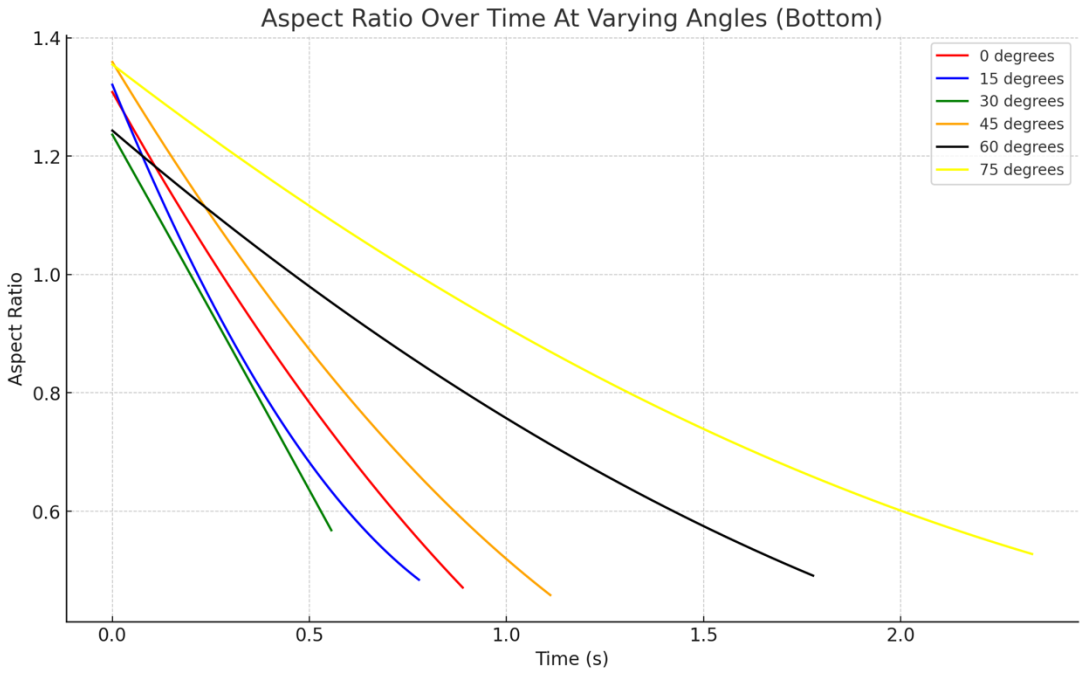

Appendix E - *Aspect ratio over time comparison of top & bottom at 0–75-degree range*

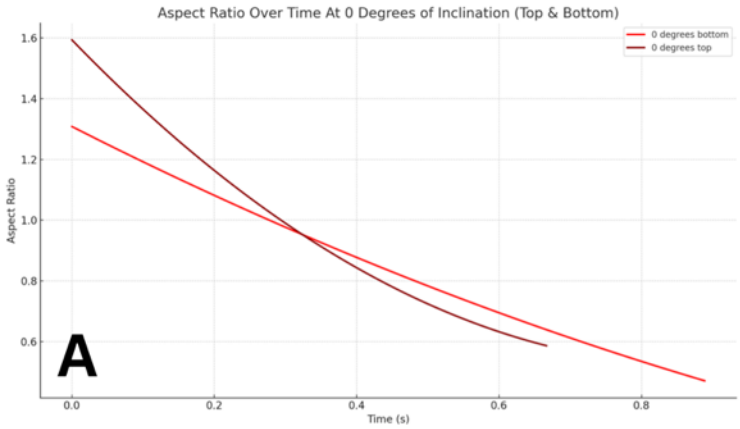

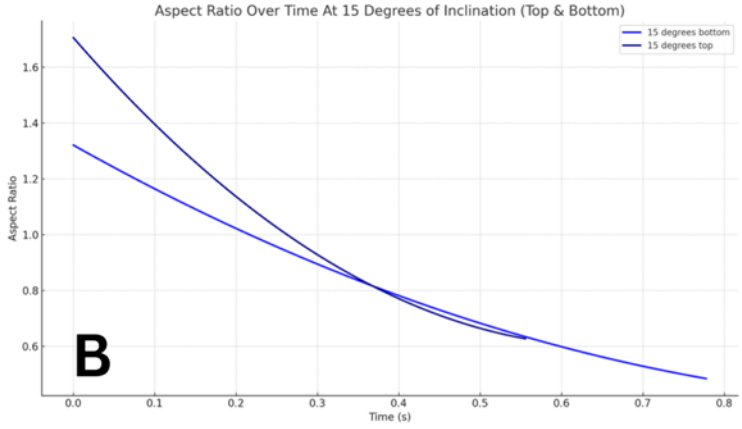

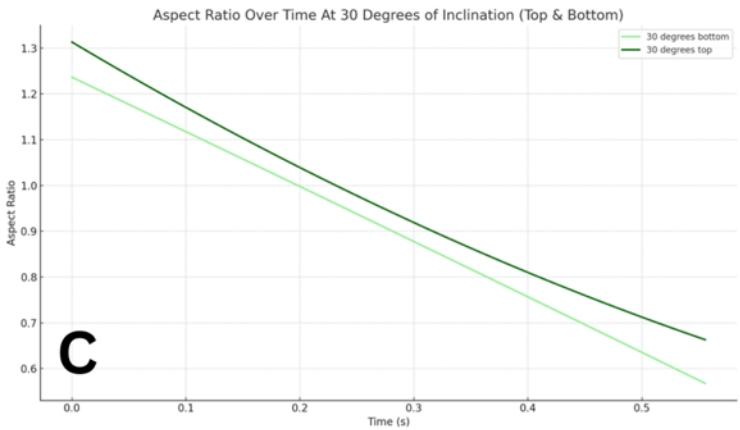

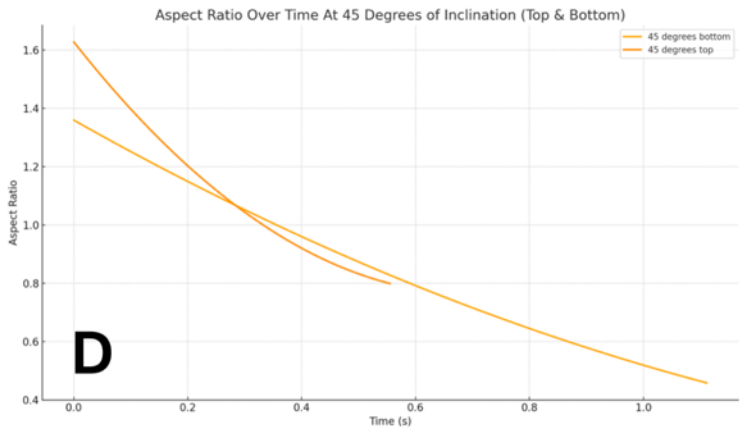

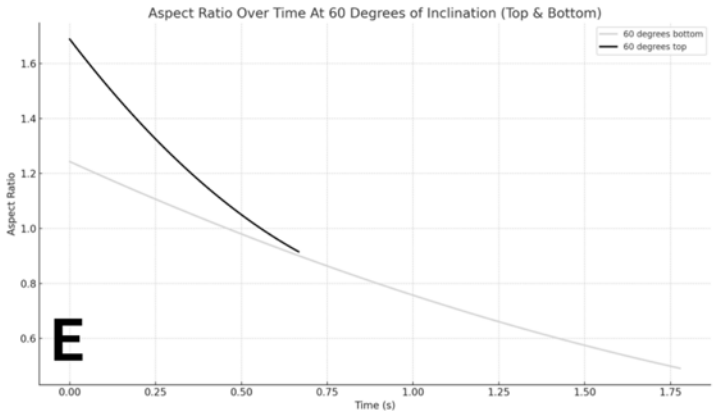

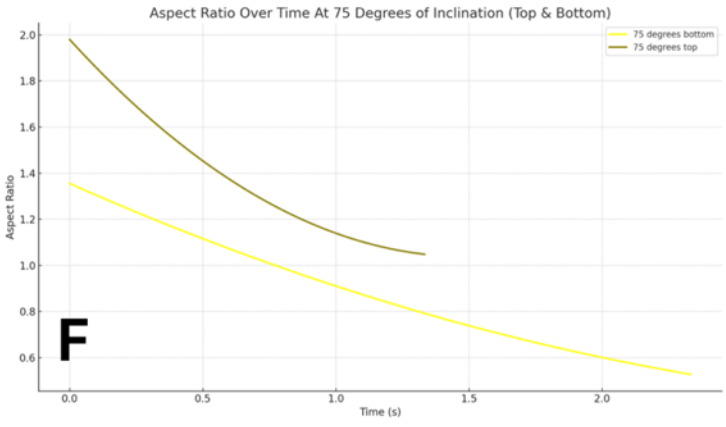

Appendix F - *Examination of droplet elongation and release at various angles of inclination, bottom chamber of the sensory light*

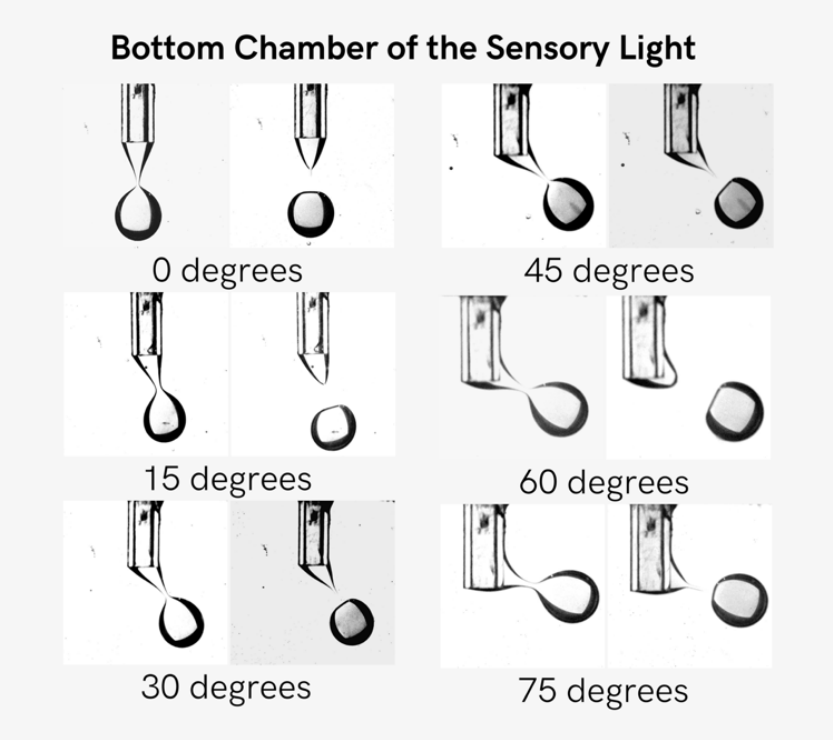

Appendix G - *Velocity of Droplets over time, 30 degrees, First vs Refined Prototype*

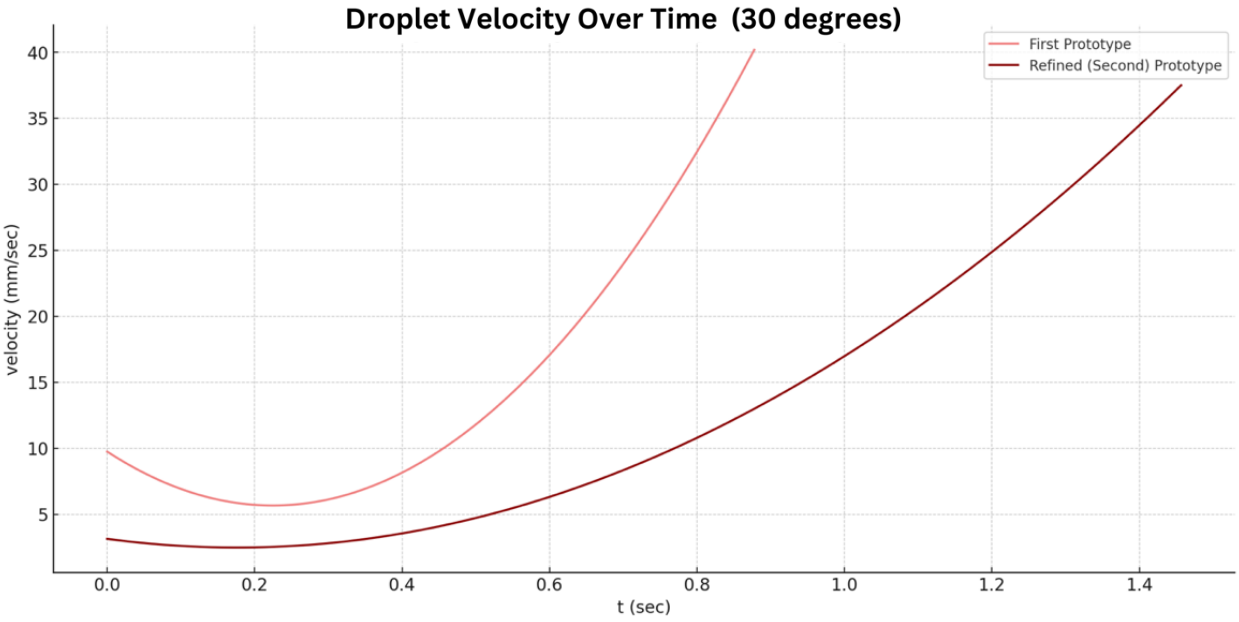

Appendix H - *Velocity of Droplets over time, 60 degrees, First vs Refined Prototype*

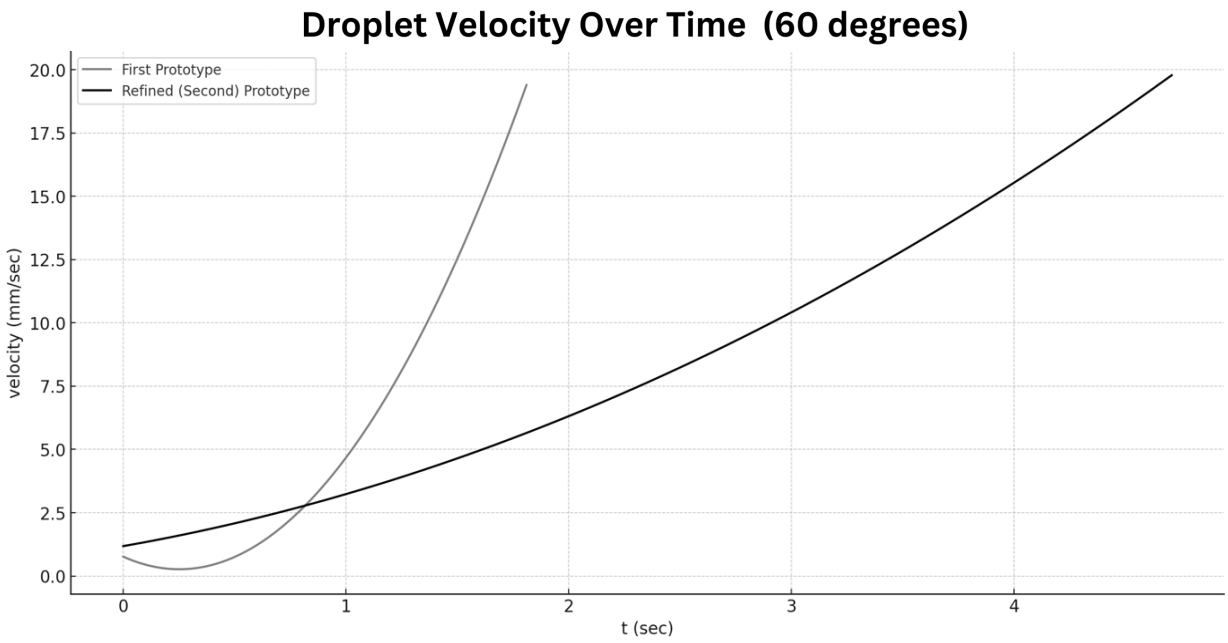

Appendix I - *Aspect ratio over time at varying angles of inclination, bottom chamber, Refined Prototype*

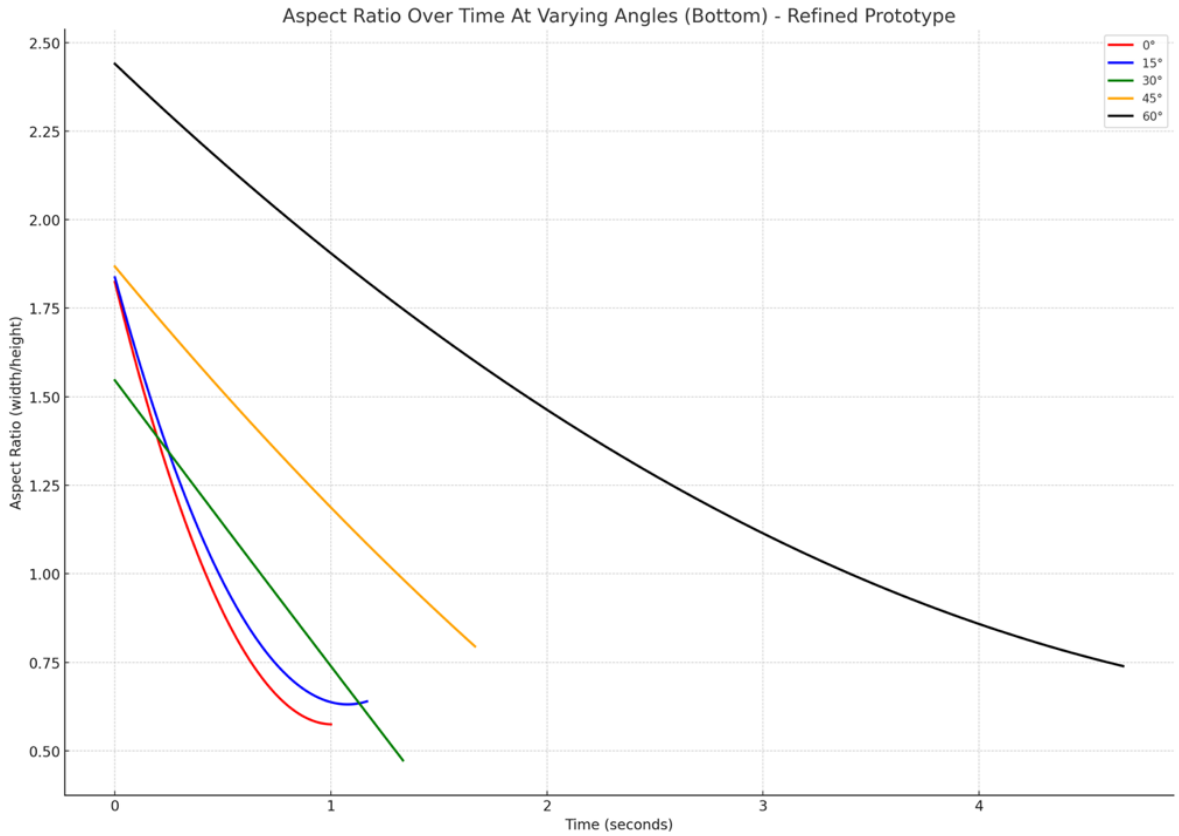

Appendix J - *Aspect ratio over time for refined vs first prototype, 0-45 degrees*

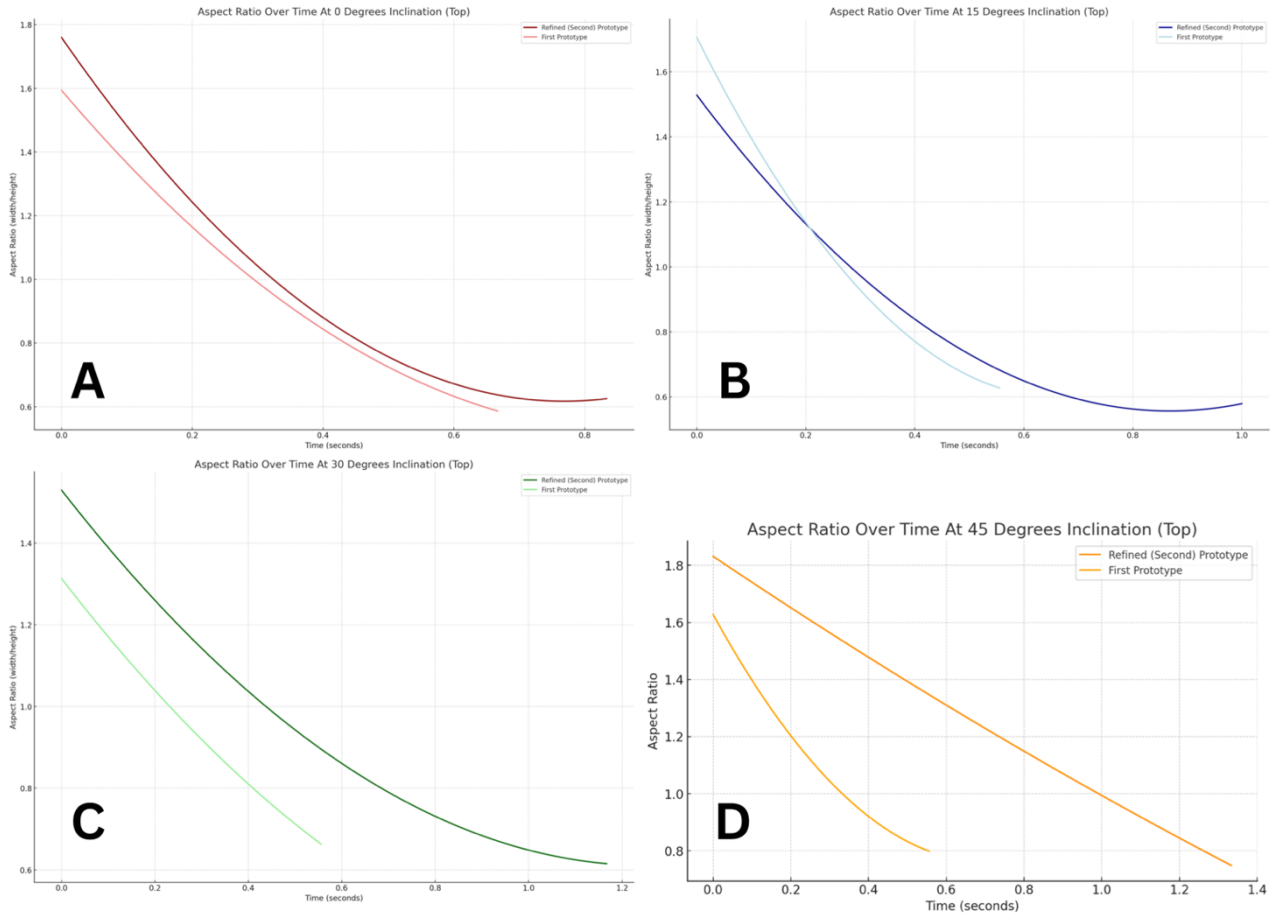

Appendix K - *Droplet generation time vs angle of inclination, top chamber, First vs Refined Prototype*

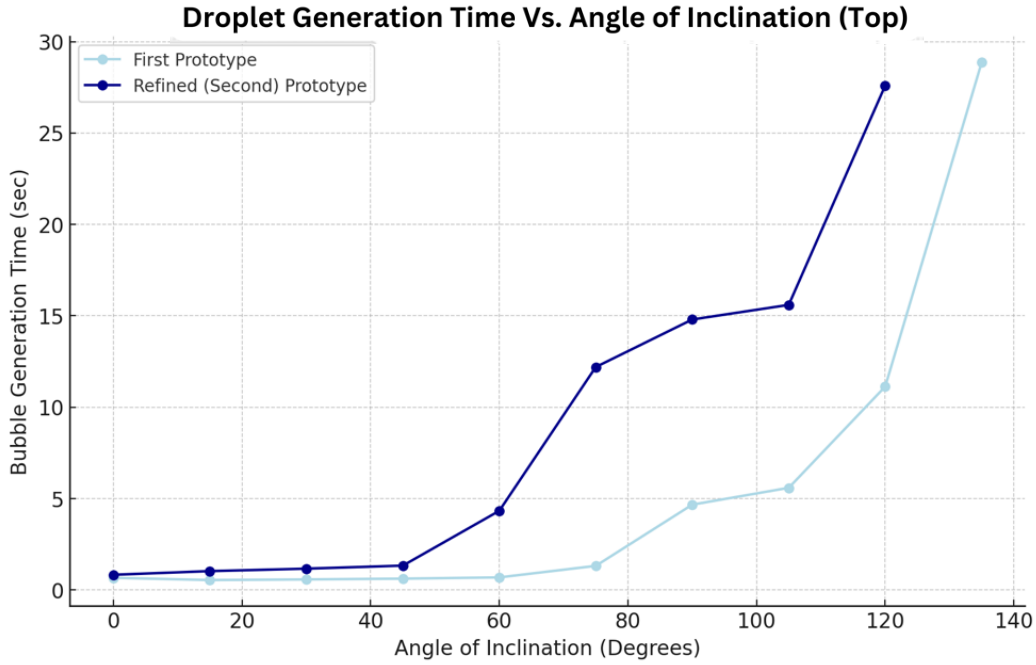

Appendix L - *Droplet size vs angle of inclination, top chamber, First vs Refined Prototype*